Classifying and Identifying Negative Poisson's Ratio.

An Examination of the Auxeticity in Zeolitic Materials

Volume 1 of 1

Submitted by Mark James Siddorn to the University of Exeter

as a thesis for the degree of

Doctor of Philosophy in Engineering

In November 2014

I certify that all material in this thesis which is not my own work has been identified and that no material has previously been submitted and approved for the award of a degree by this or any other University.

Signature……………………………………………………

Abstract

The aim of this thesis is to advance the understanding of auxeticity. This is achieved by developing a more accurate way to classify materials exhibiting the property, by carrying out high-throughput atomistic simulations of framework materials based on the SiO_2 and GeO_2 chemistries, and by exploring mechanistic models and possible correlations with directional density variations. At first this thesis outlines the development of a typographic system for negative Poisson's ratio. Materials are given classifications based on the degree to which auxetic behaviour is observed along specific axes of deformation and the frequency of occurrence of these axes. A systematic study is then performed on the elastic properties of zeolitic silicon dioxide and germanium dioxide structures. The typology is applied to these materials to better understand their auxetic behaviour. The JST framework is identified as isotropically auxetic, the first crystal to exhibit such general negative Poisson's ratios. An exploration into the effects of local density variations between parallel planes on Poisson's ratio is undertaken, but no clear correlation is found. Finally, software for systematically creating and evaluating two dimensional networks of triangles is produced. The geometrical analysis of these rotating structures predicts a high level of auxeticity and further work into three dimensional equivalents is recommended.

Table of Contents

List of Figures

List of Tables

Acknowledgments

This thesis would not have been possible without the excellent supervision and guidance of Dr Arnaud Marmier, whose passion and enthusiasm is infectious. I feel extremely fortunate to have had the benefit of his calming influence throughout. I would also like to thank Dr Ken Evans for his uncanny ability to cut to the heart of an issue, which has brought much needed clarity on many occasions.

Finally, I would like to express my gratitude to my family and friends; I have never received anything less than complete support and encouragement from every one of them, especially my partner Rebecca who has been endlessly patient.

Chapter 1: Introduction

This thesis describes the search for crystalline materials with extreme auxeticity (negative Poisson's ratio –PR–), based on atomistic simulations, geometric considerations and meta-analyses of previously published experimental studies. In the context of anisotropic auxeticity, extreme can relate to different quantities such as minimum values of PR, minimum average (where different definitions are available) or even range of angular distribution of negative PR. A major result of this work has therefore been the development of a completely novel classification of auxetic materials which brings much clarity to the field. The other major success is that I have identified a structure which is more auxetic (as in auxetic for more directions) than α-cristobalite, the previously best candidate; the cubic zeolite JST shows a negative PR in every direction, which had never been observed for a crystalline material.

For non-isotropic materials, elastic properties are complex. They are best described by tensors of order four with up to 21 independent values (only 2 in the isotropic case). Even cubic symmetries with "only" 3 independent elastic constants can give rise to a variety of very different Poisson's ratio behaviour. In fact, it has only been recently discovered that negative Poisson's ratio (NPR) is not as rare and exotic as previously thought and that the simplest form of auxeticity is present in 37% of crystals. The two descriptors, auxetic and NPR, are simply not precise enough to convey important differences and the community needs a way to describe the property more accurately, a useful yet manageable intermediate between simplistic adjectives and almost impossible to grasp four dimensional isosurfaces.

Many applications for auxeticity have been proposed, ranging from nano-actuators and sensors to blast mitigation curtains. A key requirement for systematic materials selection using Ashby indices and charts is that materials properties are available in tabulated forms; it is likely that different types of auxeticity will be required for different applications. For example and somewhat tentatively, strain amplification will require PR as large as possible, however the range of directions will not matter much, assuming of course that mono-crystals can be produced and aligned accurately. For stress-controlled molecular sieves, the ability to deform in many directions will be important, and a more generic auxeticity will be the relevant property. Isotropic, quasi-isotropic or average auxeticity is also likely to be useful in situations where the production method creates polycrystalline devices with no texture[1].

While materials with some limited auxeticity are quite common, materials with some sort of "average" auxeticity (often ill defined) are significantly more scarce, especially crystals. Auxetic foams created by crushing and based on re-entrant ribs are essentially isotropic, and therefore their PR is negative in all directions. But only one crystal has been shown to have NPR for a wide range of directions, the silicate α-cristobalite. The mechanism responsible for such generalised NPR has not been fully elucidated, in part because it had not been realised widely how unique α-cristobalite is. It would be very useful to have access to other crystals with generalised auxeticity to help understand the mechanism(s) responsible. As the obvious route of collating experimental data has already been explored, few options remains to expand the database of elastic constants of crystals. A first option consists in simulating families of crystals with reputable models to extract elastic

---

[1] Otherwise, the negative directions would be swamped by the positive ones, resulting in an isotropic, positive Poisson's ratio.

constants and corresponding auxetic typologies. The zeolite family is an attractive starting point for many reasons: it is large with more than 200 frameworks (with new structures regularly identified), it is based on the same chemistry as α-cristobalite for which numerous models of quality are available, and it has been suggested than the porous nature of zeolites might be conducive to NPR. The second option is more powerful, but much more complex: it consists of generating networks and optimising them (still using an underlying potential energy model) for energetic stability and auxeticity. Finally, it is well worth trying to correlate NPR with simpler quantities. For crystals it is generally difficult to measure NPR experimentally (either directly or through elastic constants), but were a positive correlation with NPR to be identified, it would at best allow direct identification and at worst narrow the field of search.

Chapter 2 reviews the current literature on auxeticity and the simulation of zeolites with an emphasis on elastic properties. For coherence, no chapter is devoted solely to collating methodological considerations and the relevant methods specific only to an individual chapter are described there. The new typology of auxeticity is developed and tested against a database of materials in Chapter 3. This has also the benefit of establishing a base-line of auxeticity for crystals. The search for actual crystals with extreme auxeticity starts in Chapter 4, where classical simulations with semi-empirical potentials explore all silica zeolites. Chapter 5 focuses on trying to establish whether features of directional density can be used to identify NPR. Chapter 6 sees a return to direct exploration of auxeticity, and an approach similar to the one used in Chapter 4 is applied to zeolitic networks of germanium dioxide. Chapter 7 describes an algorithm to automatically generate networks of 2D triangles for NPR optimisation. Finally in Chapter 8 I summarise the main results from the thesis and suggests possible ways to expand the tools I have developed.

Chapter 2: Literature Review

2.1 Negative Poisson's Ratio

2.1.1 Introduction to auxeticity

The elastic properties of a material are described in terms of its strain (ε) relative to an applied stress (σ), where ε is the ratio of extension (ΔL) to original length (L_0), and σ is the applied force (F) per cross sectional area (A)

$$\varepsilon = \frac{\Delta L}{L_0} \tag{2.1}$$

$$\sigma = \frac{F}{A}\ . \tag{2.2}$$

There are multiple stresses and strains found within a material corresponding to the different cross sectional areas or axes which may be examined. For example, under the same stress a material will experience longitudinal strain (ε_L) in the same direction as the applied force, and also transverse strain (ε_T) in directions perpendicular to the force. The relationship between these stresses and strains in isotropic materials are known as the elastic moduli, with the most commonly used being Young's modulus (E), bulk modulus (K), shear modulus (G), and Poisson's ratio (v). The following equations describe E and v in terms of the stress and strain of an isotropic material, with K and G being described in terms of their relationship to both E and v

$$E = \frac{\sigma}{\varepsilon} \tag{2.3}$$

$$\nu = \frac{-\varepsilon_T}{\varepsilon_L} \tag{2.4}$$

$$K = \frac{E}{3(1-2\nu)} \tag{2.5}$$

$$G = \frac{E}{2(1+\nu)} \ . \tag{2.6}$$

The Poisson's ratio has historically been the least explored,[1] though it is associated with some interesting and unusual properties particularly when in a range not normally encountered. Defined as the ratio of lateral to axial strain in a structure or material, the Poisson's ratio contributes to both *G* and *K*.[2] It has been accepted theory that *v* can have negative values for over 150 years[3] and in 1991 the term auxetic was first used to describe materials with this property.[4] Auxetic materials may prove beneficial to current materials technology with potential improvements to mechanical properties such as hardness, indent resistance, fracture toughness, shear strength, and sound absorption,[1, 5–7] or by exploiting geometrical properties such as maintaining the shape of pores within molecular sieves, or allowing for a double curvature within a honeycomb panel.[8–10]

For a material with any degree of anisotropy these four scalar constants, which can be derived from any two, are no longer sufficient to fully describe its elastic properties. Instead, a 4th order tensor is used to express stress in terms of strain (stiffness), or strain in terms of stress (compliance).[11] It is often convenient to represent these tensors as 6x6 matrices, using the well-established Voigt[12] notation, in order to aid visualisation and allow for easier manipulation. The maximum number of coefficients used to fully define the elastic properties of a material is 21,[11] but this number decreases with increased crystal symmetry. As a consequence, the Poisson’s ratio of anisotropic materials is a complex function (dependant on three directional parameters, two angles describing the axial vector, one describing the perpendicular lateral vector). The prevalence or even simply the existence of auxeticity depends on the complex interplay between the tensor elements.

To simplify analysis of anisotropic materials, their elastic properties can be averaged to simulate how they may behave whilst part of an isotropic polycrystalline structure. The four main ways in which these properties are averaged are the Voigt,[12] Reuss,[13] and Hill[14] schemes along with a direct averaging method. Both the Voigt and Reuss averaging schemes provide values for the bulk modulus *K* and the shear modulus *G*, Voigt deriving these from the stiffness matrix (with coefficients C_{ij}) and Reuss from the compliance matrix (with coefficients S_{ij}). The Voigt averages are given by

$$K_V = \frac{A + 2B}{3} \tag{2.7}$$

$$G_V = \frac{A - B + 3C}{5} \tag{2.8}$$

where

$$A = \frac{C_{11} + C_{22} + C_{33}}{3} \tag{2.9}$$

$$B = \frac{C_{23} + C_{13} + C_{12}}{3} \tag{2.10}$$

$$C = \frac{C_{44} + C_{55} + C_{66}}{3} \tag{2.11}$$

and the Reuss averages are given by

$$K_R = \frac{1}{3a + 6b} \tag{2.12}$$

$$G_R = \frac{5}{4a - 4b + 3c} \tag{2.13}$$

where

$$a = \frac{S_{11} + S_{22} + S_{33}}{3} \tag{2.14}$$

$$b = \frac{S_{23} + S_{13} + S_{12}}{3} \tag{2.15}$$

$$c = \frac{S_{44} + S_{55} + S_{66}}{3}. \tag{2.16}$$

.

The Hill scheme uses the arithmetic mean of the Voigt and Reuss values and the direct method takes a numerical average of the properties found on a sample of axes.

By rearranging Equations (2.5) and (2.6) to get the following

$$E = \left(\frac{1}{3G} + \frac{1}{9K}\right)^{-1} \tag{2.17}$$

$$\nu = \frac{1}{2} \times \left(1 - \frac{3G}{3K + G}\right), \tag{2.18}$$

the bulk and shear modulus (found with any of the averaging schemes) can be used to find an averaged value for both the Young's modulus *E* and the Poisson's ratio *v*.

2.1.2 Examples of auxeticity

Although materials such as iron pyrites,[3] bone,[15] and cat skin[16] had been found to be auxetic at various times in the mid-20th Century, it was not until the manufacture of auxetic re-entrant foams in 1987[17] that interest in negative Poisson's ratio materials began to increase. With additional studies the occurrence of auxetic properties was found to be much more prevalent than previously expected; 69% of cubic metals were found to exhibit a negative Poisson's ratio,[18] and 25% of monoclinic crystals.[19] The SiO_2 polymorph α-cristobalite has been shown to have a high level of auxeticity[20] compared even with other materials with a negative Poisson's ratio, causing much interest in α-cristobalite itself, and also in other similar materials. Complex silicates and zeolites such as the all-silica zeolite MFI (ZSM5-$Si_{96}O_{192}$) have been predicted with a negative Poisson's ratio.[21] It is hoped that these materials, if exhibiting a negative Poisson's ratio, could be used as tuneable molecular sieves, giving rise to an active interest within the academic community.

2.1.3 Applications of auxeticity

There are many applications for auxetic materials which, due to their unusual and somewhat unobserved properties, have only recently become apparent. Highly negative Poisson's ratios ($v < -0.5$) can produce large values for indent resistance,[1] a desirable property in foam mattresses where increased support could be produced without a reduction in comfort as a consequence. The increased acoustic absorption of auxetic foams leads to their potential use as damping materials for use in audio recording.[7] The increased hardness of auxetic materials[6] or the properties of auxetic warp knit textile structures[22] could allow for use in the defence or sporting industries as light but strong personal protection equipment. Auxetic fabrics also hold much potential as blast curtains, capable of preventing glass or other small pieces of debris from passing through.[23] There is interest in auxetics as the passive phase of piezoelectric composites,[24] where their negative Poisson's ratio is not used for direct mechanical benefits but instead as a way of reducing large-scale strains whilst allowing the small-scale strains necessary for producing the desired electrical current.

Of all commercial applications of these special materials perhaps the most promising comes with their use as molecular sieves.[21, 25, 26] By utilising the conservation of pore shape under external pressures, the size of the molecules that are allowed through can be dynamically altered, allowing for greater control in chemical systems where porosity is involved.

2.1.4 Mechanisms in auxetic materials

The mechanisms behind auxetic behaviour can be found at almost every size scale with many larger mechanisms being analogous to smaller ones (e.g. replacing electrostatic bonds at the molecular level with beams at the macro level). These mechanisms occur due to many different structural concepts possibly suggesting why so many different classes of materials have been found with auxetic behaviour. The two dimensional re-entrant foam structure,[27] that can be seen in Figure 2.1, was one of the earliest structural arrangements shown to have auxetic properties.

Figure 2.1 – Auxetic, two-dimensional, re-entrant foam structure. Elongation in the longitudinal direction will cause the 'middles' of the re-entrant hexagons to separate, causing expansion in the transverse direction.

Since then many structures exhibiting a negative Poisson's ratio have been identified as; chiral, where a central unit is rotated and the material is 'wrapped' around it;[28] rotating units with squares,[29] triangles,[30] and tetrahedra[31] as well as rigid, or semi-rigid units within a material;[32, 33] angle-ply laminates with stiff inclusions and a compliant matrix;[34] hard molecules in arrangements to give negative Poisson's ratio when modelled with intermolecular potentials;[35] micro-porous polymers of interconnected nodules and fibrils, where 'tightening' fibrils cause expansion in the system;[36] and liquid crystalline polymers with chains of rigid rod molecules connected by flexible spacer groups.[37] Figure 2.2 shows a few examples of auxetic mechanisms, all following a central theme of rotating units within a structure. Shown are the mechanisms for a) chiral structure, b) rotating square structure, and c) rotating triangle structure. All three of these structures deform isotropically and have Poisson's ratios of −1.

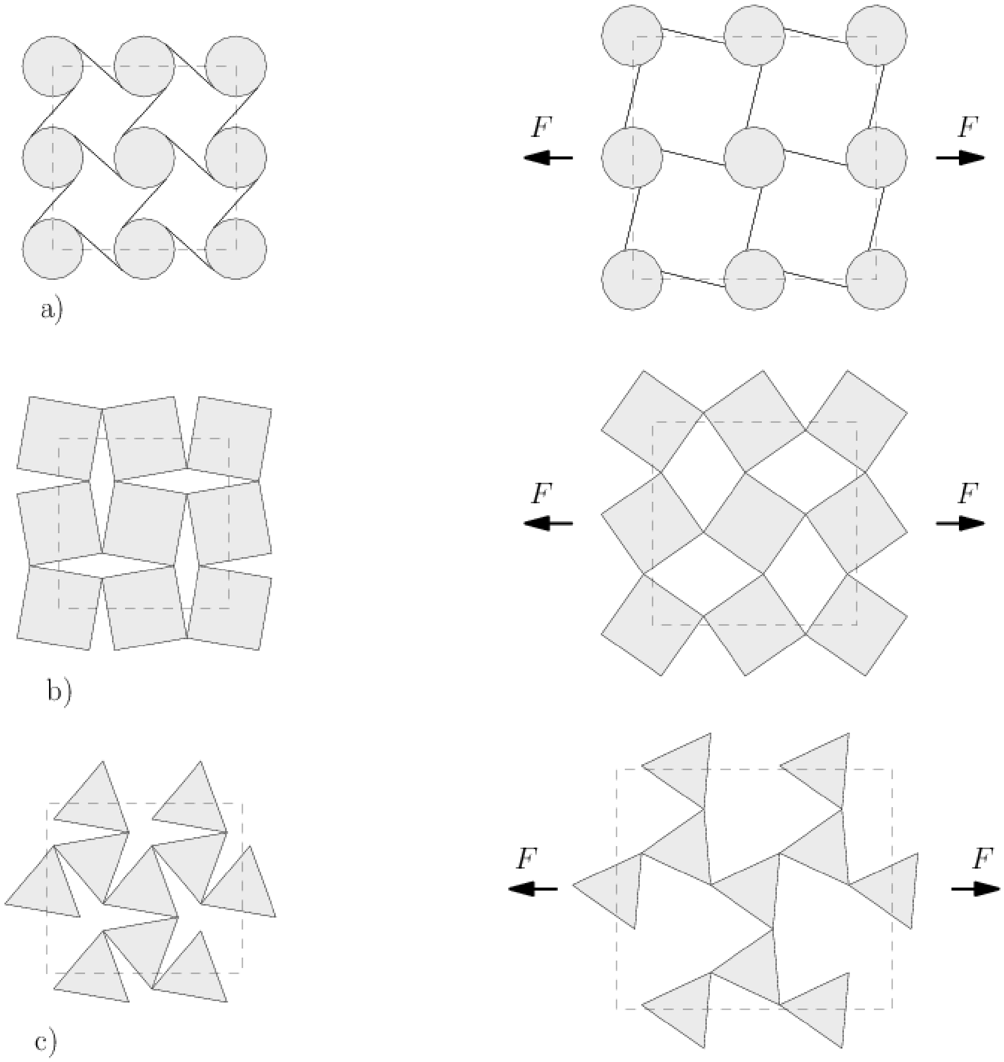

Figure 2.2 – Demonstration of the mechanisms for a selection of auxetic structures. The left hand side of parts a), b), and c) shows the structure in a more compressed form; the right hand side shows an expanded form of the same structure, when a force (*F*) is applied and the mechanical constraints are maintained. The expanded form exhibits elongation in both the longitudinal and transverse directions indicating a negative Poisson's ratio. a) a chiral structure, where rotation of the central unit wraps material around itself; b) corner connected squares which form larger vacant regions when rotated; c) corner connected triangles for which the distance between units depends solely on the angle of rotation.

The elastic properties of the crystal paratellurite, found by examination using resonant ultrasound spectroscopy with a piezoelectric tripod, show a negative Poisson's ratio in the (110) plane.[38] This auxeticity has been explained as being a result of its star shaped arrangement shown in Figure 2.3, where the stars are formed when the atoms are projected onto the (001) plane. For this example, dilation of the stars is the cause of auxetic behaviour, and not rotating units.

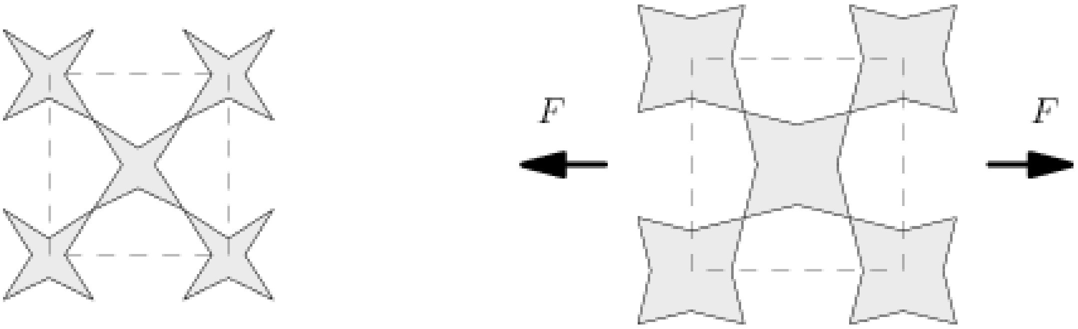

Figure 2.3 – A star arrangement as can be found in the (001) plane of paratellurite. The negative Poisson's ratio is caused by dilation of the stars under an applied force (*F*) and results in expansion in both the lateral and transverse directions.

2.1.5 Relationship between auxetic behaviour and other elastic properties

As discussed in Section 2.1.1, the Poisson's ratio of a material depends entirely on the tensors of elastic stiffness or compliance. As a result, it is closely linked to other elastic properties such as the bulk modulus, shear modulus, or anisotropy. In this section, I describe previous attempts to find an explicit link between auxetic behaviour and other, simpler, properties: at first elastic properties, then density.

For isotropic materials, v can be expressed as a function of two other elastic constants, as follows:

$$\nu(G,K) = \frac{3K-2G}{2(3K+G)} \,. \tag{2.19}$$

Auxetic materials, with a negative value for v, must therefore have a shear modulus greater than 3/2 times that of their bulk modulus.[39] For anisotropic materials the relationship between G, K and v is more complicated, but negative Poisson's ratios in particular directions are still associated with high shear strengths in others.[40]

Highly anisotropic materials have been found to have increased likelihood of experiencing extreme highs and lows for Poisson's ratio.[41] Various measures for the anisotropy of a material have been developed which aim to describe the extent to which elastic properties vary. Two such measures are the Zener[42] anisotropy index (Z), which applies only to cubic symmetries, and the Ledbetter and Migliori[43] ratio (A^*) which is a more general quantity determined by the maximum and minimum velocity of sound waves passing through the material (v_{max} *and* v_{min}). The following equations define Z and A^* respectively:

$$Z = \frac{2(C_{44})}{C_{11} - C_{12}} \tag{2.20}$$

$$A^* = \frac{v_{max}^2}{v_{min}^2}. \tag{2.21}$$

The absolute maximum and minimum Poisson's ratio exhibited by a material are correlated to the A^* measure for anisotropy for both cubic and non-cubic structures. Furthermore, this correlation was found to be independent on the scale of mechanism responsible for the auxetic behaviour.[41]

The density of silica glass has been linked to its Poisson's ratio. Glasses with loosely packed atoms exhibit smaller values for v, whereas those with more tightly packed atoms tend to have higher values for v.[44] This is believed to be due to empty space within the loosely packed structures allowing for longitudinal deformation of the material without causing as much lateral deformation. It should be noted that this phenomenon can only explain different extents of positive Poisson's ratios, and does not result in auxetic properties being linked with low density. When examining auxetic structures of two-dimensional, re-entrant honeycombs, it was found that the density variation between axes (altered by changing thickness of selected ribs in the honeycomb but not others) has an effect on the Poisson's ratio.[45] The study showed that, when the density in a particular axis was altered, the auxetic properties remained constant in some directions, but changed in others.

2.1.6 Classification of auxeticity

As complicated a property as auxeticity is, attempts have been previously made to distinguish between different materials with varying levels. Acknowledging that the term 'auxetic' is often used as a substitution for 'completely auxetic',[46] Brańka outlines three distinct classifications of materials based on the directions of longitudinal (*m* direction) and transverse (*n* direction) strains. These classifications are limited to positive values for all combinations of *m* and *n*, negative for all combinations of *m* and *n*, and negative for some but not all combinations of *m* and *n*.[46] Whilst this auxetic classification is able to distinguish between materials with no auxetic properties, fully auxetic materials, and 'others', it is the 'other' category in which the majority of materials with auxetic properties fall. There are several degrees to which a material can exhibit a negative Poisson's ratio, which existing classification systems fail to distinguish between. A new system of typology is developed and explained in Chapter 3 to enable these distinctions between auxeticity levels.

2.1.7 Experimental determination of auxeticity

Experimental techniques capable of determining the elastic properties of a material fall essentially into two categories, mechanical or acoustic. Mechanical testing, such as a tensile test to obtain Young's modulus, involves placing a sample of a material inside a specifically designed piece of machinery, applying forces to the sample to create stress, and then measuring the strain within the sample. These techniques require a minimum size of sample to be available, which may be difficult to obtain for single crystals, and the tests are often destructive. An alternative method of discovering the elastic properties of a material is through Brillouin scattering. This is an non-destructive technique which uses direct measurements of sound velocities along general directions[47] and can accurately measure the properties of a material with samples greatly smaller than those needed for mechanical testing. Both mechanical and Brillouin scattering methods require a sample of a material to be first obtained and then prepared in order to measure its elastic properties.

2.2 Silica polymorphs

2.2.1 Introduction

Silicon dioxide is one of the most abundant materials on the planet, accounting for over 60% of the earth's continental crust by weight[48] much of which is in the form of α-quartz. As well as being extremely abundant, silica can also exist in a large number of polymorphs. The structure of the majority of crystalline silica polymorphs can be described as three dimensional networks of corner sharing tetrahedra. These tetrahedra are able to rotate and dilate.[31] Within these networks the silicon atoms are at the centre of each tetrahedron and the oxygen atoms at the connection between them. The Si-O-Si bond angle in silica is more flexible than the O-Si-O bond angle.[49] Therefore, mechanisms which include rotating tetrahedra, where the Si-O-Si bonds are allowed more freedom, are likely to represent the deformations that are occurring within all-silica crystals. A change in the bond distance between silicon and oxygen is represented by a dilation of the tetrahedra, and mechanisms which allow for this dilation can model bond length changes. As all the bonds in SiO_2 materials are silicon to oxygen there is no area where we might expect increased or decreased bond extension when compared with the other bonds within a structure.

2.2.2 "Dense" polymorphs

2.2.2.1 Quartz

The most commonly occurring polymorph of silica is quartz, which exists as a low temperature trigonal phase (α) and a high temperature hexagonal phase (β).[50, 51] The structure of quartz follows that of the majority of silica described earlier, with corner sharing tetrahedra formed of a central silicon atom bonded to four oxygen atoms. Due to its piezoelectric properties[52] quartz is used extensively in electronics as a clock timing source. As α-quartz occurs naturally in atmospheric conditions and can be grown as large crystals (above 0.1 kg)[53] its elastic properties can be obtained mechanically or through Brillouin scattering.[54] These elastic properties show that the α-quartz exhibits negative Poisson's ratios for only a small number of axes, with a minimum value of −0.1.

2.2.2.2 Cristobalite

The silicon dioxide polymorph cristobalite has two crystalline phases. A low temperature (α) form and a high temperature (β) form.[55] Brillouin spectroscopy on a single crystal of α-cristobalite showed it to be highly anisotropic and yet still have an aggregate isotropic Poisson's ratio of −0.133, −0.191, and −0.163 for the Reuss, Voigt, and Hill averages respectively.[20] The spectroscopy showed that the crystal had a shear modulus of roughly 2.4 times that of the bulk modulus. Due to the instability of β-cristobalite its elastic properties can only be derived through the use of computational modelling. A molecular dynamics study showed that the high temperature phase of cristobalite remains averagely auxetic.[56] This study also showed a change in direction for the maximum negative Poisson's ratio: with $v_{23} = -0.59$ being obtained by rotating S_{ij} 42° from the *b* axis about the *a* axis in α-cristobalite at 300K, and $v_{12} = -0.28$ being obtained by rotating S_{ij} 45° from the a axis about the c axis in β-cristobalite at 1800 K.

2.2.3 Low density SiO_2 polymorphs – zeolites

2.2.4 Auxetic aluminosilicates

The elastic properties of several zeolite structures have been simulated using molecular mechanics techniques with various force fields, including NAT (natrolite – $Al_{16}Si_{24}O_{80}$), THO (thomsonite $Al_{20}Si_{20}O_{80}$), APD ($Al_{16}Si_{16}O_{64}$), and JBW ($Al_{12}Si_{12}O_{48}$).[57] It was predicted that THO and NAT would exhibit auxetic behaviour in the (001) plane (though 45° out of phase due to their alignment) and that APD and JBW would show auxetic behaviour in the (010) plane. The Poisson's ratio predicted in these materials can be explained using the rotating squares mechanism for all but JBW, which follows a rotating triangles mechanism. Brillouin spectroscopy produced experimental data on NAT which contradicted the atomistic study,[47] however further work explained how the experimental values did show auxeticity in certain directions, supporting the original prediction of auxeticity in natrolite.[58] An analytical model was produced which further supported the presence of auxetic behaviour in natrolite.[59]

2.2.5 Simulation of silicates

The many potential uses for silicates, both with and without what we might think of as unusual properties, have prompted much interest in the subject area. A large proportion of this interest has been in theoretical materials which have not yet been synthesised. This is due to the number of possible polymorphs available and the impracticalities in manufacturing samples of each to discover their properties.

Force field potentials for silica have been developed and used to predict the elastic constants of materials,[60, 61] model their phase transforms,[62] and explore their reactions with organics.[63] Zeolite silica have great potential as molecular sieves. The performance of these sieves depends on the way molecules are able, or not able, to migrate through the structure. By using molecular dynamic techniques it is possible to predict how this mass transfer will occur without synthesis of the zeolite in question.[21] The most comprehensive, but also computationally expensive, way of predicting the properties of silica (or any material) is through quantum mechanical techniques such as density functional theory (DFT). As with other modelling methods, the properties of theoretical materials can be predicted without the need for synthesis. DFT simulations have been used to predict the structure, elastic properties, and reactivity of silica as well as more exotic properties such as negative linear compressibility.[64, 65]

2.3 Atomistic modelling techniques

2.3.1 Background

The experimental methods used to measure elastic properties are discussed in section 2.1.7. For practical reasons, chiefly that sizeable monocrystalline samples must be available, but also because so many possible materials exist, it is impossible to experimentally determine the elastic properties of them all. Atomistic modelling techniques offer attractive alternatives, even if one has to be mindful of their limitations. Measuring the properties of future, hypothetical, materials, is not possible experimentally. It is therefore desirable to be able to calculate, computationally or otherwise, the expected elastic properties of a material prior to obtaining a physical sample.

In the early part of the 20th Century, especially with the advent of quantum theory, our understanding of the interactions within materials developed considerably. However, with such complex systems analytical solutions are sometimes impossible and numerical approaches require a great deal of work for all but the simplest of cases. When computers, which had been developed during and after the Second World War, became available in peace time, the possibility of predicting the properties of a material using numerical techniques became more and more feasible.[66] As computational power has increased, we are now able to simulate bigger structures, with more accurate ways of describing the chemistry inside a material.

2.3.2 Force field optimisation

A number of computational methods can be used to obtain the mechanical properties of a material. Of these, density functional theory (DFT) is the most fundamental that can practically be used to access elastic properties and can be used to solve the Schrödinger equation of the electronic structure.[67] However, DFT techniques are still computationally expensive and in many cases a good approximation of the atomistic energy can produce comparable results at a greatly reduced cost. To simplify the problem it can be assumed that the effect of the electrons in a material can be combined into effective atoms, and that the energy *U* can then be described as an expansion in terms of interactions between these atoms[68]

$$U = \sum_{i=1}^{N} U_i + \frac{1}{2}\sum_{i=1}^{N}\sum_{j=1}^{N} U_{ij} + \frac{1}{6}\sum_{i=1}^{N}\sum_{j=1}^{N}\sum_{k=1}^{N} U_{ijk} + \dots , \tag{2.22}$$

where *N* is the total number of atoms, the first term represents the self energies of the atoms, and each term thereafter the multiple body interactions. As *N* is finite, the energy is exact if calculated to a high enough order, though this comes at a high computational cost. Given that the higher order terms tend to decrease (as they are multiplied by increasingly small fractions), we can again simplify our system by ignoring these contributions and compensating to a degree with parameterisation of the lower order terms used. The Hartree-Fock method[69] is a commonly used quantum mechanical first approximation which only includes up to four-body terms, justifying our decision to limit the number of terms used. Furthermore, it is also possible to ignore interactions between atoms which are further apart than a desired cut off distance. This can be done because, although there is no upper limit on the equations governing the force between atoms, the strength of these interactions approaches zero as distance increases.

2.3.3 Potential models

A potential model is a way of describing a system as a number of functions for the internal energy associated with each interaction. By minimising the total energy of all interactions, an optimised configuration (which may be only locally optimised) can be determined, and from this properties can be calculated. Energy functions vary in form and can represent a multitude of forces within a molecular structure. The internal energy of a solid is a many body quantity which depends on all electrons and nuclei.[68] Due to this, approximations are made to simplify the energy equations, often limiting them to a finite number of terms of a converging sequence. The choice of parameters for a potential model is a subtle one, usually chosen to approximately match experimental results. However, even with advances in both the hardware and software used, potential models still need to minimise computational cost to lower the time taken to achieve optimisation. As previously mentioned, by solving the Schrödinger equation a system can be accurately modelled. However, whereas *ab initio* calculations are expensive in terms of computer time, empirical methods can be used to calculate large molecules and real lattices.[70]

2.3.4 Coulomb interactions

It is well known that two oppositely charged objects will be attracted to one another. Coulomb's law describes the energy of the interaction between these two objects in terms of their charge and the distance between them. It is the dominant term within ionic materials, representing up to 90% of the total energy.[68] Coulomb's law is given by Equation (2.23), where q_i is the charge on atom *i*, r_{ij} is the distance between atoms *i* and *j*, and ε_0 is the permittivity of free space

$$U_{ij}^{\text{Coulomb}} = \frac{q_i q_j}{4\pi\varepsilon_0 r_{ij}} \, . \qquad (2.23)$$

Despite the simplicity in calculating a single (two body) interaction, with large systems the number of calculations which need to be undertaken quickly increases. This is because although the energy decreases inversely proportional to the distance between atom *i* and atom *j*, the number of interactions which need to be considered increases proportionally to the square of the distance away from the initial atom. To increase the efficiency of this model it is often necessary to use the method of Ewald,[71, 72] leading to a convergent series with a well-defined limit.[68]

2.3.5 Short-range two-body interactions

When two bodies are close together they experience strong repulsive forces which arise from electron repulsion. In combination with the Coulomb interactions these repulsive forces describe the strong intramolecular bonds between atoms in a covalent structure. There are a number of ways of approximating these forces in terms of the potential energy of the bond relative to the distance between the two atoms. Common potential models used are the Buckingham potential, where an exponential repulsive term is included; the Lennard-Jones potential, where an inverse repulsive term is used; and the Morse potential, where the interactions are coulomb subtracted.[68] A four range Buckingham potential can be defined where the potential has different components depending on the distance between atoms. This has a purely repulsive term when r_{ij} is below a lower bound and a purely attractive term when r_{ij} is between and upper bound and a cut-off distance. The function is splined to have continuous first and second derivatives.[73] The following equations give the form of the Buckingham, Lennard-Jones, Morse, and four range Buckingham potentials respectively. All terms other than r_{ij} (sometimes referred to as just r) are parameters of the potential models

$$U_{ij}^{\text{Buckingham}} = Ae^{\left(\frac{-r_{ij}}{\rho}\right)} - \frac{C_6}{r_{ij}^6} \tag{2.24}$$

$$U_{ij}^{\text{Lennard-Jones}} = \frac{A}{{r_{ij}}^m} - \frac{B}{{r_{ij}}^n} \tag{2.25}$$

$$U_{ij}^{\text{Morse}} = D_e\left[\left(1 - e^{\left(-a\left(r_{\text{ij}}-r_0\right)\right)}\right)^2 - 1\right] \tag{2.26}$$

$$U_{ij}^{\text{Buckingham-Four}} = \begin{cases} Ae^{\left(\frac{-r}{\rho}\right)} & : \ r < r_1 \\ a_0 + a_1 r + a_2 r^2 + \\ a_3 r^3 + a_4 r^4 + a_5 r^5 & : \ r_1 < r < r_2 \\ b_0 + b_1 r + b_2 r^2 + b_3 r^3 & : \ r_2 < r < r_3 \\ -\dfrac{C}{r^6} & : \ r_3 < r < r_c \end{cases} . \tag{2.27}$$

2.3.6 Short-range three-body interactions

Often, two-body interactions are not enough to describe what is happening within a system. Especially in large frameworks, the bond angles, or three-body interactions, play a significant part. The most common potential describing three-body interactions is harmonic, with an ideal bond angle (θ_0), and a positive energy associated with any deviation from this angle. The Urey-Bradley potential has a positive energy associated with deviations from an ideal bond distance (*r_{23}*), where this distance is between the atoms at either end of the bond. The Vessal potential model combines the effect of bond angles and the distances from the central atom to the other two. Equations (2.16), (2.17), and (2.18) give the form of the harmonic three, Urey-Bradley, and Vessal potentials respectively. All terms, other than the bond angle (*θ*), and the interatomic distances (*r*) are parameters of the potential models

$$U_{ijk}^{\mathrm{Harmonic}} = \frac{1}{2}k_2(\theta - \theta_0)^2 \tag{2.28}$$

$$U_{ijk}^{\mathrm{Urey-Bradley}} = \frac{1}{2}k_2\left(r_{jk} - r_{jk}^0\right) \tag{2.29}$$

$$U_{ijk}^{\mathrm{Vessal}} = \frac{k_2((\theta_0 - \pi)^2 - (\theta - \pi)^2)^2}{8(\theta_0 - \pi)^2} \times e^{\left(-\frac{r_{ij}}{\rho_{ij}}\right)} \times e^{\left(-\frac{r_{ik}}{\rho_{ik}}\right)}. \tag{2.30}$$

2.3.7 Electron Shells

Depending on the potential models being used it is often preferable to represent atoms using the shell model.[74] For this model, ions are represented by a pair of point charges with a positive core and a negative massless shell connected by a harmonic spring. Subsequently, all short-range interactions act on the shell part of the atom rather than the nucleus.[75] The spring potential has the following form, where *k* is a constant, and *r* is the distance between the centre of the atom core and the electron shell

$$\mathrm{U}_{ij}^{\mathrm{Spring}} = \frac{1}{2}k_2r^2. \tag{2.31}$$

2.3.8 Fitting potential models

Once a potential model is decided upon the parameters must be chosen to fully define the energy equations. Usually a material is chosen for which the distances and angles between bonds is well known. Then, the chosen parameters used are fitted to this known material in order to produce a force field model able to accurately predict materials with similar chemistry.[61] A great deal of importance is placed on the ability of a potential model to simulate a wide range of materials, as well as the accuracy associated with each one. This combination of robustness and reliability is the ideal for any potential model used in predictive work.[63]

For this work, force fields are required for calculation of the elastic properties of both high density and low density silicon dioxide polymorphs. A total of fourteen potential libraries are taken from the work of various authors and are examined in detail later in this thesis.[61, 64, 76–87] They each combine a variety of different models, including the Buckingham, Morse, and four-range Buckingham models for two-body interactions and the harmonic, Urey-Bradley, and Vessal models for three-body interactions. Seven of the fourteen potential libraries represent oxygen as a core-shell atom, with the silicon interacting with the oxygen electron shells, and the oxygen cores harmonically linked to the oxygen shells. The other seven libraries do not use oxygen shells, instead directly modelling the interactions between silicon and oxygen cores (rigid ions model).

In addition to the silicon dioxide potentials, three libraries for germanium dioxide potentials were also taken from literature.[82, 88, 89] These follow the same format as the SiO_2 potentials and are composed of atomic charges and Buckingham two-body potentials. Only one of the libraries uses a shell model for oxygen atoms, with the other two treating both germanium and oxygen atoms as rigid ions.

Chapter 3: Typology of auxetics

3.1 Existing methods of describing auxetic materials

It has been known for over 100 years that it is possible for a material to exhibit a negative Poisson's ratio (v). Despite this, the way in which this is described is still often limited to a simple binary criterion (does or does not exhibit auxetic behaviour). Details may be given on the valule of the minimum and maximum v, or the longitudinal or transverse directions for which these maxima are observed, but rarely is the extent of a materials overall auxeticity or in what way it displays auxetic behaviour described. Poisson's ratio is defined as the following ratio between strains

$$\boldsymbol{\nu} = -\frac{\boldsymbol{\varepsilon_T}}{\boldsymbol{\varepsilon_L}}\ , \tag{3.1}$$

where ε_T is the transverse strain and ε_L is the longitudinal strain. As a dimensionless constant describing the strains in all perpendicular directions as a result of loading strains in all longitudinal directions, the Poisson's ratio is a four dimensional tensor and cannot easily be represented graphically. Comparisons between two materials traditionally rely overly heavily on extreme data or various bulk averaging techniques. The values of minima might misrepresent a crystal's Poisson's ratio as a whole, whereas bulk averaging can cause subtleties in the directions distribution to be overlooked.

A crystal which exhibits, due to its particular anisotropy, a negative Poisson's ratio in a very narrow range of directions when deformed along a very particular set of axes (Figure 3.1 shows how the Poisson's ratio for one such material may look) is clearly 'less' auxetic than a completely isotropic foam which exhibits a negative

Poisson's ratio in every possible direction. However, currently there exists no clear way of quantifying the difference between these two extreme cases, or more similar cases where a distinction may be even harder to determine. By assigning the 'auxetic' tag to both materials the foam’s highly auxetic behaviour is not assigned enough weight over the crystals relatively common one, and conversely by using bulk averages the crystals unusual properties, which may have applications if alignment is possible, will be washed out in the noise of the many 'normal' direction properties.

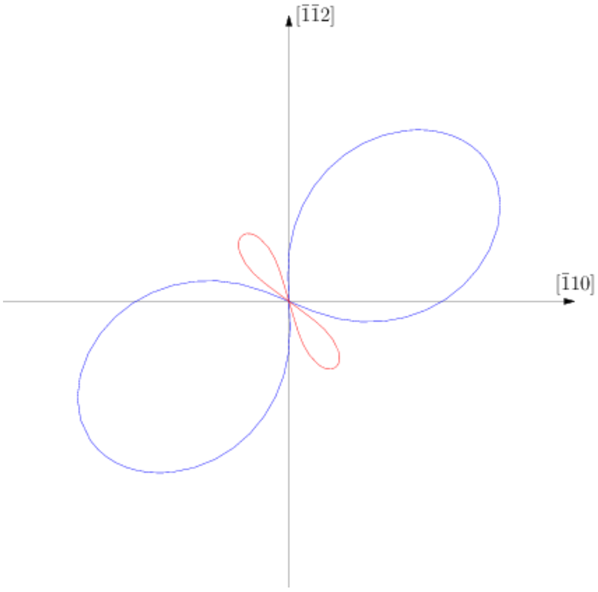

Figure 3.1- The Poisson's ratio in the (111) plane of an auxetic crystal (all silica ATV simulated with the SLC potential model). This example shows a radial plot of Poisson’s ratio in a plane, where the value observed in the transverse directions are represented by the distance away from the origin. The blue line indicates positive Poisson’s ratio values and the red line indicates negative values. In this example, although a negative Poisson’s ratio is present, it is only found in a small percentage of transverse directions and has a lower average magnitude than the average of positive ratios.

In this chapter a typology of auxetic behaviour is proposed which distinguishes between the many different ways a material can display auxeticity. By using this typology system we can identify, describe and compare materials with auxetic behaviour in the following way:

- Identification.

  To aid in identification of auxetic materials the typology system can be seen as a series of increasingly auxetic criteria, which must be satisfied by a material in order for it to be classified in a particular way. By separating different extents of auxeticity, materials which meet higher level classifications can be distinguished from those which do not at every degree, and therefore a large list of potentially interesting materials can be subdivided into as many smaller groups as there are distinct classifications used. These distinctions allow for materials to stand out from others even within sets of materials which are known to exhibit auxetic behaviour.

- Description.

  To avoid long, potentially confusing descriptions of a material’s auxetic characteristics the typology system can be used to quickly sum up the extent to which the Poisson's ratio is negative. There are a total of twelve binary indicators which fully describe the auxeticity in terms of this typology, with a thirteenth (no auxeticity at all) being the inverse of the very lowest level of auxetic behaviour. However due to the inference of lower levels from higher levels, the number of indicators to describe auxeticity can be reduced to 4. To accompany classifications with appropriate values of Poisson's ratio, twelve numbers are still needed, as although a value might be inferred to be negative, the extent to which it is would not be known.

- Comparison.

  If the typology of two or more materials is known, the classifications which they satisfy can easily be compared to one another to analyse which material exhibits a greater or lesser degree of auxeticity. In the case of materials with identical typology classifications the associated values could be examined more closely if needed. This is an improvement of the current system of comparing only the average, or extreme values of Poisson's ratio and instead allows a comparison at all levels of auxeticity.

In the context of this typology system I use the term 'direction' to refer to the transverse direction for which Poisson's ratio is observed and 'axis of deformation' or simply ‘axis’ to refer to the longitudinal axis of loading. Figure 3.2 shows a non-auxetic material under a tensile load in the *x*-axis. If discussing v_{xy} in this situation, the 'transverse direction' is the *y*-axis (perpendicular to the load) and the 'axis of deformation' is the *x*-axis (parallel to the load).

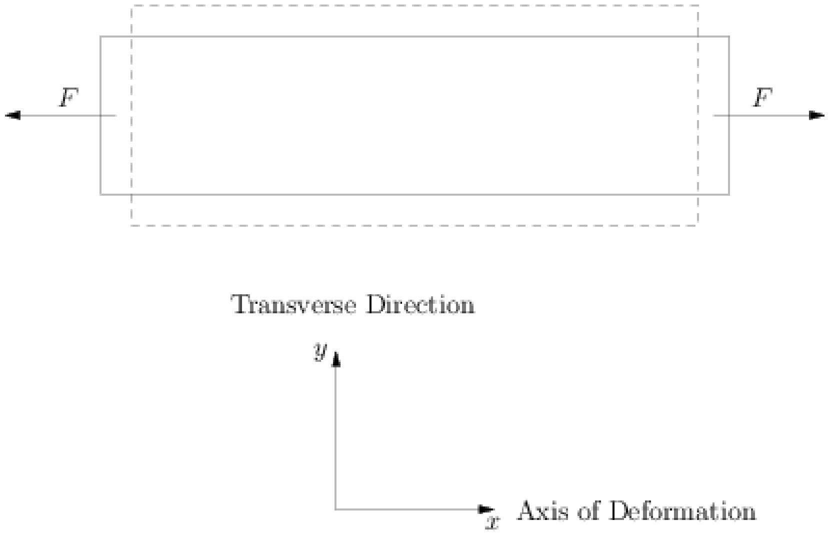

Figure 3.2 – A non-auxetic material under tensile load *F* in the *x*-axis. Demonstrating the terminology used to discuss Poisson's ratios between different axes. The dotted outline shows the shape of the pre-loaded structure, the solid line shows the outline of the structure after the load has been applied.

3.2 Description of auxetic typology

The typology system includes thirteen distinct classifications split into three 'classes' (A, B, and C) each with four 'types' (1, 2i, 2ii, and 3), plus the additional classification of a material without auxetic behaviour. Each axis of deformation has its own class of auxetic behaviour, and the extent of which this class is present throughout the material determines its type. To satisfy a particular class, the Poisson's ratios observed in the transverse directions around an axis must meet specific criteria.

- Class A is the most trivial case and is satisfied if any direction around any axis exhibits a negative Poisson's ratio. This corresponds to a single value, the minimum Poisson's ratio of all directions around an axis, being less than zero.
- Class B is satisfied if the average of all Poisson's ratios around any axis is negative. Although some transverse directions may have a positive Poisson's ratio and others a negative one, by using the average of all directions (again a single numerical value), a particular axis can be quantified as being 'averagely' auxetic. The number of directions in which auxetic behaviour is displayed contributes to the B classification, and the magnitude of the Poisson's ratios in these directions also affects the decision. This is advantageous to describe how a material is likely to behave in a polycrystalline environment, where single crystal directions are unlikely to be aligned.
- Class C is satisfied if every transverse direction around an axis has a negative Poisson's ratio. The magnitudes of the ratios are likely to fluctuate in non isotropic materials, but crucially none can have a positive value. Similarly to the classification for classes A and B, a single value can be used to determine the

satisfaction of class C. In this case it is the maximum Poisson's ratio around an axis which must be negative, as opposed to the minimum or mean value to satisfy A and B respectively.

To classify a material’s Poisson's ratio entirely we must also consider every axis of deformation. The prevalence of axes exhibiting a class is used to determine the type of that class, with increasing values for type corresponding to more axes being of a particular class.

- Type 1 classifications are satisfied if there are any axes which are of a particular class. They represent the minimum level at which a material could be said to have auxetic properties of that class and can only distinguish between materials with axes exhibiting classes and those without. A single numerical value may be used to determine satisfaction of type 1 classifications during calculation of the Poisson's ratios. This value is the minimum of each of the three values used when determining an axes' class. For example, if we determine class A by the minimum Poisson's ratio in all transverse directions around an axis, the minimum of the minimums for all axes can be used to determine if a material is '1A' (satisfied if this minimum of minimums is negative). '1B' and '1C' classifications are determined by the minimum of averages and the minimum of maximums respectively, again satisfied if these values are negative.
- The classification of type 2 is split into two types: 2i and 2ii. Both types are satisfied if the average of axes can be said to be of a particular class; the distinction occurs in the averaging method used to determine this. Type 2i uses a median average of the class of every axis, if more than half the axes exhibit a class then type 2i is satisfied. Type 2ii uses the mean of the value used for

determining a class in each axis. It follows that if the average of minimums, average of averages, or average of maximums is negative; '2iiA', '2iiB', and '2iiC' are satisfied respectively. Classifications of 2ii are perhaps more useful than those of 2i in determining the behaviour of a polycrystalline material, as the Poisson's ratio magnitude is incorporated. Additionally, the use of a relevant value calculated from the combined class definition values to determine the type fits more naturally with the other type classifications. However, for the purpose of a comparison between materials, or a description of a material, the subtlety different method of measuring the average class for type 2i, is worthy of inclusion in this typology system.

- Type 3 classifications require every axis to be of a particular class in order to be satisfied. While this classification is extremely hard to satisfy, a material which fits type 3 can be said to exhibit the particular auxetic behaviour no matter which direction of loading is chosen. By taking the maximum of the associated values for the class definitions type 3 satisfactions can be determined. Once again this maximum of minimums, averages, or maximums must be below zero for 3A, 3B, or 3C to be present respectively

Table 3.1 - Description of typology system with the associated values to determine satisfaction of each classification

Type	Class	Description of Poisson's ratio for materials of this classification	Criteria to determine classification
0	N/A	Positive for all directions around all axes of deformation	Minimum of minimums
1	A	Negative for at least one direction around at least one axis of deformation	Minimum of minimums
	B	Negative when averaged over all directions around at least one axis of deformation	Minimum of averages
	C	Negative for all directions around at least one axis of deformation	Minimum of maximums
2i	A	Negative for at least one direction around more than half of axes of deformation	Percentage of class A
	B	Negative when averaged over all directions around more than half of axes of deformation	Percentage of class B
	C	Negative for all directions around more than half of axes of deformation	Percentage of class C
2ii	A	Negative for at least one direction around a mean average of axes of deformation	Average of minimums
	B	Negative when averaged over all directions around a mean average of axes of deformation	Average of averages
	C	Negative for all directions around a mean average of axes of deformation	Average of maximums
3	A	Negative for at least one direction around all axes of deformation	Maximum of minimums
	B	Negative when averaged over all directions around all axes of deformation	Maximum of averages
	C	Negative for all directions around all axes of deformation	Maximum of maximums

Table 3.1 summarises the typology system, with the associated values used to determine satisfaction of each classification. With the exception of the values for 2i, which satisfy the classifications if they are greater than half, each value corresponds to a classification being satisfied when this value becomes negative.

The classifications of a particular class or type are not exclusive as each class can have many types, and each type can be satisfied by many classes. Lower classes and types are implied by higher ones provided the respective type and class do not change. That is to say, a '3B' classification implies those with a lower type ('1B', '2iB', and '2iiB'), and also those with a lower class ('3A'). In this example '2iiC' is not implied as although the type is lower the class has been raised (depending on the material '2iiC' may be satisfied in its own right). This inheritance comes as the result of the cumulative nature of these classifications. If the maximum Poisson's ratio around an axis is negative, then the average, and also the minimum Poisson's ratio must be negative too. Similarly, if the maximum of all class determining values is negative, the average and minimum will also be negative. Of particular interest are crystals which can be said to be '2iiB' auxetic. These crystals have a negative value for the average for each axis of the average Poisson's ratio for each transverse direction. Therefore, if present in a polycrystalline material, and orientated in a truly random way, they should exhibit isotropic auxetic behaviour. Further to this it is suggested, that any material which satisfies '2iiB' can be used to create a structure which is '3C' and any material which does not satisfy '2iiB' cannot.

3.3 Modification of ElAM for calculation of typology

The ElAM (Elastic Anisotropy Measures) software uses the elastic constants in the principal axes to calculate the off axis elastic properties, by implementing the standard tensor rotation formulae:[90] among these is the Poisson's ratio. Currently a user can request a two or three dimensional display of the maximum or minimum Poisson's ratio for each axis of loading; a direct, Reuss, Voigt, or Hill measure of average Poisson's ratio; and the value, longitudinal axis, and transverse axis of the minimum and maximum Poisson's ratio in the crystal. Aside from the graphical outputs these values relate to the minimum of the minimums, the average of the averages, and the maximum of the maximums of Poisson's ratios in all axes. These values alone could be used to distinguish between '3C', '2iiB', '1A', and no auxetic behaviour, but do not allow for any further distinction. It is therefore necessary to modify the ElAM source code to create this additional data for classification purposes. During Poisson's ratio calculations ElAM examines the transverse direction at every degree (180 values due to symmetry) for a particular longitudinal direction and the maximum, minimum, and average for this direction is calculated. By sampling the unit sphere with user defined theta and phi increments many longitudinal directions are then used to calculate the maximum of all maximums, minimum of all minimums, and average of all averages. Using the data already given for each longitudinal direction, and keeping track of the minimum, maximum and average of each, the remaining measures relating to auxetic classification can be obtained. This calculation of the typology of a material can only ever be an approximation due to the continuous nature of Poisson's ratio and the discrete way in which sampling is implemented. More accurate typologies can be produced with higher sampling rates but at the cost of increased computational expense. However, it is expected that, with the possible exception of those materials close to the threshold of a classification, a coarse search may be sufficient to determine the typology of most materials.

3.4 Typology system applied to common materials

To demonstrate the potential use of our typology system a large number of materials are classified according to the criteria set out in the previous section. With a large and sufficiently varied array of materials used the typology data obtained are expected to be a reliable representation of all materials. By including materials from many different groups, a single group of materials with unusual properties should not skew the results to suggest an auxetic typology of greater or lesser extent than actually occurs. With these data, showing 'normal' auxetic typology, a benchmark can be created and used as a comparison against any specific group of materials chosen to be researched. If particular typologies are more or less prominent in a study than in materials as a whole it is reasonable to suggest the studied materials have different auxetic behaviour than what might be expected.

The stiffness matrices from 471 materials, used by Lethbridge *et al*. to study the correlation between anisotropy and auxeticity in materials,[41] were collated into an ElAM database file and run through the modified program to output typology (the full input file and subsequent typology data for each of the 471 materials can be found in the supplementary data for this work). The percentage, and the number of the 471 materials that satisfied each classification can be seen in Table 3.2. The traditional measure of what is, or is not an auxetic material is represented by this system’s '1A' classification. As can be seen in Table 3.2, 37.2% of the materials studied satisfied the '1A' classification. This supports the work suggesting that a relatively high percentage of materials exhibit at least some level of auxetic behaviour.[18] However, the percentage of materials which satisfy greater levels of auxeticity decrease rapidly, with only 3.2%, 6.6%, and 7.9% considered to be '1B', '2iA', and '2iiA' respectively. The silicon dioxide polymorph α-cristobalite is the only material studied which satisfies the '2iB', '2iC', '2iiB', and '2iiC' classifications, highlighting its unusual properties. The associated values for percentage of class B, percentage of class C, average of averages, and average of maximums shown by α-cristobalite are 99%, 53%, −0.1401, and –0.0022 respectively. There are three materials which belong to the '3A' category: α-cristobalite again, and two forms of beryllium copper alloy. These have the related auxetic value (maximum of minimums) of −0.0626, −0.0026 and 0.0 with the most auxetic of these relating to α-cristobalite. There are no materials in this study which meet the criteria to satisfy the '3B' or '3C' classifications. Whilst these typologies are possible, and can be found in isotropic foams with a negative Poisson's ratio, due to the requirement that every longitudinal direction must be of a class for satisfaction, they are not expected in anisotropic single crystals such as those in this study.

Table 3.2 – The prevalence of auxetic typologies in the sample of 471 typical materials used by Lethbridge *et al.*[41]

Type	Class	Number	Percentage of total
0	N/A	296	62.8
1	A	175	37.2
	B	15	3.2
	C	11	2.3
2i	A	31	6.6
	B	1	0.2
	C	1	0.2

2ii	A	37	7.9
	B	1	0.2
	C	1	0.2
3	A	3	0.6
	B	0	0.0
	C	0	0.0

3.5 The typology of experimental α-cristobalite

As shown in section 3.4, α-cristobalite can be considered to be highly auxetic, and is unusual even among those materials which exhibit a negative Poisson's ratio. It is the only material of the 471 used in the study to satisfy '2iB', '2iC', '2iiB', or '2iiC' and the value used to determine '3A' is more negative than other materials which satisfy the same criteria. The full classification of α-cristobalite can be seen in Table 3.3, where negative values for types 1, 2ii, and 3, and a value greater than 50% for type 2i, indicate satisfaction of the associated classification. The material is shown both to exhibit a highly negative Poisson's ratio (up to −0.51), and also experience negative Poisson's ratios in a large number of directions (A in 100%, B in 99%, and C in 53%).

Table 3.3 – Typology of experimental α-cristobalite, the associated values of each typology classification and their value present in single crystal α-cristobalite

Type	Class	Associated Value	Value in α-
1	A	Minimum of	−0.5073
	B	Minimum of	−0.2603
	C	Minimum of	−0.0696
2i	A	Percentage of	100%
	B	Percentage of	99%
	C	Percentage of	53%
2ii	A	Average of	−0.2781
	B	Average of average	−0.1401
	C	Average of	−0.0022
3	A	Maximum of	−0.0696
	B	Maximum of	0.0009
	C	Maximum of	0.0956

Given the unusual nature of α-cristobalite and its highly auxetic properties, studying similar materials with similar chemical structure and their elastic behaviour would appear justified. These include simple dense polymorphs of silicon dioxide such as quartz, but also the more complex and open structures of all-silica zeolites. For these, the central atom of each tetrahedron within the structure (known as a T-site), is occupied by a silicon atom. In the next chapter the elastic matrices of many of these polymorphs are calculated and used to obtain typology data for materials which bear a better comparison to α-cristobalite.

Chapter 4: Properties of siliceous zeolites

4.1 Chapter Overview

This chapter aims to characterise the Poisson's ratio of all-silica zeolites and identify exceptional structures. The motivation to study NPR silicates arises from the attention zeolites have received for many years due to their very low density and potential use as molecular sieves.[25] These early studies have been far from systematic and in light of recent results it is timely to compare the auxeticity of silicas (zeolites in particular) with that of crystals in general. Additionally, the SiO_2 mineral cristobalite has been recognised to have exceptional properties among crystals, and it is hoped that by understanding the way in which its polymorphs behave a better understanding might be gained of its auxetic properties. By replacing every T-site in a number of zeolite frameworks with silicon a large variety of all-silica theoretical structures can be created. Potential models for silicon and oxygen are validated and then used to calculate the stiffness matrices of these structures allowing us to explore their elastic properties.

4.2 Input parameters for modelling SiO_2 structures

4.2.1 SiO_2 potentials

Atomistic potentials used to model materials are primarily obtained through either *ab initio* techniques, where intermolecular forces are derived from quantum mechanical calculations, or through experimental results, which are used as known properties with which to fit parameters of pre-defined functions. Difficulty in finding a consistent model for SiO_2, which is able to match predicted properties closely with real ones, arises as the bonding within SiO_2 polymorphs is neither completely ionic, nor completely covalent. Therefore, empirical models incorporating both features must be used.[91] In addition to this, SiO_2 exists as both high density (quartz, cristobalite), and low density (zeolites) polymorphs, meaning a potential model which has been fitted to a dense form may not be as well suited to a more expanded framework. However, it has been shown that potentials derived for α-quartz,[76] when coupled with earlier potentials derived for Al_2O_3, are able to yield excellent energy-minimized structural models for a wide range of zeolites.[91]

A recent review on the modelling of silica zeolites, by Combariza *et al*.,[92] collates a wide range of potential models developed by various other authors. With the addition of a force field model developed by Sastre and Gale in 2003,[82] this work utilises these libraries for calculations of the elastic properties of all-silica zeolites. For clarity the naming convention used by Combariza will be maintained throughout this work, with the name of the potential and source publication given below in Table 4.1.

Table 4.1 - The potential libraries used for the calculation of the elastic properties of all-silica zeolites

Library Name	Reference
Shell Model	
Gale	Gale[78]
PMM08	Pedone *et al.*[80]
Sastre	Sastre and Gale[82]
SC1	Sastre and Corma[79]
SLC	Sanders *et al.*[76]
SS96	Schröeder and Sauer[77]
SS97	Sierka and Sauer[64]
Rigid Ion	
AHCM	Auerbach *et al.*[85]
BKS	Van Beest *et al.*[61]
JA	Jaramillo and Auerbach[84]
JC	Jackson and Catlow[83]
PMM06	Pendone *et al.*[81]
TTAM	Tsuneyuki *et al.*[87]
Vessal	Vessal[86]

The atomic charges, parameters for two-body interactions, and parameters for three-body interactions used in these potential models are given in Appendix A. Wherever possible the values for cut-off distances were taken from the literature. For those where no cut-off was given, a value of 12.0 Å was used with two-body potentials, and 2.9 Å for three-body potentials.

4.2.2 All-silica zeolite crystallography

In order to model SiO_2 structures, crystallographic information files listing the atomic arrangement and unit cell parameters for zeolite frameworks are taken from the 'Database of Zeolite Structures',[93] which is maintained by the International Zeolite Association (IZA) and has crystallographic data for 218 unique zeolite frameworks (as of August 2014). The lengths of the unit cell (*a, b,* and *c*), internal angles of the unit cell (*α, β,* and *γ*), space group, and fractional coordinates of atoms are listed for each framework. Also included in these crystallographic files are the direct symmetry operations which can be used to map the primitive atoms to symmetrically equivalent ones within the periodically repeating unit cell. When simulating frameworks all atom locations can be obtained with these direct symmetry operations or, if the modelling software is able, the space group given can be used to automatically infer the crystal symmetry. The zeolite structures used list 'O' sites (for oxygen atoms) and 'T' sites (for the centre of the tetrahedra formed by a central atom surrounded by four evenly spaced oxygen atoms). Each framework is modelled as all-silica with every 'T' site being populated by a silicon atom.

4.3 Methodology for the calculation of the elastic properties of SiO_2 zeolites

The elastic constants of all-silica zeolites were calculated using energy minimization techniques with the potential models previously discussed in this chapter. The framework information, combined with a species library and potential library, is used to create an input file for the simulation software GULP (General Utility and Lattice Parameter).[68] GULP is an atomistic modelling program with the ability to calculate stiffness matrices from initial lattice parameters and a force field model. Using the inter-atomic two-body and three-body potential models the structures are optimised with respect to total lattice energy under a constant pressure. Several iterations of the Broyden-Fletcher-Goldfarb-Shanno[94] algorithm are implemented until the lattice energy stabilises and a minimum has been found. Once this optimisation has been achieved, the final lattice parameters and elastic constants are collated into a database. ElAM is then used to produce the full

Poisson's ratio from each of the stiffness matrices found. This allows for the identification of interesting properties such as a highly negative Poisson's ratio in a particular, possibly off-axis, direction.

4.4 Validation of the SiO_2 potential models

To ensure that the results obtained are reasonable and accurate, validation of the methods and potential models used is critical. A high correlation between existing experimental results and those simulated allows theoretical predictions, for materials which may not have been examined experimentally, to be more readily trusted. Additionally, conclusions gathered from these simulations are likely to be more representative of real systems. To validate the potential models used simple, dense polymorphs of SiO_2 were simulated and their elastic moduli compared to those obtained through Brillouin scattering.[47] Unfortunately due to the difficulties in experimenting on small single crystals there are relatively few SiO_2 crystals for which experimental data exist. In addition to this, most of the frameworks used in this study, which are populated solely by silicon and oxygen, are entirely theoretical and therefore impossible to obtain experimental data on. Whilst it is technically possible for these structures to exist naturally, in practise most will have sites populated with other elements, changing their chemical makeup and consequently their elastic properties. However, it has been shown to be possible to produce all-silica forms of some zeolites with careful control of the crystallization time and various other parameters.[95] For the validation of the fourteen potential models discussed earlier in this chapter, experimental results for the dense silica polymorphs α-quartz[54] and α-cristobalite[20] along with the all-silica zeolite version of the MFI structure[96] will be used for comparison with simulated results. Figure 4.1 shows the simulated values for the stiffness coefficients, for all fourteen potential models, plotted against the experimental values. The solid black line represents the ideal case where the simulated value matches exactly that of the experimental. It can be seen that the AHCM, JA, JC, and Vessal potentials perform poorly, with the majority of points lying away from the equality line. The PMM06 and PMM08 both match experimental results closely, but only PMM06 has results for the MFI crystal. As many of the coefficients of the stiffness matrices are either zero or dependant on other values, the ones used for validation in each case vary. For the trigonal crystal α-quartz, C_{11}, C_{12}, C_{13}, C_{14}, C_{33}, C_{44}, and C_{66} are used; for the tetragonal crystal α-cristobalite C_{11}, C_{12}, $C_{13,}$ C_{33}, C_{44}, and C_{66} are used; and for the orthorhombic crystal MFI C_{11}, C_{12}, C_{13}, C_{22}, C_{23}, C_{33}, C_{44}, C_{55}, and C_{66} are used.

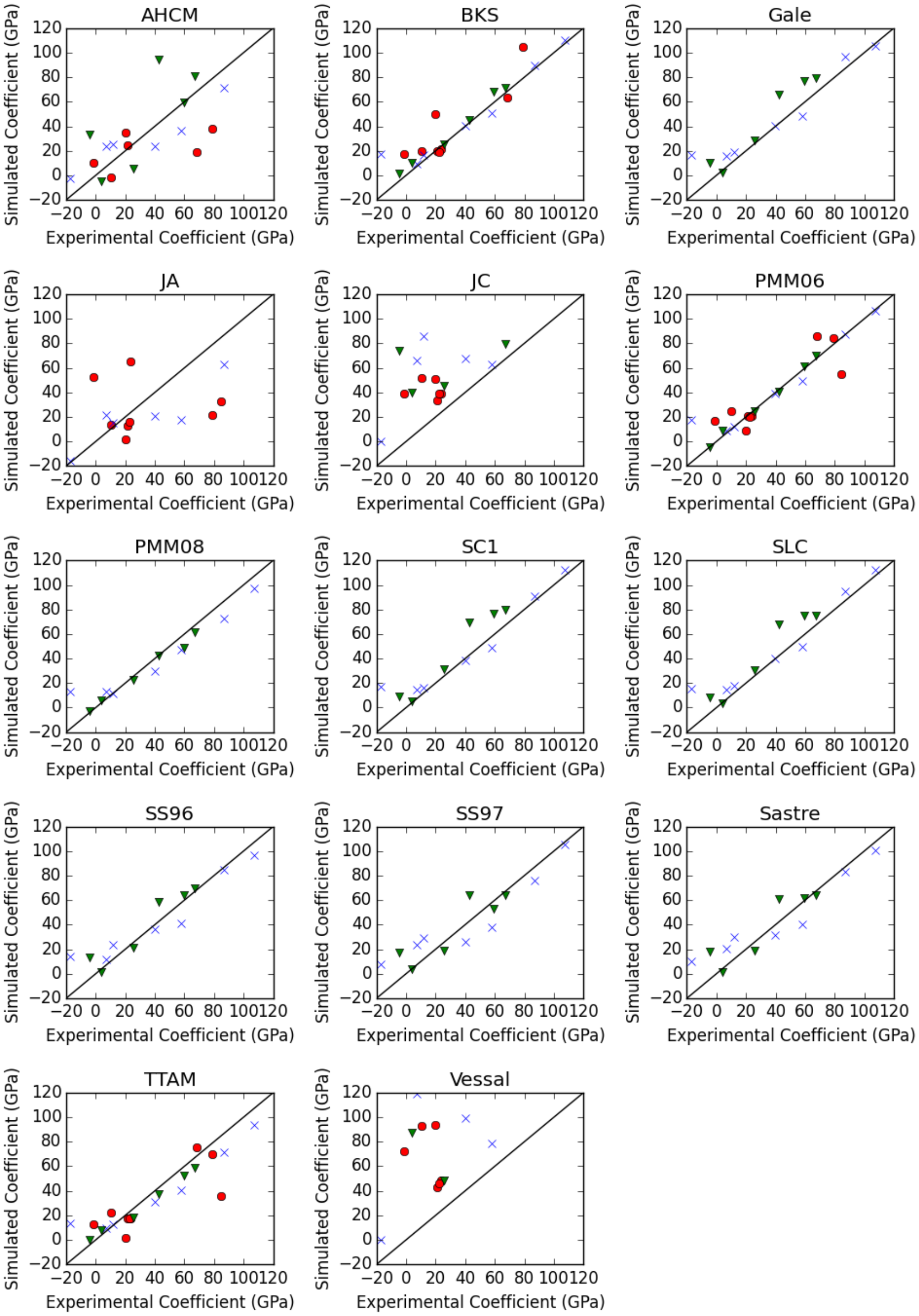

Figure 4.1 – A comparison between the simulated stiffness coefficients, when using fourteen potential models, and the experimental results for known crystals. Blue crosses represent the stiffness coefficients for α-quartz, red circles those of MFI, and green triangles those of α-cristobalite. The solid black line is the line of equality where the simulated results exactly match experimental ones.

Comparison of the stiffness matrices to experimental results also allows for a distinction to be made between different potential models, and for these models to be rated in terms of their performance in modelling all-silica zeolites. A root mean squared error (RMSE) value can be obtained by finding the square root of the average of all squared errors, where the error is the difference between the experimental and calculated value. By performing this test, a single value can be used to compare the performance of each force field. This RMSE test was performed on the data for each inter-atomic potential, when compared to the experimental data which are available, giving a picture of which models could most likely be trusted to give accurate results. Table 4.2 lists the RMSE values for the potential models calculating the elastic properties of the crystals.

Table 4.2 – The RMSE (in GPa) of the stiffness coefficients for each potential when compared with the experimental value for α-quartz, α-cristobalite, and all-silica MFI.

Potential Model	α-Quartz	α-Cristobalite	MFI
AHCM	31.10	28.27	65.11
BKS	13.53	5.59	20.55
Gale	14.41	14.40	
JA	27.31	351.22	71.82
JC	70.32	84.41	42.24
PMM06	13.60	2.53	14.61
PMM08	14.50	5.27	
Sastre	15.53	12.25	
SC1	14.20	15.30	
SLC	13.86	13.69	
SS96	14.82	10.15	
SS97	16.47	13.09	
TTAM	15.88	6.39	19.06
Vessal	135.54	164.79	89.25

Among those potentials which are able to model all three experimental crystals, PMM06 has a consistently low RMSE of 13.6, 2.53, and 14.61 for α-quartz, α-cristobalite, and MFI respectively. Simulations using PMM06 also give the closest match to the stiffness components of a set of experimental results (2.53 for α-cristobalite) whilst the other two sets of results are also reasonable. As can also be seen in Figure 4.1, the errors found using the AHCM, JA, JC, and Vessal potentials are the highest of all those used, with some RMSE values greater than 100, indicating they are perhaps not suited to modelling all-silica zeolites. The remaining ten potentials appear to produce somewhat reasonable correlation to experimental results. It is important to note that the extremely low number of crystals with experimental results does not allow for a more substantial conclusion, whilst the ideal potential will model silica in all frameworks, with such a small sample a single erroneous value is likely to skew the results substantially.

4.5 Results and Discussion

Comparison of the minimum and maximum calculated Poisson's ratio to the structure's anisotropy (A*) bears good relation to previous work carried out by Lethbridge *et al*.[41] It was found that the extreme Poisson's ratio all lie on two curves approximately symmetrical around a single point of intersection at A* = 1. Figure 4.2 shows the graph of minimum and maximum Poisson's ratio plotted against the anisotropy of the structure, where crosses represent minimum and maximum Poisson's ratio of all-silica zeolites studied in this thesis, and squares the materials from the Lethbridge *et al*. case study.[41] Due to their poor correlation with experimental results, the AHCM, JA, JC, and Vessal potential models have not been included in this analysis.

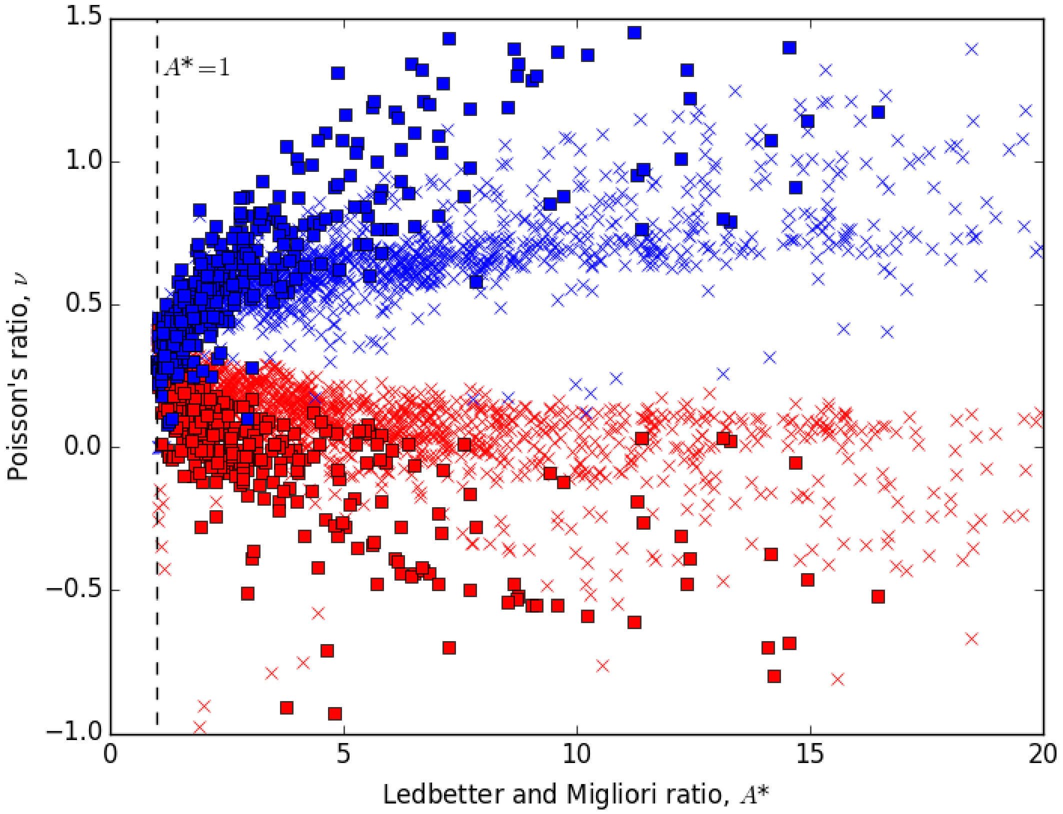

Figure 4.2 - Min and max Poisson's vs Anisotropy for all-silica zeolites and other materials. Crosses represent silica structures from this work, squares represent those from the Lethbridge *et al.*[41] study of general materials. The maximum Poisson's ratio found is shown in blue and the minimum is shown in red.

It was suggested by Lethbridge that there was no relationship between crystal symmetry and the distribution of points and also that there is no relationship between the direction at which extreme Poisson's ratios occur and all crystal systems. The results obtained in this study support this hypothesis and suggest that zeolite frameworks behave no differently from other more dense materials. It can also be seen that, in general, the extreme values for SiO_2 polymorphs fall within those of general materials. This suggests that for a similar level of symmetry within a crystal, there exists less variation between the extents to which Poisson's ratio is observed.

4.5.1 Typology of α-Cristobalite

In the Chapter 3 the typology of α-cristobalite was explored to demonstrate the extent of its auxeticity. To compare how each of the potential models represents the typology classification for α-cristobalite the different stiffness matrices, obtained using the different force fields, can be run through the typology software. By examining the classifications satisfied by each model of cristobalite it is possible to identify which potentials are likely to predict more auxeticity than others.

Table 4.3 shows the associated values from the typology classifications for α-cristobalite when modelled using the fourteen potential models, alongside the same values when calculated from the experimental stiffness matrix. The PMM06, PMM08, and TTAM potentials best represent the auxeticity of α-cristobalite, being the only ones to show the crystal as having typology classifications of 3A, 2iB, and 2iiB, as is the case with the experimental results. The BKS potential also shows a reasonable match with experimental α-cristobalite by matching the 2iB and 2iB classifications. However, none of the potentials reflect the true extent to which cristobalite exhibits a negative Poisson's ratio, with the 2iC and 2iiC classification only being found in the experimental results, and not in any of the fourteen sets of simulated results. The JA, JC, and Vessal potentials are again among the furthest away from experimental results, with none of the models successfully giving a 2iA or 2iiA auxetic classification. This is to be expected given the high RMSE for the stiffness coefficients of α-cristobalite these potentials have.

Table 4.3 – The associated values for the typology classifications of α-cristobalite when using the elastic constants calculated with the fourteen potential models and from experimental results. The values which indicate a classification has been satisfied are highlighted in a bold font.

Type	Class	Experimental	AHCM	BKS	Gale	JA	JC	PMM06	PMM08	Sastre	SC1	SLC	SS96	SS97	TTAM	Vessal
1	A	**-0.5073**	**-0.7297**	**-0.4629**	**-0.3660**	0.1454	0.0411	**-0.5308**	**-0.4820**	**-0.3352**	**-0.3496**	**-0.3358**	**-0.3710**	**-0.3361**	**-0.4850**	**-0.0627**
	B	**-0.2603**	**-0.1072**	**-0.1660**	**-0.1099**	0.2264	0.1957	**-0.2514**	**-0.2286**	**-0.0390**	**-0.1053**	**-0.1045**	**-0.0853**	**-0.0325**	**-0.1867**	0.2374
	C	**-0.0696**	**-0.1053**	0.0232	0.0315	0.2264	0.2010	**-0.0702**	**-0.0508**	0.0199	0.0570	0.0461	0.0160	0.0448	**-0.0032**	0.2489
2i	A	**100.00%**	**55.38%**	**82.81%**	**58.57%**	0.00%	0.00%	**100.00%**	**100.00%**	**50.84%**	**61.93%**	**62.61%**	**54.06%**	46.63%	**100.00%**	11.19%
	B	**99.00%**	5.66%	**60.69%**	39.64%	0.00%	0.00%	**88.83%**	**88.31%**	8.04%	42.30%	43.90%	26.82%	8.58%	**76.23%**	0.00%
	C	**53.00%**	0.40%	0.00%	0.00%	0.00%	0.00%	43.28%	40.32%	0.00%	0.00%	0.00%	0.00%	0.00%	8.68%	0.00%
2ii	A	**-0.2781**	**-0.0509**	**-0.1925**	**-0.0914**	0.2266	0.1788	**-0.2900**	**-0.2512**	**-0.0114**	**-0.0947**	**-0.0924**	**-0.0572**	**-0.0099**	**-0.2202**	0.1818
	B	**-0.1401**	0.3132	**-0.0352**	0.0243	0.2760	0.2584	**-0.1267**	**-0.1110**	0.1284	0.0145	0.0115	0.0728	0.1287	**-0.0548**	0.3276
	C	**-0.0022**	0.6774	0.1220	0.1401	0.3254	0.3380	0.0365	0.0293	0.2682	0.1238	0.1154	0.2028	0.2672	0.1106	0.4733
3	A	**-0.0696**	0.6131	0.0344	0.1316	0.3155	0.3090	**-0.0702**	**-0.0508**	0.2794	0.1142	0.1090	0.2051	0.3030	**-0.0032**	0.3848
	B	0.0009	0.6131	0.1267	0.1396	0.3379	0.3090	0.0344	0.0301	0.2794	0.1164	0.1112	0.2051	0.3030	0.1161	0.3848
	C	0.0956	1.3461	0.2268	0.2161	0.4160	0.4287	0.1691	0.1177	0.4106	0.1748	0.1642	0.3105	0.3996	0.2377	0.6647

4.5.2 Auxetic Typology of all SiO_2 structures

Using the typology system developed in the previous chapter a small number of structures were found to be type '2B' auxetic which are thought to have not been identified previously. Due to the variations in the potential models, the frameworks which are shown to meet this criterion are different for each data set. However, there are a few structures which are shown to be consistently auxetic with the majority of potential models used. The frameworks of NPO and JST are suggested to exhibit a negative Poisson's ratio when averaged over all directions, a property shared with cristobalite, when simulated with seven and nine of the potential models used respectively. These structures might have applications if their negative Poisson’s ratio nature could be coupled with other properties, rendering them suitable for specific functions, such as in piezoelectric devices or as molecular sieves. This thesis is unable to provide a link between the structures exhibiting auxetic behaviour which could point at ways of identifying future materials or the fabrication of structures to fit specifications. Whilst the Poisson's ratios of 210 all-silica structures were examined in this study only one is suggested to have increased auxetic performance over α-cristobalite. As well as being found to be 2iiB by the majority of potentials, JST is also predicted to have 3A classification by eight of the fourteen potentials, these being Gale, PMM06, JC, SC1, SLC, SS96, SS97, and TTAM. Of the remaining six potentials, half of them (AHCM, JA, and Vessal) were among the least reliable when validated against experimental results.

After calculation of the off axis elastic properties of 204 all-silica zeolite frameworks and 6 dense silica polymorphs, the typology of auxeticity was calculated. By collating the results from each individual potential, a percentage of the structures that satisfy each degree of auxetic behaviour can be calculated. Table 4.4 shows the percentage of siliceous materials that exhibit a certain type of auxeticity, for the elastic constants produced using the fourteen potential models. It can be seen that the differences in the potential models give rise to varied percentages, with the JA and AHCM potentials simulating on average more auxetic properties. The extremely low percentage of auxeticity shown by crystals modelled with the JC potential is suspicious when compared to the percentages calculated with other models. However, it is perhaps less surprising when we consider JC's poor performance in matching the elastic constants of experimental results.

Table 4.4 - Percentages of auxetic typology for SiO_2 zeolites using the fourteen potential models in this study

Type	**Class**	AHCM	BKS	Gale	JA	JC	PMM06	PMM08
1	A	76.2%	49.7%	25.7%	81.5%	7.1%	44.7%	65.6%
	B	50.3%	23.0%	8.2%	63.5%	0.5%	17.9%	37.4%
	C	19.5%	8.6%	2.3%	31.5%	0.5%	5.8%	14.1%
2i	A	50.8%	23.5%	7.0%	64.6%	0.5%	19.5%	33.7%
	B	7.0%	3.7%	1.2%	9.6%	0.5%	3.7%	5.5%
	C	0.5%	1.1%	0.6%	1.7%	0.5%	0.5%	0.6%
2ii	A	53.0%	26.2%	9.9%	68.0%	0.5%	21.1%	39.3%
	B	12.4%	3.7%	1.8%	14.0%	0.5%	3.7%	7.4%
	C	0.5%	0.5%	0.6%	1.1%	0.5%	0.5%	0.6%
3	A	1.6%	1.1%	0.6%	2.8%	0.5%	1.6%	1.2%
	B	0.5%	0.5%	0.6%	0.6%	0.5%	0.5%	0.6%
	C	0.0%	0.0%	0.6%	0.6%	0.5%	0.0%	0.6%
		Sastre	SC1	SLC	SS96	SS97	TTAM	Vessal
1	A	25.0%	33.1%	28.5%	18.3%	45.0%	50.6%	11.5%
	B	9.5%	10.8%	8.1%	2.4%	18.5%	25.0%	0.5%
	C	1.2%	0.6%	1.7%	0.6%	1.3%	8.5%	0.5%
2i	A	10.1%	13.9%	7.6%	4.3%	15.2%	27.8%	1.1%
	B	1.2%	1.2%	1.2%	0.6%	1.3%	5.1%	0.5%
	C	0.6%	0.6%	0.6%	0.6%	0.7%	1.1%	0.5%
2ii	A	11.3%	14.5%	8.7%	4.9%	21.9%	30.7%	1.1%
	B	1.8%	1.2%	1.2%	0.6%	2.6%	3.4%	0.5%
	C	0.0%	0.6%	0.6%	0.6%	0.7%	1.1%	0.5%
3	A	0.0%	0.6%	0.6%	0.6%	0.7%	1.7%	0.5%
	B	0.0%	0.6%	0.6%	0.6%	0.7%	0.6%	0.5%
	C	0.0%	0.6%	0.6%	0.6%	0.7%	0.6%	0.5%

Type 1A auxetic behaviour bears the most relevant comparison to previous studies, as this type represents a material exhibiting at least some negative Poisson's ratio. In general the percentages of 1A structures is perhaps lower than we might have expected when we consider that this figure for cubic metals is closer to 69%.[18] However, when compared with the 471 materials from the case study, with a 1A percentage of 37.2% we find a much closer correlation. On average all-silica zeolites appear to have a marginally higher level of auxeticity than the materials from the case study, with an increased percentage satisfying '2iiA' and '1B', but follow the same trend of decreasing rapidly above these classifications, with few if any materials displaying type 3 or class C auxeticity.

4.5.3 Auxeticity of all-silica JST

Despite the wide range of auxetic properties simulated with the fourteen different potential models, JST is consistently shown to have a high degree of auxeticity. Ten potentials simulate JST as having some auxetic properties (1A), of those nine calculate it has being averagely auxetic (2iiB), and eight predict it to be completely auxetic in every direction (3C). This level of completeness in the structure’s auxeticity surpasses that of all other siliceous polymorphs, including α-cristobalite.

Pure silica JST is cubic (space group PA-3, number 205), its primitive cell, shown in Figure 4.3, contains 96 oxygen and 48 silicon atoms. Due to this complexity it can be described in many ways. The following description is especially relevant to its auxeticity and helps understand the underlying mechanism. It is first useful to abstract the bent Si-O-Si bonds by straight Si-Si segments as in Figure 4.4.

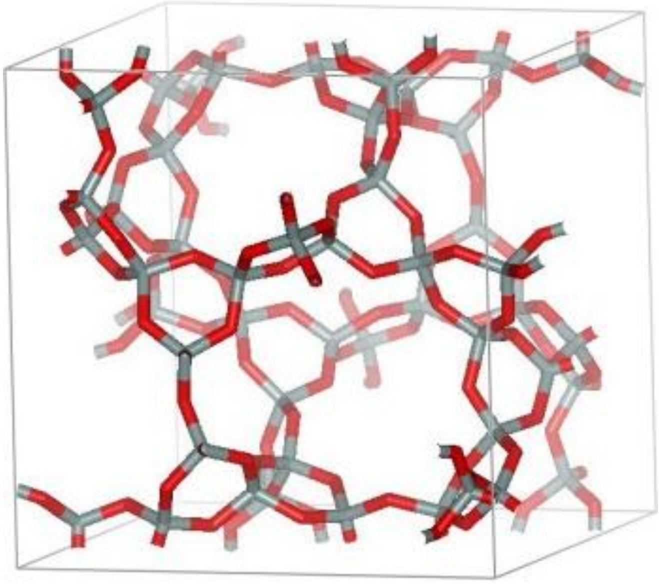

Figure 4.3 - The primitive cell of all-silica JST

Figure 4.4 - Abstracted structure of the JST framework where bent Si-O-Si bonds are represented by straight Si-Si segments

JST can then be seen as having a face centred cubic structure, where the motifs are four three-dimensional 6 sided stars. These stars (12 silicon each), are composed of a quasi-planar central hexagon surrounded by 6 sides alternating pointing up and down at angles of ±60.4°. The central hexagons lie in the four $\{111\}$ planes, and connect to each other through connecting triangles; in other words, each silicon belongs to a single star. If one assumes very stiff Si-Si connection, a tensile deformation flattens the stars, and makes them larger, leading to in-plane NPR. This simple mechanistic analysis is confirmed by studying the deformation of a unit cell. Under a 1% (100) strain, the Si-Si bonds remain largely unchanged, most bonds deforming by 0.02% with a maximum of 0.18%, while the out-of-plane side angle varies from 60.4° to 58.9°, a change of 2.4%. At this stage, JST has only been recently produced, and in a complex gallogermanate form with cationic templates in its pore.[97] While pure silica JST has not been synthesised yet, it might be necessary to obtain further confirmation of its framework's extraordinary auxeticity by mechanistic methods such as finite element analysis or fabrication of macro-scale models.

The lattice parameters and elastic constants for all-silica JST were optimised successfully (an energy minima was found) by thirteen of the potential models, with the Sastre potential running into an error during optimisation. With no known experimental results the properties obtained with different potentials can only be compared with one another, though the large number of models used should highlight any erroneous data. Table 4.5 gives the single lattice parameter, a, and the stiffness coefficients C_{11}, C_{12}, and C_{44} for each potential used.

Table 4.5 – The lattice parameters and elastic properties of all-silica JST when simulated with thirteen potential models

Potential	a(Å)	C_{11}(GPa)	C_{12}(GPa)	C_{44}(GPa)
AHCM	12.17	−102.17	63.80	14.30
BKS	13.47	89.93	7.98	25.53
Gale	15.29	33.19	−6.08	20.74
JA	11.11	105.79	116.76	60.84
JC	15.77	40.77	−3.01	22.43
PMM06	13.55	91.58	16.78	26.56
PMM08	15.43	25.36	−3.98	16.43
SC1	15.41	40.10	−4.69	22.91
SLC	15.24	36.77	−5.49	21.37
SS96	15.59	32.21	−1.42	17.42
SS97	15.62	30.20	−1.52	16.81
TTAM	15.71	14.12	−9.75	12.62
Vessal	15.79	34.64	−3.83	22.14

It can be seen that the results obtained with the AHCM, JA, and PMM06 potentials vary significantly from the remaining data sets. These differences could have been caused by errors in the geometrical optimisation, and are not necessarily true representations of JST's properties. Ignoring these suspicious models gives a unit cell length of a little over 15 Å and stiffness coefficients of ~30 GPa for C_{11}, ~ −6 GPa for C_{12}, and ~20 GPa for C_{44}. The potentials which are largely in agreement for the elastic properties of JST are the same as those which predict high levels of auxeticity. The potentials which are inconsistent (with both the general consensus and among the outliers themselves) are those which predict less auxetic properties for JST.

To fully explore the extent of auxeticity predicted for JST by each potential the typology system is applied to the stiffness matrices obtained. Table 4.6 shows the associated values of typology, described earlier, for each potential.

From the associated typology value for the 1A classification found using the JA potential it is clear that the simulation of the structure has failed to optimise successfully. The rest of the potentials (with the exception of AHCM) give a very narrow range of minimum Poisson's ratio (associated value for 1A) to maximum Poisson's ratio (associated value for 3C), with the largest of just 0.25 with BKS. This suggests an extremely isotropic material where the Poisson's ratio varies very little when examined in different axes. Excluding AHCM and JA, there are no potentials which predict JST to exhibit a small amount of auxeticity without also simulating a complete 3C auxetic classification. Nine of these thirteen potentials predict JST to be isotropically auxetic with a 3C classification. These repeatedly auxetic calculations are sufficient to expect a real sample all-silica JST to have a high chance being auxetic, and to exhibit this auxeticity over a large proportion of directions.

Table 4.6 – The associated values for the typology classifications of all-silica JST when using the elastic constants calculated with thirteen of the fourteen potential models. Values which correspond to a classification being satisfied are highlighted in a bold font.

Type	Class	AHCM	BKS	Gale	JA	JC
1	A	**−1.6631**	0.0614	**−0.2501**	**−195.3931**	**−0.0919**
	B	**−1.6631**	0.0815	**−0.2448**	**−21.3500**	**−0.0885**
	C	**−1.6631**	0.0815	**−0.2442**	0.4848	**−0.0882**
2i	A	**100.00%**	0.00%	**100.00%**	**50.81%**	**100.00%**
	B	**100.00%**	0.00%	**100.00%**	4.16%	**100.00%**
	C	**60.38%**	0.00%	**100.00%**	0.00%	**100.00%**
2ii	A	**−0.6723**	0.0994	**−0.2394**	**−1.587**	**−0.0867**
	B	**−0.4963**	0.1548	**−0.2349**	0.5355	**−0.0843**
	C	**−0.3203**	0.2101	**−0.2303**	2.658	**−0.0819**
3	A	**−0.0560**	0.2022	**−0.2243**	0.5246	**−0.0798**
	B	**−0.0404**	0.2085	**−0.2243**	9.3742	**−0.0798**
	C	0.1821	0.3080	**−0.2243**	152.6934	**−0.0798**
		PMM06	PMM08	SC1	SLC	SS96
1	A	0.1253	**−0.2401**	**−0.1437**	**−0.1812**	**−0.0638**
	B	0.1549	**−0.2284**	**−0.1409**	**−0.1799**	**−0.0585**
	C	0.1549	**−0.2271**	**−0.1406**	**−0.1798**	**−0.0580**
2i	A	0.00%	**100.00%**	**100.00%**	**100.00%**	**100.00%**
	B	0.00%	**100.00%**	**100.00%**	**100.00%**	**100.00%**
	C	0.00%	**100.00%**	**100.00%**	**100.00%**	**100.00%**
2ii	A	0.1589	**−0.2175**	**−0.1390**	**−0.1789**	**−0.0561**
	B	0.2013	**−0.2078**	**−0.1369**	**−0.1778**	**−0.0525**
	C	0.2436	**−0.1981**	**−0.1348**	**−0.1768**	**−0.0489**
3	A	0.2323	**−0.1863**	**−0.1326**	**−0.1756**	**−0.0462**
	B	0.2373	**−0.1863**	**−0.1326**	**−0.1756**	**−0.0462**
	C	0.3160	**−0.1863**	**−0.1326**	**−0.1756**	**−0.0462**
		SS97	TTAM	Vessal		
1	A	**−0.0820**	**−2.3375**	**−0.1929**		
	B	**−0.0735**	**−2.3149**	**−0.1760**		
	C	**−0.0727**	**−2.2937**	**−0.1744**		
2i	A	**100.00%**	**100.00%**	**100.00%**		
	B	**100.00%**	**100.00%**	**100.00%**		
	C	**100.00%**	**100.00%**	**100.00%**		
2ii	A	**−0.0695**	**−2.2050**	**−0.1635**		
	B	**−0.0636**	**−2.1872**	**−0.1505**		
	C	**−0.0577**	**−2.1694**	**−0.1375**		
3	A	**−0.0531**	**−1.000**	**−0.1243**		
	B	**−0.0531**	**−1.000**	**−0.1242**		
	C	**−0.0531**	**−1.000**	**−0.1240**		

Chapter 5: Local Density Variations

5.1 Chapter Overview

There have been hints in the past that negative Poisson’s ratio behaviour might be associated with low density, with “more space” for unusual mechanisms to unfold. But whereas a crystal structure usually has many different Poisson's ratios (v) in different directions, its density is unique. However, the local density, and in particular the way it varies along a specific axis, can also be directionally dependent. This chapter attempts to establish a link between the density variation in a given axis and the Poisson's ratios arising in directions relating to this axis.

To measure the density variation for a particular axis within a crystalline array, the area densities on planes normal to the axis are measured. The intersection area between each atom and these planes is calculated, and the changes in these areas are a measure of density variation. Only rational Miller vectors can be used for density variation calculations as the intersection area is assumed to be periodic within the structure. Sampling planes from an irrational Miller vector results in a quasi-crystalline pattern where the intersection area cannot be calculated exactly.

The stiffness matrices of a structure (here obtained from GULP and the SLC potential model)[68, 91] can be used to calculate the Poisson's ratio in the chosen directions through standard tensor rotation techniques. From this, the density variation in the same direction can be compared with the relevant Poisson's ratios. These are those caused by a longitudinal deformation along this axis, those for a transverse response on this axis caused by deformations which are perpendicular, and finally those where both longitudinal deformation and transverse response are perpendicular to the axis.

By analysing a large number of siliceous zeolite crystals, for a wide range of Miller vectors, it is anticipated that some form of correlation between the density variations and Poisson's ratios associated with any chosen axis will be found. A correlation of this nature could help suggest future materials which may have auxetic properties, or uncover trends which may be used to tailor materials to have particular Poisson's ratios in designed directions.

After brief background notes on anisotropy and functional programming languages, the methodology and implementation are detailed. The last section discusses the results from this work, first on body central cubic structure, then on siliceous zeolites.

5.2 Background

5.2.1 Anisotropy and Density

Since all the siliceous zeolites examined in the previous chapter are chemically identical it is clear that the differences in their elastic properties are likely to arise from purely structural variations. In 2010 it was shown that the anisotropy of a crystal is highly correlated to its elastic properties, in particular the minimum and maximum Poisson's ratio,[41] and siliceous zeolites follow the same pattern. Although it is possible that the anisotropy of the different crystals is the major contributing factor to their varied Poisson’s ratio, the correlation between the two properties does not imply causation, and both could occur as a result of an additional property of the structure. It is perhaps self-evident that those crystals which are less symmetric will have a greater range of inherent Poisson's ratios, as they occur within a more varied set of geometrical conditions. A more fundamental relationship could exist between the density of a crystal and its range of Poisson's ratios. However, due to the highly directional nature of Poisson's ratio, a more directionally relevant measure of density may be required.

5.2.2 Body centred cubic crystals – preliminary hypothesis

To look for correlation and produce hypotheses between Poisson's ratio and density variations the body centred cubic (BCC) crystals can be considered first. From analysis of the mechanisms involved in BCC deformation the minimum and maximum Poisson's ratios have been shown to be $\nu(110,1\bar{1}0) = -1$, and $\nu(110,001) = 2$ respectively.[18] The three axes of interest inferred from this are the $[110]$ direction, the $[001]$ direction, and the $\left[1\bar{1}0\right]$ direction. As the minimum and maximum Poisson's ratios share a deformation axis ($[110]$) it is proposed that the properties relating to this axis are responsible for the existence of Poisson's ratio extremes. It is also suggested that the directional properties of the $[1\bar{1}0]$, and $[001]$ axis may be linked to negative or positive ratios respectively. Due to the symmetry of the cubic system the Miller indices used in the directions discussed will directly correspond to the Miller indices of the planes for which these directions are the normal vectors; however, this is not the case for all crystal symmetries. Before calculating directional density a hypothesis can be drawn that more extreme Poisson's ratios can be found when the axis of deformation has properties similar to those found in the $[110]$ axis of BCC, more negative Poisson's ratios can be found when the transverse direction has directional properties similar to those found in $[1\bar{1}0]$ of BCC, and more positive Poisson's ratios can be found when the transverse direction has directional properties similar to those found in [001] of BCC. It is unclear whether these predictions will hold true in the case of more complex symmetries and structures, such as zeolites.

5.2.3 Functional programming

In order to access this density directionality, dedicated software had to be produced to calculate the way in which the density varies along specific axes (albeit restricted to those with rational Miller indices). Initially a preliminary script in the Python programming language was created to test the principles and functions to be used. Whilst this prototype software was able to produce the desired information, the code produced was too computationally expensive to be used for the large data set intended. Although proven computationally efficient languages such as FORTRAN were considered for the software, the highly functional quality of the problem (repeated use of mathematical functions for calculating intersection areas etc.) meant a functional language was more suitable.

Functional programming languages offer a few key advantages over imperative ones and often are more suited to highly modular problems, such as in this case, where the result can be derived from the repeated use of many smaller functions. Most functional languages make use of lazy evaluation (where operations are only implemented at the point at which they are needed,[98] rather than when the program loop reaches them as is the case in most imperative languages) and referential transparency (where each function, given the same inputs, will always return the same result, with no side effects on any other part of the program).[99] Lazy evaluation allows the program to run faster without taking up excessive memory when working with large data sets, allowing for more directions to be analysed within an acceptable time frame. Through the use of referential transparency the problem of finding the density variations along an axis can be split into more modular functions, allowing the software to be written in terms of what is mathematically true rather than the more conceptually difficult task of creating an order of execution. The functional language Haskell[100] was chosen as a purely functional language with both lazy evaluation and referential transparency as features.

5.3 Methodology

5.3.1 Directional density variation: geometric principles

To calculate the density variations along an axis in a crystal structure the individual atoms are represented as spheres, described by atom locations and atomic radii (taken as those for quartz where *r* is 0.65 Å and 1.17 Å for oxygen and silicon respectively).[101] Axes are systematically chosen, by iterating Miller indices, along which to measure density variation, and planes along these axes are sampled for their area of intersection with the atoms. This area is defined as the total area of intersection between the plane and each atom, per unit cell in the structure. Although discussing density variations and calculating intersection areas, the area found is equivalent to a local volume when expressed as a percentage of total area of the plane per unit cell, and then multiplied by the distance between samples. Figure 5.1 shows how the intersections between atoms and a plane form a measurable area, where a simple cubic structure is being intersected by the (101) plane. By moving the planes along the axis (the same normal vector), and examining the variation in intersection area (and therefore plane density), a function for density variation is obtained.

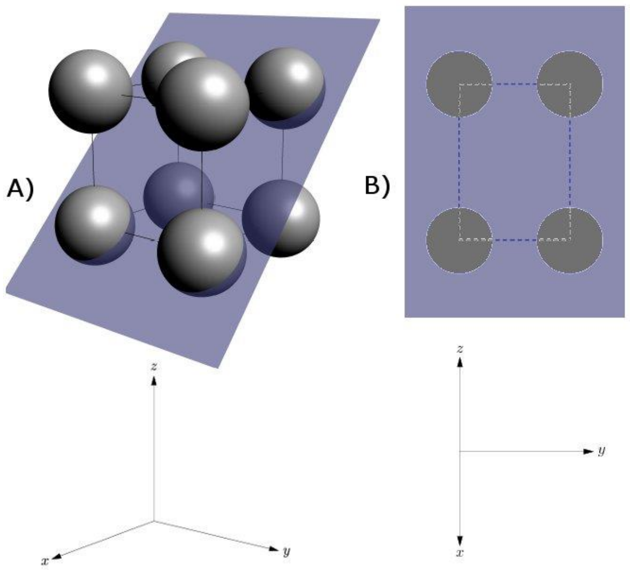

Figure 5.1 – The intersection of atoms, modelled as spheres, with a selected plane on the chosen axis. A) The (101) plane intersecting a simple cubic structure intersecting the atoms at [100], [110], [001], and [011]; B) The projection of the (101) plane, the grey areas shown represent the total intersection area between the plane and a primitive cubic unit cell.

To select axes for examination, Miller indices are produced by looping through valid combinations of integers (arbitrarily limited to those with a magnitude less than 6 to reduce computation cost). The Miller indices are forced to be both unique and rational by checking that the greatest common factor is one in each case. Each Miller index describes a lattice plane, with a normal vector of the axis for which density uniformity will be measured. This axis will only be identical to the Miller vector with the same index in cubic systems. As the chosen axis must have rational Miller indices, the atoms within the unit cell suffice to find the intersection area of a plane for the entire periodic structure. This can be shown in the following way: if a primitive lattice plane is represented by a normal vector and a displacement from the origin (equivalent to the shortest reciprocal lattice vector), integer factors of this displacement (*d*) will intersect the unit cell in *N* distinct ways (where *N* is equal to the sum of the Miller indices) before becoming periodic. Figure 5.2 shows how the (320) plane intersects any unit cell 4 distinct times, and how this is equivalent to four offset planes intersecting just one unit cell. The intersection at zero displacement, also equivalent to a displacement of 5 times the offset distance (*d*) in this case, has no intersection area associated with it as it passes through the origin. This explains why only four offset planes are needed rather than five, which is the sum of Miller indices (in Figure 5.3, an offset reveals the 5 planes).

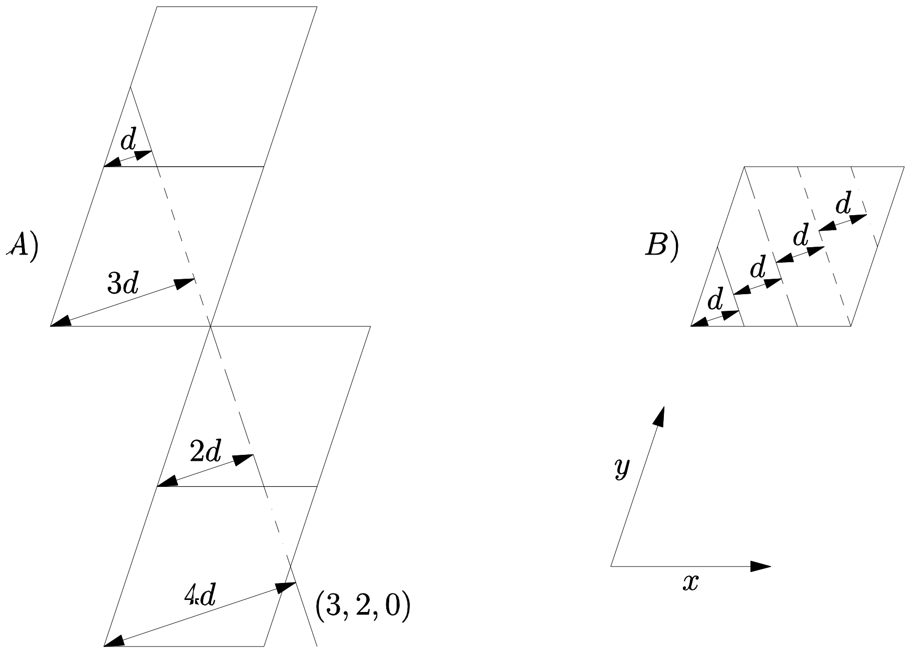

Figure 5.2 - The different ways the (320) plane intersects the unit cell. A) A continuous plane intersecting four different periodic cells at integer factors of d (the displacement of the primitive lattice plane); B) Four different representations of the same plane intersecting a single unit cell, each with a separation of d. The intersection area associated with both A and B will be identical. Note the different line types.

If the Miller indices of the lattice plane were irrational, it would intersect the unit cell in an infinite number of ways, and be impossible to evaluate. The atoms in the unit cell do not need to be replicated in order to establish the intersection area. Instead, the intersection areas for all parallel planes, which intersect the atoms within just one unit cell, can be summed to give an area of intersection for this whole plane.

After choosing a set of Miller indices, the Cartesian equation for the plane can be obtained in terms of a vector (*a b c*) normal to the plane, and a displacement *d* from the origin. This can be achieved by satisfying the following equations, where the intercepts between the plane and the unit cell are (x_1 y_1 z_1), (x_2 y_2 z_2), and (x_3 y_3 z_3).

$$a = \frac{-d}{D}\begin{vmatrix} 1 & y_1 & z_1 \\ 1 & y_2 & z_2 \\ 1 & y_3 & z_3 \end{vmatrix} \tag{5.1}$$

$$b = \frac{-d}{D}\begin{vmatrix} x_1 & 1 & z_1 \\ x_2 & 1 & z_2 \\ x_3 & 1 & z_3 \end{vmatrix} \tag{5.2}$$

$$c = \frac{-d}{D}\begin{vmatrix} x_1 & y_1 & 1 \\ x_2 & y_2 & 1 \\ x_3 & y_3 & 1 \end{vmatrix} \tag{5.3}$$

where the non-zero term *D*, is the determinant of the coordinates:

$$D = \begin{vmatrix} x_1 & y_1 & z_1 \\ x_2 & y_2 & z_2 \\ x_3 & y_3 & z_3 \end{vmatrix} \tag{5.4}$$

The values for *a*, *b*, and *c* give a Cartesian vector normal to the Miller plane and are initially found by setting *d* to equal one. By dividing all four values by the magnitude of the normal vector, a Cartesian equation for the initial lattice plane is produced, where the vector (*a b c*) has been normalised (has a magnitude of 1) and the *d* value is equal to the distance from the origin to this primitive plane. The intersection area of a plane can now be calculated using the above method, by substituting integer factors of *d* into the plane equation with constant values of *a*, *b*, and *c*.

To calculate the variation of densities along the chosen axis it is necessary to examine planes at different displacements other than those with integer multiples of *d*. The same logic used earlier when dealing with the initial lattice plane, also applies with offset planes. Therefore, the atoms within only one unit cell are sufficient to solve the intersection area for any plane parallel to the initial (provided the separation between the planes examined equals *d*). Figure 5.3 shows how the intersection areas of planes with an offset displacement of 0.25*d*, 0.5*d*, and 0.75*d* from the initial Miller plane can be calculated from the unit cell atoms. This allows the intersection area of any plane offset from the initial lattice plane to be calculated.

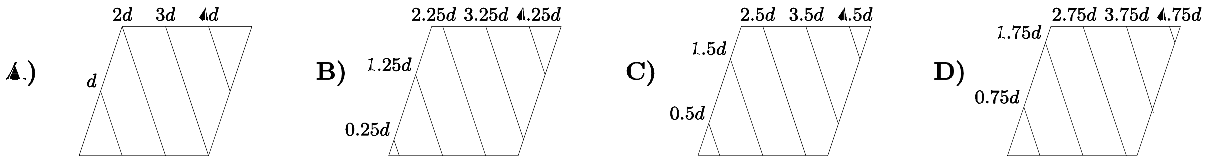

Figure 5.3 – The values of d needed to find the intersection area for the initial, 0.25d displacement, 0.5d displacement, and 0.75d displacement lattice planes. Each plane can be evaluated by incrementing the desired displacement by whole multiples of d. A) The initial plane with d, 2d, 3d, and 4d as displacement values in the plane equation; B) The 0.25 offset plane with 0.25d, 1.25d, 2.25d, 3.25d, and 4.25d as displacement values; C) The 0.5d offset plane with 0.5d, 1.5d, 2.5d, 3.5d, and 4.5d as displacement values; and D) The 0.75d offset plane with 0.75d, 1.75d, 2.75d, 3.75d, and 4.75d as displacement values.

Unlike simpler elastic properties like Young's modulus which relates to a single axis, the Poisson's ratio describes the relative strains between two perpendicular axes. Therefore, when examining the density variation along a chosen axis, a number of different Poisson's ratios could be considered as relevant; they fall into three categories. Firstly, the Poisson's ratios resulting from deformations along the same axis as that used for density variation calculations. Secondly, the Poisson's ratios with a transverse direction the same as the axis used in the density variation calculations, which arise from perpendicular deformations. Thirdly, the Poisson's ratios for which both the longitudinal and transverse directions are perpendicular to the axis used in the density variation calculations. As there is a one-to-many relationship between the density variation and each of the three classes of Poisson's ratios the minimum, maximum, and average Poisson's ratio are considered for each case. Figure 5.4 shows the directions used for determining the Poisson's ratios, where the first direction, *a*(*i*), is the axis used for density variation calculations; the second direction, *a*(*ii*), is perpendicular to *a*(*i*) and found by varying the angle *γ*; and the third direction, *a*(*iii*), is perpendicular to both *a*(*i*) and *a*(*ii*).

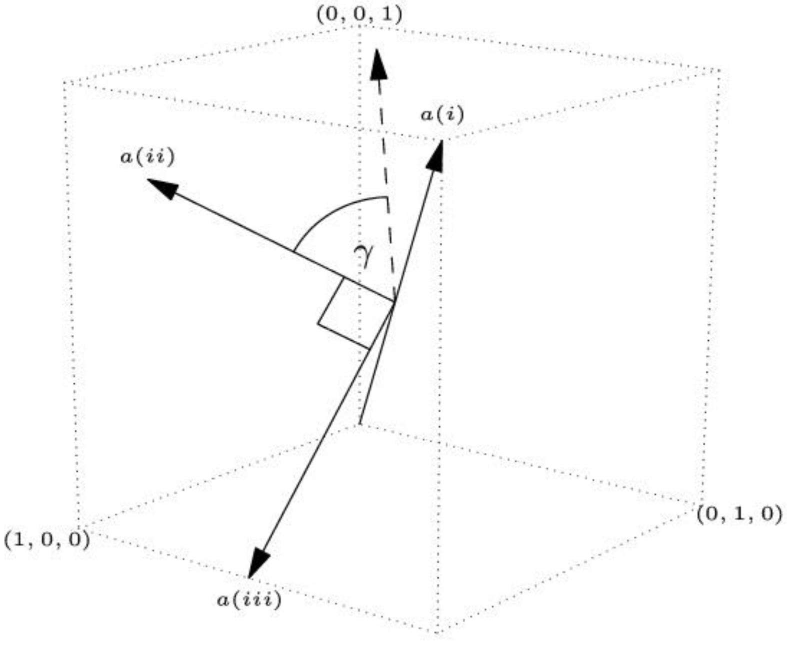

Figure 5.4 – The three axes used for Poisson's ratios calculations. *a*(*i*), the axis for which density variation is calculated; *a*(*ii*), the axis perpendicular to *a*(*i*) created by sampling different values of γ between 0 and π; and *a*(*iii*) the axis perpendicular to both *a*(*i*) and *a*(*ii*), found by taking the cross product of the two others.

If *γ* is sampled between 0 and π, the three sets of Poisson's ratio data will be calculated from a deformation in *a*(*i*) and a transverse direction *a*(*ii*), a deformation in *a*(*ii*) and a transverse direction *a*(*i*), and a deformation in *a*(*ii*) and a transverse direction *a*(*iii*).

5.3.2 Directional density variation: software implementation

For the reasons discussed in Section 5.2.3, the functional programming language Haskell was used to create the directional density software. Haskell is a statically typed, lazy, purely functional language, quite different from most other programming languages.[102] Its lazy evaluation of code allowed for a fast and error free way of producing the required results, as well as ensuring a low level of computational cost. The functional aspect of Haskell also allowed for extremely flexible code, which could be quickly changed to examine a different aspect of the density variations.

The software consists of various functions used to obtain local density results for a series of planes along an axis through the crystal structure. The primary function takes three Miller indices and a set of atom locations as its input and produces the standard deviation for density variation within this family of planes. The Cartesian plane equations are produced in the form given in Equation (5.5), where the coefficients *a*, *b*, and *c* are found using Equations (5.1), (5.2), (5.3), and (5.4). The displacement, *d*, is sampled from 0 to 1 to examine different planes, and added to increasing factors of the plane separation (the distance from the origin to the primitive plane) to scan the entire unit cell without using periodic atoms (as outlined earlier)

$$ax + by + cz - d = 0\,. \tag{5.5}$$

The distance between each atom and the plane is calculated using Equation (5.6), where *x*, *y*, and *z* are the atom coordinates; *a*, *b*, *c*, and *d* are the normal vector and distance from the origin to the plane; and *R* is the minimum distance from the atom centre to the plane. Equations (5.5) and (5.6) are closely related (*a*, *b*, *c*, and *d* are the same), this simply implies that the plane equation holds true whilst the point (*x*, *y*, *z*) lies on the plane, and therefore there is a separation of zero. Equation (5.7) gives the area of the intersecting circle between an atom and the plane, assuming the two intersect, where *r* is the atomic radius and *A* is the area of intersection

$$R = \begin{pmatrix} a \\ b \\ c \end{pmatrix} . \begin{pmatrix} x \\ y \\ z \end{pmatrix} - d \tag{5.6}$$

$$A = 2\pi \times \sqrt{r^2 - R^2} \, . \tag{5.7}$$

By summing the combined areas of all atoms which intersect each instance of the measured plane, the total intersection area for this plane is calculated. By normalising, according to the number of plane samples taken (fractions of the plane separation), and the known absolute density of the structure, a measure of local density is assigned to each plane. Once all plane samples are taken, and a local density is acquired for each one, the standard deviation is calculated for the set of Miller indices originally passed to the software.

This standard deviation for an axis is used to compare minimum, maximum, and average Poisson's ratios which can be found in the first, second, and third families. The code used for density variation calculations can be found in the supplementary material of this thesis.

5.3.3 Elastic properties: Implementation

To compare the minimum and maximum Poisson's ratios of siliceous zeolites to the density variations within the crystal structures, a script was written in the Python programming language. This script cycles through a compiled list of zeolite structures, and produces data for a number of axes for each one. Rational Miller indices are chosen by looping through three integer values ranging within a specified minimum and maximum size. The values are filtered to be both unique and have a greatest common divisor of 1. To calculate the density variations of a zeolite crystal the atom locations, listed as fractions of the crystal cell parameters, are taken from crystallographic files found in the international database of zeolite structures,[93] and atomic radii, taken as the distance from the atomic centre to the valence electron pair, with oxygen and silicon having an atomic radius of 0.65 Å, and 1.17 Å respectively.[101] This information is passed into the density variation code described earlier, to calculate a standard deviation of density for a particular zeolite structure within a specified Miller plane family.

Once the Miller plane indices have been chosen, the intercepts (produced by taking the reciprocals) are converted into Cartesian coordinates and used to find the normal vector of the defined plane. This Cartesian vector is expressed as Z'', a transformation of the Z axis after it has undergone a rotation of α degrees around the original Z axis, followed by a rotation of β degrees around X' (the transformed X axis). By performing a final rotation of γ degrees around Z'', a perpendicular vector X''' can be produced which is used as the *a(ii)* direction for Poisson's ratio calculations. By taking the dot product of Z'' and X''' (*a(i)* and *a(ii)*) a third vector, perpendicular to both, can be found which is used as *a(iii)* to calculate Poisson's ratios. This vector *a(iii)* is equivalent to the transformed *Y* axis, following the same *ZXZ* rotation to give *Y'''*.

The compliance matrix for each crystal structure is calculated using GULP[68], with the crystallographic files and the SLC (Sanders *et al.*) [76] potential library. If the longitudinal axis (*k*), transverse axis (*v*), and compliance matrix (*S*) are written in Voigt notation as in Equation (5.8), where $A_{BC} = A_B \times A_C$

$$\begin{bmatrix} k_1 \\ k_2 \\ k_3 \\ k_4 \\ k_5 \\ k_6 \end{bmatrix} = \begin{bmatrix} k_{11} \\ k_{22} \\ k_{33} \\ k_{23} \\ k_{13} \\ k_{12} \end{bmatrix} , \tag{5.8}$$

then Equations (5.9) and (5.10) describe the value of S'_{11} and S'_{12} respectively, where *S'* is the rotated compliance matrix.

$$S'_{11} = \sum_{i=1}^{6} \sum_{j=1}^{6} S_{ij} \times k_i \times k_j \tag{5.9}$$

$$S'_{12} = \sum_{i=1}^{6} \sum_{j=1}^{6} S_{ij} \times k_i \times v_j \ . \tag{5.10}$$

The Poisson's ratio can now be simply calculated between the axes *k* and *v* by the negative ratio between transverse and longitudinal strain

$$\nu = \frac{-S_{12}}{S_{11}} \,. \tag{5.11}$$

By repeating this process for each crystal structure, sets of Miller indices, γ rotations about Z'', and family of Poisson's ratio, an extremely large set of data is produced. In order not to discriminate between different crystal structures only the standard deviation data for each axis will be compared with Poisson's ratio information. This is to try to establish a link between density variations which do not depend on the structure being examined.

5.4 Results and Discussion

5.4.1 BCC crystals

Due to the symmetry of the BCC structure the density variation for both the $[110]$ axis and the $[1\bar{1}0]$ axis are identical, and have a standard deviation of 0.12. This is a larger variation than that of the density in the $[001]$ axis which has a standard deviation of 0.08. The symmetry in the crystal means that the only valid comparison between the axes, relating to the maximum and minimum Poisson's ratios in the structure, are between $[110]$ (or $[1\bar{1}0]$) and $[001]$. As both the extremes for Poisson's ratio have [110] as an axis of deformation it is possible that a higher variation in the density results in a more varied Poisson's ratio in the first family of ratios. It could also be suggested that a low variation in density results in a more negative Poisson's ratio found in the third family of ratios. However, both of these conclusions are only supported by a single datum value and any conclusions drawn are self-fulfilling. To better understand whether the density variation has some significance to the Poisson's ratio in general materials, the Miller indices of a large number of materials, in this case silica zeolites, will be systematically examined.

5.4.2 Siliceous zeolites

The following figures show the results for minimum, maximum and average Poisson's ratios, when plotted against the standard deviation for density found in the relative axis. Data are shown for the first, second, and third family of Poisson's ratios respectively.

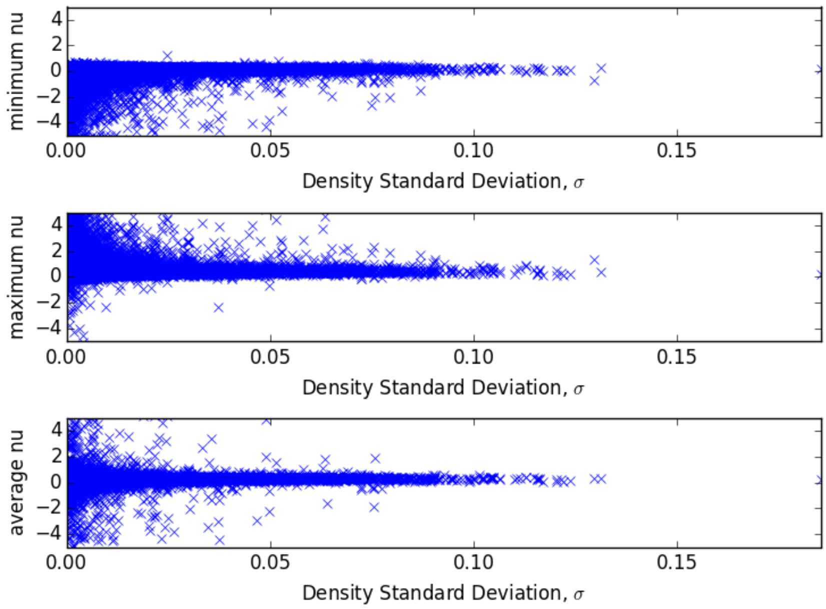

Figure 5.5 – The minimum, maximum, and average Poisson's ratio, when compared with the standard deviation of the density, for the first family of Poisson's ratios.

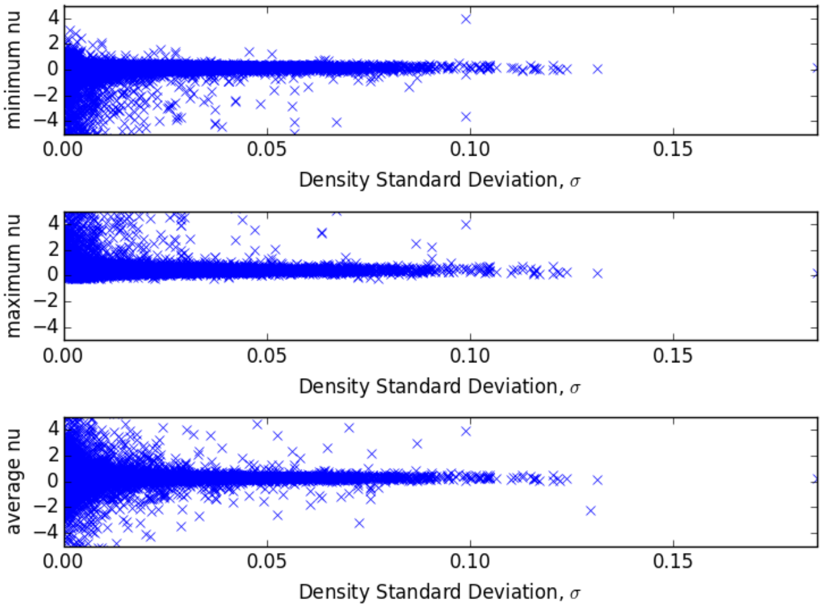

Figure 5.6 – The minimum, maximum, and average Poisson's ratio, when compared with the standard deviation of the density, for the second family of Poisson's ratios.

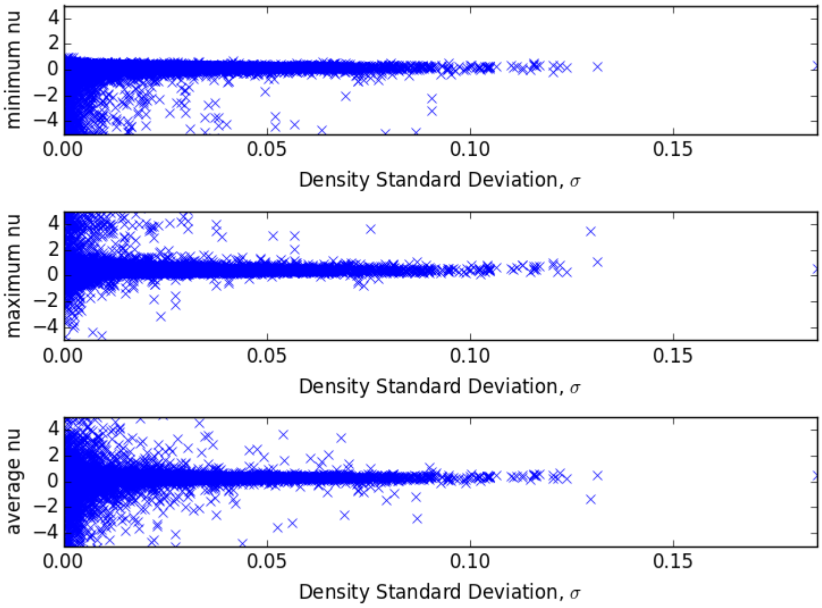

Figure 5.7 – The minimum, maximum, and average Poisson's ratio, when compared with the standard deviation of the density, for the third family of Poisson's ratios.

The data appear to suggest an increased likeliness of very large positive or negative Poisson's ratios when the standard deviation of density is low. However, due to the high proportion of Miller indices which would normally be considered 'off-axis' being chosen, there is a large concentration of data points at the lower end of the standard deviation scale. This can be shown with the histogram in Figure 5.8 which plots the number of data points within a range of standard deviations.

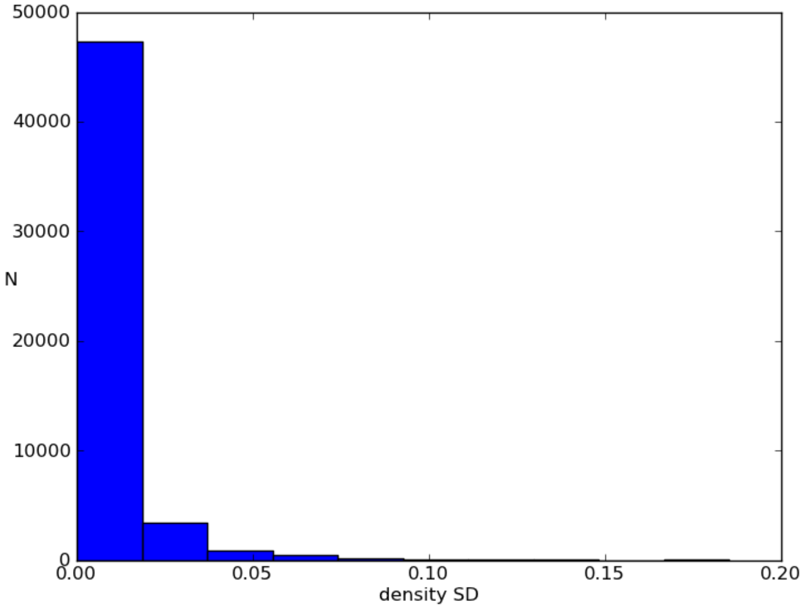

Figure 5.8 – The histogram of data points for the standard deviation of density.

This suggests that most axes examined have very little repeating crystal structure and their density approaches an even distribution. As the skew may lead to misinterpretation of the spread of Poisson's ratio values, the following figures smooth the distribution by plotting the data on a log scale in the x-axis.

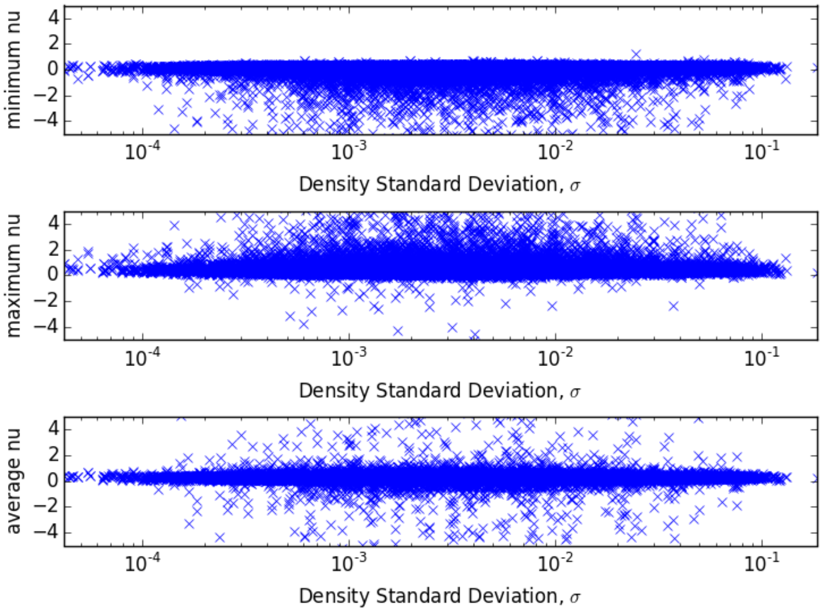

Figure 5.9 – The minimum, maximum, and average Poisson's ratio, when compared with the standard deviation of the density on a log scale, for the first family of Poisson's ratios.

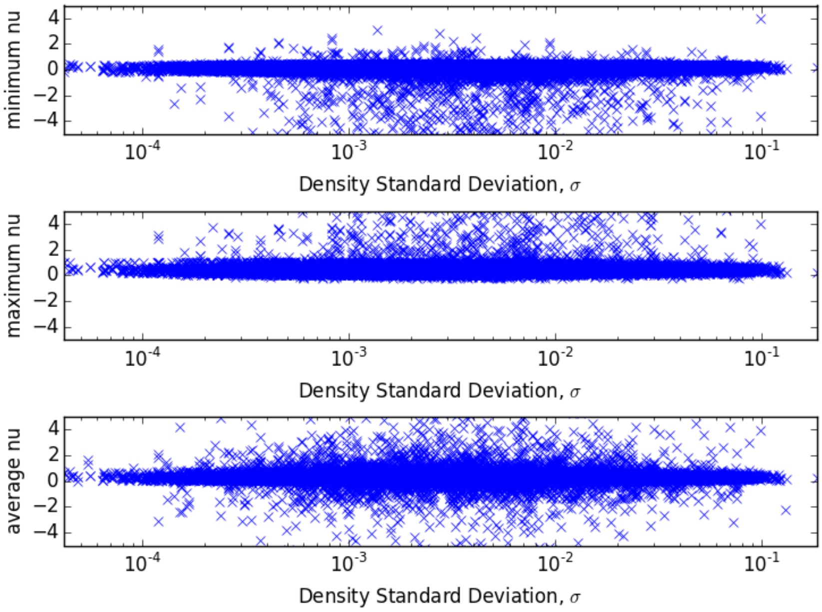

Figure 5.10 – The minimum, maximum, and average Poisson's ratio, when compared with the standard deviation of the density on a log scale, for the second family of Poisson's ratios.

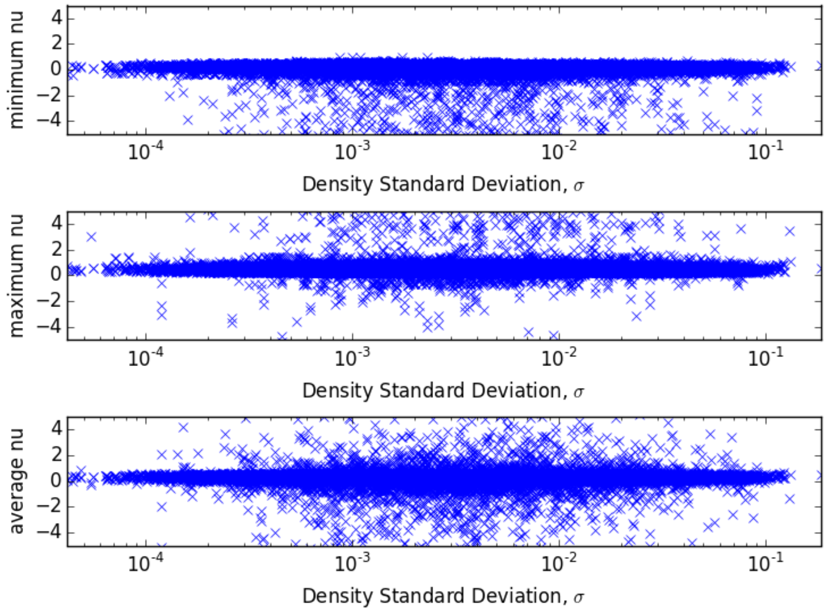

Figure 5.11 – The minimum, maximum, and average Poisson's ratio, when compared with the standard deviation of the density on a log scale, for the third family of Poisson's ratios.

The new histogram shows how, after plotting on a log scale in the x-axis, the skewed distribution of the data has been successfully altered to give a smoother range of points, which appear to be roughly normally distributed between the minimum and maximum of the range.

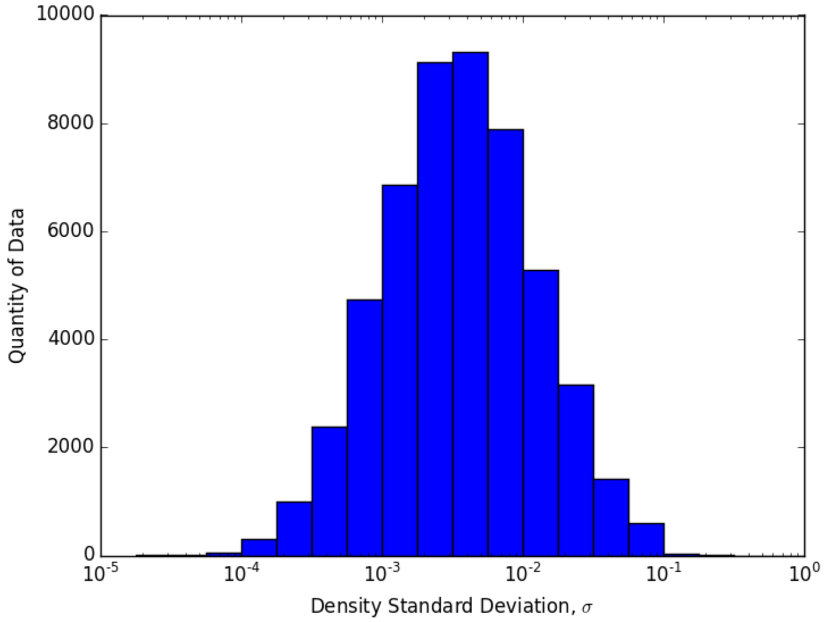

Figure 5.12 – The histogram of data points for the standard deviation of density when plotted on a log scale.

5.4.3 Discussion

When examining the log scale figures, there does not appear to be any correlation between the standard deviation and either the minimum, maximum, or average for any of the three families of Poisson's ratios. This is supported by the Pearson product-moment correlation coefficient (PPMCC) of each of the nine data sets used for comparison (minimum, maximum, and average for each of the three Poisson's ratio families). The PPMCC gives a measure of linear correlation between two variables and is defined in Equation (5.12), where *E*(*x*) is the expectation of *x*

$$PPMCC_{\nu,\sigma} = \frac{E(\nu\sigma) - E(\nu)E(\sigma)}{\sqrt{E(\nu^2) - E(\nu)^2} \times \sqrt{E(\sigma^2) - E(\sigma)^2}} \ . \tag{5.12}$$

A PPMCC value of 1 indicates a perfect correlation and a value of 0 indicates no correlation at all.

Even the largest PPMCC value for the data sets found is below 0.01, strong evidence suggesting that there exists no correlation between direction density variation and the Poisson's ratios associated with this axis. It is suggested that more complex factors are contributing to the specific Poisson's ratio values other than the way in which density changes along specific axes in the crystal. It may be that specific arrangements and mechanisms are responsible for the maxima we see present which vary relatively unpredictably as the structure changes. In itself, it is interesting to note that there exists no link between the periodicity of an axis and the way in which the Poisson's ratios related to it vary, as the initial justification for this work, with similar chemistry the reasons for varied elastic properties must be geometric, is still valid. It is still unknown which other contributing factor, and not the local density variations, account for this behaviour. Further work into the reasons why structure can play such a pivotal role should be undertaken, with an emphasis on discovering what it is about a structure which creates an interesting set of elastic properties, given the chemical similarities in a crystal group such as zeolites.

Chapter 6: Properties of GeO_2 zeolites

6.1 Chapter overview

The modelling of silica zeolites structures performed in chapter three produces elastic properties of one group of materials, and focuses on one chemical makeup. However, the open tetrahedral frameworks which they form can also be formed by other classes of materials with similar chemistry, such as germanium oxides (GeO_2), aluminium phosphates ($AlPO_4$), or gallium phosphates ($GaPO_4$).[103–105] Of these the most chemically similar to SiO_2 is GeO_2, which also forms tetrahedra of oxygen atoms, but with germanium in place of silicon at the centre of each tetrahedron.

The elastic properties of GeO_2 crystals can be compared with their SiO_2 equivalent, allowing a distinction to be made between extreme Poisson's ratios resulting from interesting chemistry, and those due to purely structural factors. If an arrangement of tetrahedra behaves differently when constructed from GeO_2 rather than SiO_2, this suggests the properties are a result of chemical interactions. Conversely, similar elastic properties resulting from arrangements which are identical, except for the central element in each tetrahedron, point to structures which are geometrically interesting.

To validate the germanium oxide potentials used a case study will be carried out on α-GeO_2, the quartz equivalent structure, which occurs naturally and has been experimentally studied.[106] The lattice cell parameters and components of the stiffness matrix can be compared with those produced by each potential to measure the accuracy of each. Ideally more GeO_2 crystals would be used for the validation of potential models. However, experimental data are limited due to a lack of stable polymorphs.

Particular attention will be given to the GeO_2 equivalent of α-cristobalite, a crystal known to have an unusual Poisson's ratio, and to JST, a framework shown to be isotropically auxetic in previous chapters. If these structures exhibit a strong negative Poisson's when composed of either SiO_2 or GeO_2, they are likely to have similar properties for other tetrahedral chemistries ($AlPO_4$, $GaPO_4$ etc.). As well as comparisons with previously studied families, this chapter enables a wider range of crystals to be examined. With more theoretical materials being studied, there is an increased chance in finding a crystal with unusual elastic properties, or with a combination of chemical and elastic properties which could be useful.

This chapter provides a background to molecular modelling using germanium and oxygen potentials, as well as a brief discussion on real GeO_2 materials and their properties. A methodology is then given for the process of finding the stiffness matrices of theoretical materials. This explains how germanium and oxygen are substituted into initial tetrahedral framework structures, followed by a description of the use of potential models to perform force field optimisation. The experimental values for α-GeO_2 are compared with those calculated and the validity of future elastic properties is considered. Finally, the results from a large number of tetrahedral frameworks are presented, with particular attention on the GeO_2 forms of α-cristobalite and JST, along with a discussion of their properties.

6.2 Background

Germanium oxide is a naturally occurring mineral which can exist in a crystalline form as connected tetrahedra. The only GeO_2 polymorph which is found un-synthesised in atmospheric conditions is argutite,[107] which shares a structural topology with the tetragonal titanium dioxide crystal rutile,[108] although it can also exist in a hexagonal from (with the structure of α-quartz), and a cubic form (with the structure of low temperature cristobalite).[107] The quartz like structure, known as α-GeO_2, has been suggested to have a greater piezoelectric effect than the SiO_2 equivalent[109] and studies have been performed to calculate its properties.[107]

Some tetrahedral frameworks which are formed by zeolites, such as ACO and AST,[110] can be observed in both silica and germania forms. However, there are those, such as LTA, which have inter tetrahedral angles (the tetrahedra-oxygen-tetrahedra angle or TOT)[111] suitable only for SiO_2, or those with TOT angles which can exist only in GeO_2, such as ASV.[111] This suitability is due to the stable TOT angles being smaller for Ge-O-Ge bonds than for Si-O-Si bonds, which limits the arrangements of tetrahedra which can be synthesised.[112] Whether these structures are physically possible or entirely theoretical has an impact on the significance of the elastic properties calculated if a real material is intended to be synthesised. However, for the purpose of examining a wide range of structures, all frameworks will be considered.

A common technique to examine GeO_2 materials is to substitute germanium into existing SiO_2 zeolite frameworks.[113] By varying the percentage of silicon sites which are replaced a comparison can be produced between structures with the same topology but with different ratios for the types Si or Ge tetrahedra. Some structures produce specific arrangements of tetrahedra (such as double four rings)[114] which have been shown to be stabilized by the substitution of germania into the framework.[115]

6.3 Input parameters for modelling GeO_2 structures

6.3.1 GeO_2 potentials

The difficulties that arise with fitting energy potentials to both the ionic and covalent behaviour of SiO_2 models also hinder the germanium equivalents. In addition to this, the smaller Ge-O-Ge bond angle (130° for the germania equivalent of α-quartz)[89] when compared to Si-O-Si in silica (141.5° for α-quartz at 10.6 kbar),[76] has been thought to create difficulties in modelling without introducing many-body terms to simulate positive germanium atom repulsions.[89] Potential models for GeO_2 found in literature are given in Table 6.1 with the source publication references.

Table 6.1 – The potential libraries used for the calculation of the elastic properties of GeO_2 equivalent structures

Library Name	Reference	Type
Woodley	Woodley *et al.*[88]	Rigid Ion
Oeffner	Oeffner and S. Elliott[89]	Rigid Ion
Sastre	Sastre and Gale[82]	Shell Model

The atomic charges, two-body interactions, and three-body interactions for these potential models are given in Appendix B. Where possible the cut-off distances for Buckingham potentials were taken from the literature. Where cut-offs were not given 12 Å, a value commonly implemented with similar potentials, is used. The Woodley and Oeffner potentials are rigid ion models, where germanium atoms interact directly with the core of oxygen atoms, whereas the Sastre potential uses the shell model, with a harmonic spring force between oxygen cores (O_c) and shells (O_s).

6.3.2 GeO_2 zeolite crystallography

The crystallographic files used for the creation of all-silica zeolites in chapter 3 are also used to create their germanium oxide equivalent. The initial lattice parameters and atom sites remain constant for both, with the only difference arising from the T-sites being populated with germanium atoms instead of silicon. This is achieved with minor alterations to the software for taking the information from the crystallographic file and using it to create an input file for GULP.

6.3.3 Validation of the GeO_2 potential models

Unlike SiO_2 structures, which exist in many stable polymorphs, GeO_2 naturally forms very few real polymorphs. Of these α-GeO_2 is the only one with experimentally measured elastic properties which can be used to validate the germanium oxide potential models. The quartz equivalent structure is modelled with the GeO_2 Woodley, Oeffner, and Sastre potentials by performing a force field optimisation with the general purpose lattice parameters program GULP.[68] The stiffness coefficients and lattice cell parameters obtained from these optimisations are compared to the results gained through experimental procedures by Grimsditch,[116] Jorgensen,[117] and Balitsky.[107] The parameters for SiO_2 α-quartz are included for comparison.

Table 6.2 – The properties of experimental silica α-quartz, experimental α-GeO_2, and the force field optimisation simulations of α-GeO_2 from this work.

Cell	Exp. α-quartz	Exp. α-GeO_2		This work		
Parameters (Å)	Bechmann[54]	Jorgensen[117]	Balitsky[107]	Woodley	Oeffner	Sastre
a = b	4.91	4.98	4.984	5.49	5.09	4.99
c	5.41	5.64	5.660	6.06	5.73	5.66
Stiffness coefficients (GPa)	Bechmann[54]	Grimsditch[116]	Balitsky[107]			
C_{11}	86.74	66.4	64.8	268.42	36.82	55.00
C_{33}	107.2	118	116	266.15	93.36	86.92
C_{44}	57.94	36.8	37.4	67.66	23.86	24.04
C_{66}	39.88	22.53	21.10	57.67	11.91	14.60
C_{12}	6.99	21.3		153.08	13.00	25.79
C_{13}	11.91	32		185.90	16.82	26.13
C_{14}	−17.91	2.2	11.7	0.00	0.07	-0.66

Figure 6.1 shows the corresponding graphs for the potential validation to aid in visualisation. The Sastre potential shows the greatest similarity to the experimental values for α-GeO_2 with a RMSE (square root of the mean squared error) for the stiffness coefficients of 14.06. The Oeffner potential provides a reasonable approximation to the real properties of α-GeO_2 with a RMSE value of 17.18. It can be seen both in Table 6.2 and in Figure 6.1 that the Woodley potential does a poor job of simulating the experimental lattice parameters and elastic properties of α-GeO_2, with an extremely large RMSE of 123.06 for the elastic coefficients.

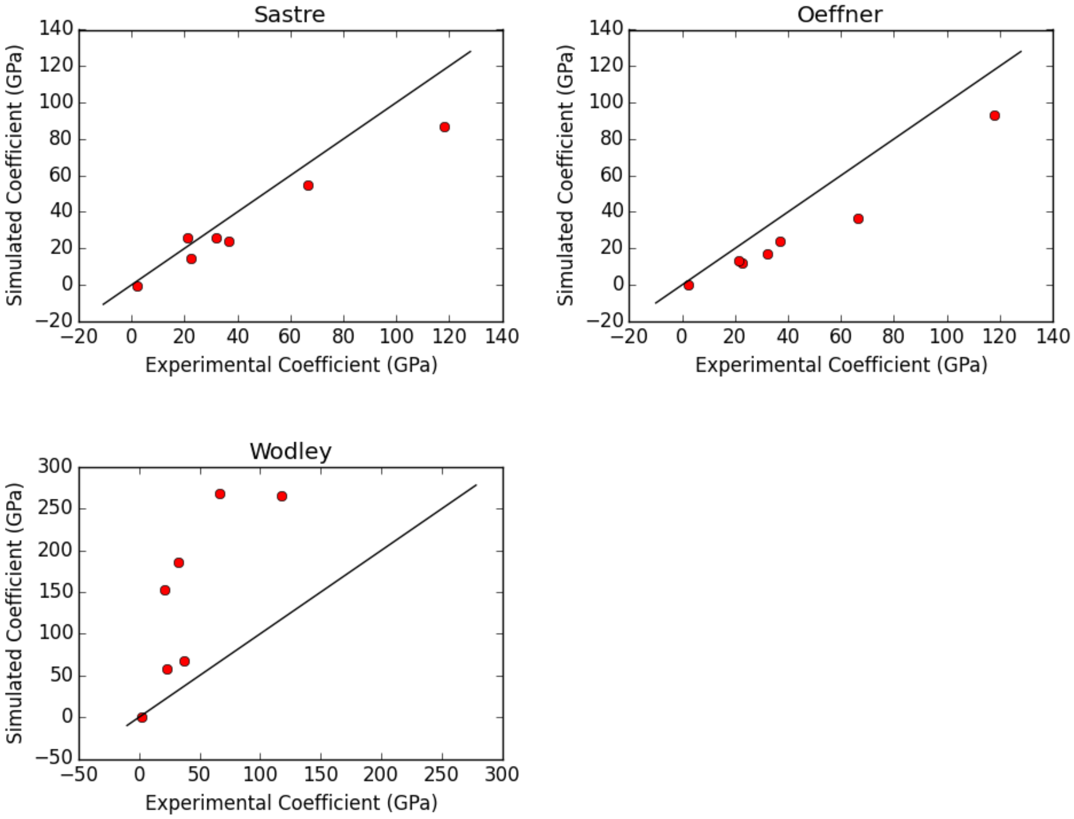

Figure 6.1 – Comparison of the simulated stiffness coefficients of the GeO_2 equivalent of α-quartz with the experimental values. The solid black line is the line of equality where the simulated results exactly match the experimental ones.

6.3.4 Calculation of GeO_2 elastic properties

The 210 zeolite frameworks used for calculating the SiO_2 elastic properties (obtained from the international database of zeolite structures)[93] are also used for calculations with GeO_2. By altering the crystallographic files to replace the silicon at each tetrahedra site with germanium, input files giving the locations of each atom within the unit cell are produced. Force field optimisation is performed within the GULP[68] software, using each potential model, giving a prediction of final lattice parameter values and stiffness coefficients. These coefficients are used to find the off axis elastic properties of each GeO_2 framework, allowing for a comparison of the minimum and maximum Poisson's ratio. As with silica the anisotropy of each structure is compared with the minimum and maximum Poisson's ratio to establish whether the trend, of more extreme properties arising with less symmetric frameworks, follows with the GeO_2 equivalent structures.

The previously developed typology system is employed to distinguish between the extents to which each structure exhibits auxetic behaviour and to aid identification those which may have interesting elastic properties. Each typology is classified in terms of the negativity of an axis and the number of axes which have this negativity. By applying these classifications structures with auxetic properties for a very small number of specific directions can be distinguished from those which may have a large degree of auxetic behaviour in many different directions. By making this distinction, potentially interesting structures are highlighted amongst those which are more common.

6.4 Results and discussion

6.4.1 Properties of the GeO_2 equivalent of α-cristobalite

The auxetic properties of the SiO_2 form of α-cristobalite are well known and have been explored in depth, both in previous literature, and in Section 2.2.2.2, Section 3.5, and Section 4.5.2 of this thesis. The lattice parameters of the GeO_2 form of α-cristobalite have been measured[118] but, due to difficulties in forming a stable crystal, its elastic properties have not. Simulations of the elastic properties of the α-cristobalite form of GeO_2 are calculated using the three potential models outlined and the stiffness matrices are obtained. Table 6.3 gives the lattice cell parameters and the stiffness matrix coefficients C_{11}, C_{12}, C_{13}, C_{33}, C_{44}, and C_{66} for the three potentials used. With the lack of experimental results for GeO_2 α-cristobalite, the properties of the SiO_2 form are given for comparison.

Table 6.3 – The lattice parameters and elastic properties of the GeO_2 form of α-cristobalite when simulated with the three GeO_2 potential models used. The experimental values for SiO_2 α-cristobalite are included for reference.

Cell Parameters (Å)	SiO_2 Exp.	GeO_2 Oeffner	GeO_2 Sastre	GeO_2 Woodley
a = b	4.96	5.099	4.922	5.586
c	6.91	6.444	7.537	7.899
Stiffness Coefficients (GPa)				
C_{11}	59.45	10.50	23.39	272.84
C_{12}	3.88	64.62	0.78	123.10
C_{13}	-4.49	18.11	14.64	175.68
C_{33}	42.47	40.70	61.15	221.25
C_{44}	67.24	28.94	50.14	74.87
C_{66}	25.74	14.67	10.04	23.29

Even though there is no experimental form to use as a benchmark, it can be seen that the Oeffner and Sastre potentials give values which are in a similar range to the stiffness matrix of the SiO_2 form. The very high values found by the Woodley potential are more unusual which mirrors the poor performance this potential showed when modelling GeO_2 α-quartz.

The stiffness matrices can be used to examine the extent to which the structure is shown to exhibit negative Poisson's ratio if any. A typological examination of the GeO_2 form of α-cristobalite can also be used to compare between the different potential models. Table 6.4 lists the associated values for auxetic typology for each of the potential models.

Table 6.4 – The associated values for the typology classifications of the GeO_2 form of α-cristobalite. The elastic constants used to obtain these values come from the three GeO_2 potential models outlined. The values which indicated a classification has been satisfied are highlighted in a bold font.

Type	Class	Oeffner	Sastre	Woodley
1	A	**−542.5025**	**−0.4449**	**−0.1098**
	B	**−31.5876**	**−0.1108**	0.3261
	C	0.2406	**−0.0566**	0.3436
2i	A	**52.66%**	**69.68%**	14.49%
	B	19.98%	30.40%	0.00%
	C	0.00%	4.88%	0.00%
2ii	A	**−2.1277**	**−0.0098**	0.2060
	B	0.6666	0.1713	0.4013
	C	3.4609	0.3524	0.5965
3	A	0.3066	0.6059	0.4412
	B	365.6528	0.6059	0.4412
	C	1273.8067	0.6667	0.8763

The results obtained from the Oeffner potential seem very far from the other two and include minima and maxima which are extreme. Although the Woodley potential predicts values which are within a generally expected range of Poisson's ratios, without an experimental form for comparison and with the potential performing badly at modelling GeO_2 α-quartz it is difficult to know if these values are accurate or not. The Sastre potential, the best performing of the potential models used to simulate GeO_2 α-quartz, predicts the highest level of auxeticity for GeO_2 α-cristobalite. The typology bears a very close resemblance to the auxeticity predicted for the regular silica form of α-cristobalite found with the Sastre SiO_2 potentials from the same literature.[82] This suggests that the different chemistry, when replacing tetrahedra sites with germanium instead of silicon, has only a small effect on the Poisson's ratio, with more contribution arriving from the geometric structure.

6.4.2 Properties of the GeO_2 equivalent of the JST framework

A newly discovered structure which could have extremely negative, and even isotropically negative Poisson's ratios, is the silica structure of the JST framework. In

Chapter 4 it was predicted to be 3C auxetic by nine of the fourteen potential models used. To further compare the elastic properties predicted with silicon or germanium, the GeO_2 form of JST is examined in terms of its lattice parameters, elastic properties, and auxetic typology. This also allows for a prediction of the properties of the JST framework itself, independent of chemistry, and the auxetic behaviour which could be expected from the structure alone. Table 6.5 outlines the lattice parameter of the cubic framework, and the components of the stiffness matrix C_{11}, C_{12}, and C_{44}.

Table 6.5 – The lattice parameters and elastic properties of the GeO_2 form of JST when simulated with the three potential models used.

Potential	a(Å)	C_{11}(GPa)	C_{12}(GPa)	C_{44}(GPa)
Oeffner[2]	16.372	15.17	−13.62	10.97
Sastre	16.374	19.89	−1.62	12.24
Woodley	17.095	38.73	5.16	16.30

Somewhat surprisingly, given the differences in modelling the α-cristobalite form of GeO_2, all three potential models give reasonably similar results, with the Woodley being the only potential not to predict a negative value for C_{12}. The elastic properties predicted give rise to the following auxetic typology, with the associated values listed in Table 6.6. The failed optimisation of the Oeffner potential creates unusually large values which causes errors within the typology software. For this reason the Oeffner potential has been omitted from the typology results for GeO_2 JST.

---

[2] The values obtained using the Oeffner potential are from a simulation which failed to find a minimum. These results should be treated with suspicion.

Table 6.6 – The associated values for the typology classifications of the GeO_2 form of JST when using the elastic constants calculated with the Sastre and Woodley potential models.

Type	Class	Sastre	Woodley
1	A	**−0.1525**	0.1157
	B	**−0.1356**	0.1176
	C	**−0.1339**	0.1176
2i	A	**100.0%**	0.0%
	B	**100.0%**	0.0%
	C	**100.0%**	0.0%
2ii	A	**−0.1251**	0.1184
	B	**−0.1126**	0.1220
	C	**−0.1000**	0.1256
3	A	**−0.0888**	0.1255
	B	**−0.0888**	0.1260
	C	**−0.0888**	0.1322

The two potential models differ significantly in their prediction of the extent of auxeticity in the structure, with the Sastre potential showing isotropic auxeticity and the Woodley potential showing none at all. Both potentials have an extremely narrow range between the associated values for the 1A and 3C classifications. This implies that despite different predictions of the elastic properties, the structure is expected to behave isotropically. The A^* ratio for JST was found to be 1.30 when modelled with the Sastre potential and 1.06 with Woodley, further supporting the prediction of largely isotropic behaviour. Given the auxetic prediction by the Sastre model it is reasonable to suggest that the negative Poisson's ratios predicted with the SiO_2 form of JST may be present in the theoretical GeO_2 form. It is suggested that the zeolite framework JST could exhibit a large degree of auxeticity, independent of its chemical makeup.

6.4.3 Typology of GeO_2 forms of the zeolite frameworks

Using the three potential models for GeO_2 the 210 structures, 204 zeolite frameworks, and 6 dense polymorphs used earlier with silica, are modelled with germanium at the centre of each tetrahedron. The stiffness matrix of the structures is calculated using force field optimisation with the GULP software and these matrices are used to predict the respective auxetic typology. By collating the results from each potential the percentage of structures which fit specific classifications can be obtained. These percentages can then be used to give an overall view of the auxeticity of the group of materials, in this case GeO_2 zeolites, predicted by an individual potential model. The potential models can also be compared with each other to identify those which may be more likely to predict a higher or lower level of auxetic behaviour. Table 6.7 shows the percentages of all GeO_2 zeolites which meet each typology classification when using the three potential models chosen.

Table 6.7 – Percentages of auxetic typology for GeO_2 zeolites using the three potential models in this study

Type	Class	Oeffner	Sastre	Woodley
1	A	80.0%	56.0%	3.9%
	B	59.4%	32.0%	0.0%
	C	30.0%	12.0%	0.0%
2i	A	55.6%	29.6%	0.0%
	B	10.6%	4.0%	0.0%
	C	2.5%	1.6%	0.0%
2ii	A	60.6%	31.2%	0.0%
	B	16.3%	7.2%	0.0%
	C	1.9%	1.6%	0.0%
3	A	3.8%	0.8%	0.0%
	B	1.3%	0.8%	0.0%
	C	1.3%	0.8%	0.0%

It can be seen that the Woodley potential, which produces outlying results for the GeO_2 equivalent of both α-quartz and α-cristobalite, again gives extreme results in this set of calculations. Given the prevalence of auxetic properties in materials (as demonstrated in Section 2.1.2) it would be extremely unusual if the percentage of auxetic GeO_2 zeolite frameworks was as low as suggested by the Woodley potential.

The Oeffner potential generally predicts more auxetic crystals than Sastre, with almost double the number of materials being predicted as 2iiA auxetic. However, the percentages obtained using the Sastre potential, which has been shown to be more reliable, are a closer fit to those found using SiO_2 structures. Both the Oeffner and Sastre potentials continue to follow the trend of the reasonably common occurrence of Type 1 or Class A behaviour, with a sharp decline in the number of crystals exhibiting higher degrees of auxeticity. Based on the limited number of potentials used for GeO_2 and the extremely small amount of experimental data available for validation it is difficult to make a solid prediction on the auxetic behaviour of GeO_2 zeolites. The data available supports the argument that replacing silicon atoms with germanium in the tetrahedral sites of zeolites does not overly affect the crystals auxeticity. It is proposed that this modest change in chemistry does not dramatically alter the deformation mechanisms of these open frameworks.

6.4.4 Anisotropy and maxima in GeO_2 zeolites

The maximum and minimum Poisson's ratio found anywhere in each zeolite framework are compared to the anisotropy of the crystal. As before the Ledbetter and Migliori[43] measure of anisotropy (A^*) is used and the results are compared graphically with a general cross-section of materials used by Lethbridge *et al.*[41] Figure 6.2 shows the results, where squares represent general materials, crosses represent GeO_2 polymorphs, blue points show maximum Poisson's ratios, and red points minimum Poisson's ratios.

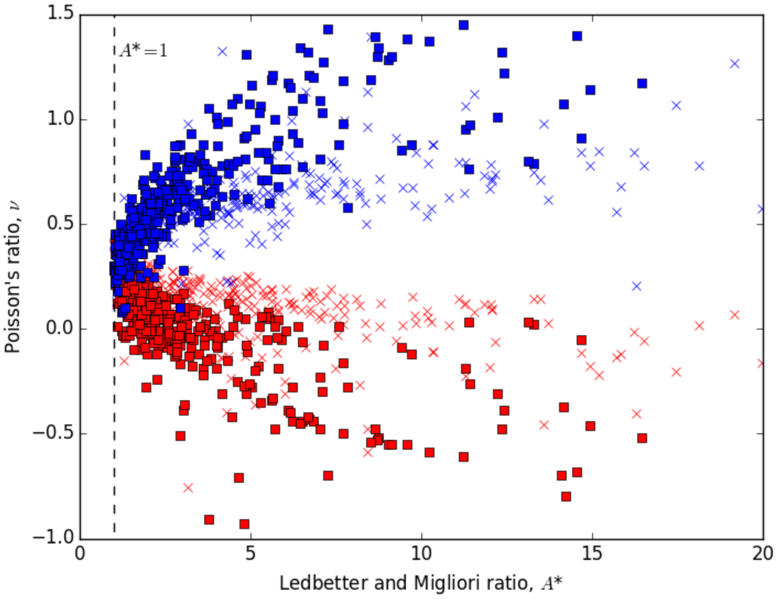

Figure 6.2 – The minimum and maximum Poisson's ratio vs the *A measure of anisotropy for both the materials from the Lethbridge *et al.*[41] study and the simulated GeO_2 zeolites. Squares represent the Poisson's ratios of general materials; crosses represent the Poisson's ratios of GeO_2 materials; blue squares give maximum Poisson's ratios; and red squares give minimum Poisson's ratios.**

The same trend observed before with SiO_2 structures, of an increased variation for Poisson's ratio at higher degrees of anisotropy, is also present within GeO_2 structures. However, like SiO_2 structures, the majority of extreme data fall within that of general materials. This indicates the Poisson's ratios found within GeO_2 structures are less varied than for general materials with a similar degree of anisotropy. The results for GeO_2 structures follow those for SiO_2 reasonably closely. This supports the suggestion that the chemistry of the zeolite structures makes very little difference to their elastic properties. This is encouraging for recreating these properties with similar structures either with a different chemical makeup or at different size scales.

6.4.5 Comparison between GeO_2 and SiO_2 structures

Due to the lack of experimental data for GeO_2 structures, along with the unreliable nature of some germania potentials, it is difficult to make reliable predictions on their general elastic properties. Some encouragement can be taken from the similarity between results obtained using the Sastre potential models for silicon and germanium. These potentials hold general agreement with specific cases and the auxetic typology percentages for all structures are similar. There are still a very limited number of auxetic materials identified with GeO_2 potentials but JST, the most auxetic material found with SiO_2 potentials, features prominently among these. From the limited data available it is suggested that the chemical composition of zeolite structures has much less of an effect on its elastic properties than the underlying structure itself, with the trends observed with silica being maintained in germania.

6.4.6 Future development of structures

As more elastic potentials are developed and more powerful computations become commonplace the properties of zeolites can be examined further. The structures such as α-cristobalite and JST have been shown to be auxetic with both SiO_2 potentials and GeO_2. However, the basic frameworks these represent can be made up of any tetrahedral forming material, and may be found to be auxetic for a wide range of chemistry.

For theoretical purposes it may be possible to construct artificial potential models which act on simulated materials which do not exist. Whilst these would hold no relevance to the creation of real materials, they could be used to help us understand the properties of specific frameworks. Additionally to this, finite element analysis, or mechanical testing could be applied to theoretical structures or macro sized models respectively. It is suggested that structures with interesting or auxetic behaviour at the microscopic level could have similar properties at a macro scale. This assumption is an over simplification of the complicated forces involved at atomic scales, but could be valid if the dominant mechanisms of the system are maintained.

Chapter 7: Triangular structures

7.1 Chapter Introduction

So far in our attempts to understand and explain the elastic properties of materials a few mechanisms have provided justifications for negative Poisson's ratios. One type of mechanisms which is often associated with zeolite structures is that of rigid units which have a fixed (or mostly fixed) size and shape, but which are relatively free to rotate within the overall framework. These rotating units are represented by geometric shapes, which are connected at corners, and repeated periodically to form a framework structure. The angles between units and the dimensions of the units themselves are often sufficient to produce analytically a measure of Poisson's ratio.[30]

In this context, a siliceous zeolite can be described as a framework of tetrahedra, formed by a central silicon atom surrounded by four oxygen atoms, where each tetrahedron connects to its neighbours at the corner oxygen atoms. In an idealized zeolite, these tetrahedra are rigid, and the corner-corner joints can rotate freely.[119] The tetrahedra are the rigid units which can rotate within the structure. These frameworks are clearly three dimensional, but it is sometimes possible to simplify the mechanisms to two dimensions. This can help to identify simpler explanations of the causes of auxetic behaviour, and also aid visualisation of the processes involved.

A variety of different units have been chosen for analysis in the past, and these units can be connected together in many different ways. The number of structures which can be produced by combinations of arrangements is particularly well highlighted by the zeolites frameworks. Even though they consist of only tetrahedral units, at the time of writing there are known to be 218 unique frameworks which are catalogued in an online database,[93] a number which is increasing every year. The aim of this chapter is to automate the process of creating a large number of two dimensional structures, in order to calculate their Poisson's ratios. In the interest of simplicity (after all this study serves chiefly for concept validation) and because they approximate well to two dimensional SiO_2 frameworks, only connected equilateral triangles are considered to build up the structures; non-equilateral triangles, squares and other shapes are not included.

With a method of producing a large number of structures and analysing their Poisson's ratios it should be possible to optimise the structures to find extreme values. Using genetic algorithms, a population of structures initially produced randomly, can be selected, mutated, and bred to produce new structures with possibly more extreme negative Poisson's ratios. The possible use of genetic programming techniques requires that each structure have a unique way of describing its creation and that breeding is possible between two structures. The software created to produce and analyse triangular network structures can then be used in conjunction with a genetic algorithm to produce structures with increased auxetic properties.

This chapter is essentially methodological. The first section is concerned with previously published geometric schemes, and is followed by a detailed exposition of the computational method used to generate 2D networks of regular triangles, and to extract Poisson’s ratios. As a demonstration of the method, the systems with two, four, six, and eight triangles are created systematically in order to examine which structures exhibit auxetic behaviour. Finally, I consider evolution of the techniques, to include future integration with genetic optimisation as well as description of 3D structures.

7.2 Background

7.2.1 Rotating rigid units

The negative Poisson's ratios found in the elastic properties of certain materials have been explained with several different mechanisms. Re-entrant honeycombs,[120] keyed brick structures,[1] and nodule-fibril[36] models have all been used to successfully identify and explain how particular structures behave, which can cause them to be auxetic. Of particular interest to the way in which SiO_2 structures (such as zeolites) deform, is the mechanisms involving the rotation of rigid, or semi rigid units.[121] These mechanisms model structures composed of units, usually with a fixed size and shape, and connected together periodically, with corner-corner joints which are free to rotate.[32] Variations of these mechanisms have been shown to exhibit auxetic behaviour for rigid squares,[29] rigid triangles,[30] and also semi-rigid units.[33] The Poisson's ratios associated with these mechanisms are often as low as -1 and uniform in every direction. The restriction in deformation for the units themselves leads to structures which are unable to shear,[32] a property associated with real auxetic materials.[122]

7.2.2 Rotating mechanisms in zeolites

Silicon dioxide frameworks such as zeolites form as corner-corner connected tetrahedra capable of existing in a large number of topological nets.[123] The increased flexibility of the Si-O-Si bonds when compared to that of the O-Si-O bonds allows for assumptions about the crystal deformations. For the purpose of indentifying mechanisms, the tetrahedra within zeolites can realistically be assumed to behave as rigid units, and the corner-corner joints (Si-O-Si bonds) can be treated as free to rotate. Whilst this ignores any deformation which may occur within the tetrahedra themselves, a mechanism causing auxetic behaviour, due to rotating units, is likely to mask other more subtle alterations within the structure.

7.3 Methodology of 2D Structure Creation

7.3.1 Software outline

The programming language Python was chosen to generate triangular structures in two dimensional space, and to calculate their Poisson's ratio. These structures can be created either randomly, systematically, or according to a pre-described recipe, with any number of internal triangles and periodic joints. By removing translation and rotation of the entire structure (by fixing one of the triangles) the Poisson's ratio can be calculated when there is only one free angle within the structure. More than one free angle will result in a many to one relationship between the angles within the framework and the lattice vectors of the crystal cell, and the structure will not be rigid. Conversely, if the structure is completely fixed then we must break our model, of rigid triangles connected with flexible joints, in order for any deformation to occur at all. To allow the created structures to be systematically and computationally analysed a ‘key’ describing each structure is generated. This key can be repeatedly used to always create an identical structure, serving as a machine readable identifier of a structure as well as a possible 'genome' when used in conjunction with a genetic algorithm.

The two dimensional structures are represented by a list of vertices, having either a known, fixed position, or an unknown range of positions. An additional list of triangles is stored as a set of three vertices, with an arbitrary vertex listed first, followed by the remaining two listed clockwise. This clockwise listing of vertices helps with traversing the structure when determining valid configurations. When a vertex is not fixed in space a locus is used to store the possible locations in which the vertex may exist whilst maintaining the rules of the structure, such as all triangles having unit length sides. For first order loci, where a vertex is attached to a fixed point, the locus represents an arc of a circle with unit radius, centred on the connected point and with bounds defined on creation. For second order loci, vertices with a connected non-fixed vertex between them and a fixed vertex, the locus represents a circular area, centred on the fixed vertex with a radius of two unit lengths. Other than defining the maximum distance away from a point a vertex can be, second or higher order loci do not limit the acceptable structure positions but can be reduced to first order or fixed once the structure becomes more defined. Figure 7.1 shows examples of three fixed vertices A_0, B_0, and C_0; two first order loci of vertices D_1 and E_1, which are connected to vertex A_0; and a second order locus of vertex F_2, which is connected to vertex D_1.

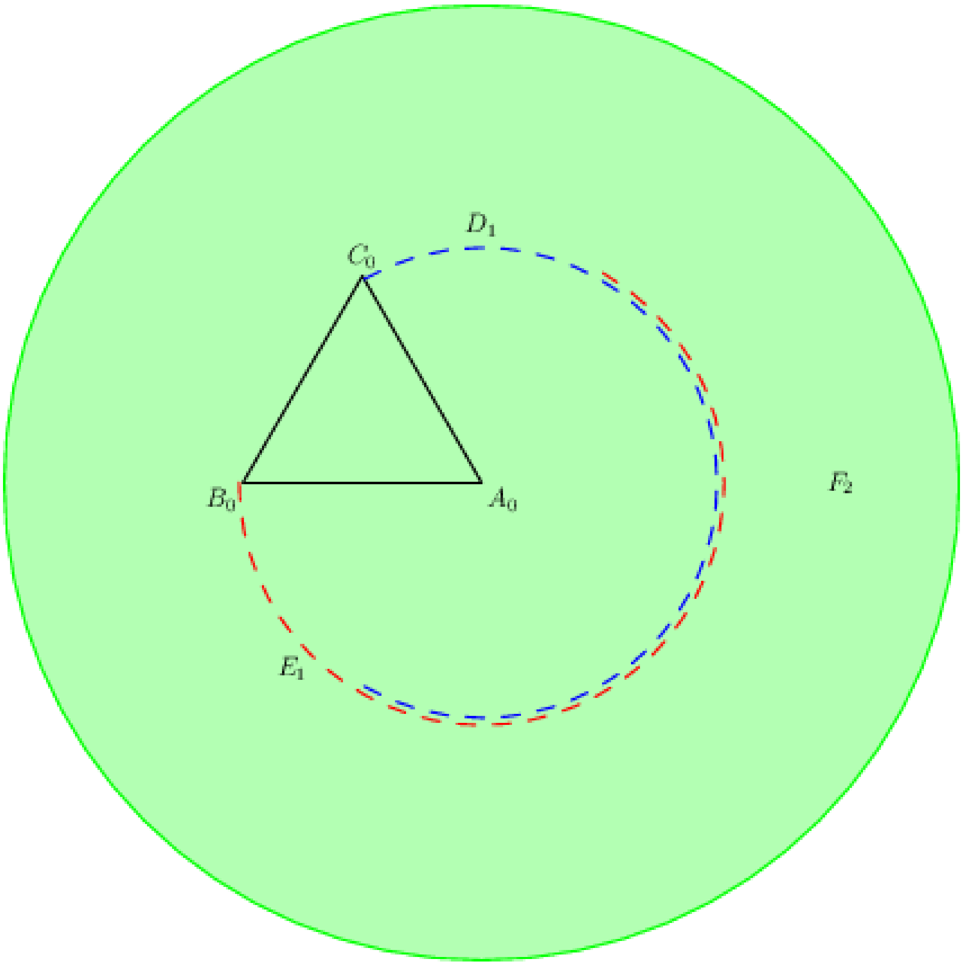

Figure 7.1 – Example of vertices with varying degrees of freedom, where N_x is the vertex *N* which has *x* degrees of freedom. The fixed vertices are A_0, B_0, and C_0 (at the corners of the triangle) which will always have this position; the loci with one degree of freedom are D_1 (blue loci) and E_1 (red loci) which can lie anywhere on their respective arcs (but are each dependant on the other); and the locus with two degrees of freedom is F_2 (green locus), which could lie anywhere within this area (provided it does not intersect existing triangles).

7.3.2 Creating a 2D network of triangles

The creation process begins with three vertices fixed in space as part of a central triangle. Two vertices are added to an available corner to simulate joining an additional triangle to the structure. Once a vertex is included in two triangles it is no longer considered available as a joining vertex, so as to maintain the analogy with hinge joints connecting only two triangles together. Further triangles are then added either systematically (if a range of structures are being explored), randomly (if a random structure is being created), or according to a pre-determined order (if a known structure is being created) until the structure consists of the desired number of triangles. When adding two vertices as a triangle the clockwise notation for vertices in a triangle is maintained. This is not only used to determine valid joints in second order or higher loci, but also affects the range of points which are defined by first order loci. As can be seen in Figure 7.1, the first order loci of vertices D_1 and E_1 are centred on the fixed vertex A_0 and form the triangle *ADE*. The first corners of *ADE* when moving in a clockwise direction from A_0 (clockwise corner) and in an anticlockwise direction from A_0 (anticlockwise corner) are D_1 and E_1 respectively. Similarly the clockwise and anticlockwise corners from A_0 in the triangle *ABC* are B_0 and C_0 respectively. When a first order locus for the clockwise corner D_1 is created, the limits of its range are defined by the anticlockwise corner of the triangle it is connecting to (vertex C_0) and a point in space 4π/3 radians (the range of movement for two connected equilateral triangles) clockwise from this corner. Conversely the locus of the anticlockwise corner E_1 has the limits of the vertex B_0 (the clockwise corner from A_0), and a point 4π/3 radians anticlockwise from B_0. The vertices contained within a triangle are stored clockwise sequentially from an arbitrary starting point (usually the first vertex created but not always, due to the possibility of later joins). This allows the clockwise corner V_c of a vertex V_n to be determined by the following relationship:

$$V_c = \mathrm{myTri}[\,(\mathrm{myTri.indexOf}(V_n) + 1)\ \%\ 3\,], \qquad (7.1)$$

where % designates a modulo operation to allow the first and last element of the triangle to loop around, myTri.indexOf(*x*) is the index of the value *x* within the triangle myTri, and myTri[*y*] is the y^{th} element of the triangle myTri. A similar relationship can be used to find the anticlockwise corner V_a

$$V_a = \mathrm{myTri}[\ (\mathrm{myTri.indexOf}(V_n) - \ 1)\ \%\ 3\ ]. \tag{7.2}$$

7.3.3 Joining triangles to form a framework: motif

Once the number of triangles reaches a desired value, or an adding sequence is finished, the structure is composed of linked chains of various lengths and generally has too much freedom for the Poisson's ratio to be found for all but the most trivial of cases. In order to reduce the freedom within the structure existing vertices must be joined to each other to close loops and reduce the possible range of movement.

To join two vertices, they first must both be determined to be available. This is done by checking that the number of triangles in which a vertex is present in is equal to one. To maintain the analogy with SiO_2 frameworks (where silicon atoms do not share more than one oxygen atom), joins will be forbidden between triangles which already share a joint at a different vertex. Within the network of triangles it is not possible to have a free vertex which can be found in only one triangle. Figure 7.2 shows the result of attempting to join vertices I_3 and C_0. As can be seen, if this joint were to be allowed vertex E_1 (part of the *BDE* triangle but no other) would be internal, and could not join to another triangle in future operations.

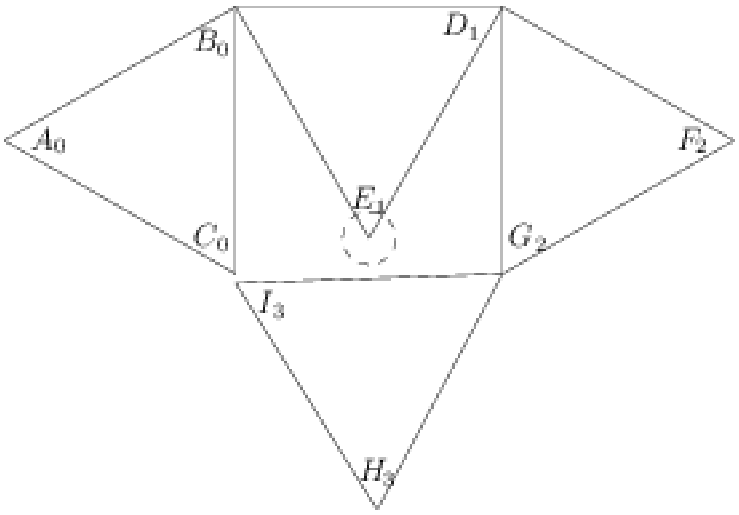

Figure 7.2 - Arrangement of a triangle structure with a, non-valid, free internal vertex

This free vertex is an analogy of an oxygen atom bonded to only one silicon atom, and does not form part of a stable framework. Vertices A_0, F_2, and H_3 are also only found within only one triangle, these being *ABC*, *DFG*, and *GHI* respectively. However, as these vertices are external[3], they are able to be either included in future joins, or used for periodical atoms when the structure is repeated, and are therefore acceptable.

The strict clockwise vertex notation within a triangle definition can be used to determine whether or not a closed ring contains a free vertex. When traversing a clockwise ring, such as in Figure 7.2, the anticlockwise corner from the current vertex is used to determine the next triangle to be examined. For this example (starting at vertex C_0 in triangle *ABC*) the anticlockwise corner is vertex B_0 and the next triangle *BDE*. However, when selecting the anticlockwise corner from B_0 within *BDE*, vertex E_1 is used, which has no other triangle associated with it to allow the

---

[3] Although it is impossible in this structure for vertex C to join with vertex I in an anti-clockwise ring as well as the clockwise ring shown in Figure 7.2, it is possible to have a chain of triangles with enough freedom to join in both directions (thus allowing both sets of vertices to be either internal or external). However, when this is the case no more than one of the directions may form a closed loop without internal vertices, and so there is never an ambiguity as to which way a join is made.

traversing to continue. If this termination of the loop occurs before the end vertex (I in this example) is located then the loop is invalid and a different join is attempted.

It is also possible to disallow joining based on the maximum lengths of both chains combined being less than the distance between the fixed points that these chains originate from. When each chain is examined, it can be seen that the joining loci is connected to another with fewer degrees of freedom. If a chain is followed far enough back it will always be found to be connected to a fixed point in space. The distance between the fixed points, associated with each chain, is calculated and used as a cut-off value to discriminate against joints that have a maximum length (the total number of connected vertices for both chains, multiplied by the length of one triangle side) less than that required to join the points with a straight line.

Once the joining vertices have been identified as valid the process of connecting them to form a new structure begins. At this stage it is still a possibility that the joint will be found to break specified conditions of the structure which are difficult to predict before attempting to create the joint. Because of this, the system state is saved and should the algorithm run into any inconsistencies during the joining process, the joint creation process will be abandoned and this saved system state will be returned.

The first stage in the joining process acknowledges that, once the joint is complete, the structure will have one vertex as a component of two triangles rather than two vertices found separately. The choice of which vertex to keep and which to remove is largely irrelevant provided the kept vertex has the correct properties once connected. The orders of the two loci are used to determine the order of the joint vertex where this is initially the lower of the two. If either of the two vertices is a fixed point, they have an order of 0, and the joint will be also be fixed. If both vertices are greater than 1, then the most defined point will determine the order of the joint loci. The only exception to this is when both loci are first order. When this occurs, the intersection between the first order loci is found using trigonometry and then fixed. Once the joint has been updated in the structure the change is cascaded down each chain. As the order of a locus depends on the number of triangle sides connecting it to the nearest fixed point in space, the order of any locus associated with a chain originating from the joint's pivot is compared to that of the existing locus order. Again, if there is a more restrictive order for this point available, then the definition for the locus is changed to match the newer, more restrictive definition. This can be seen in Figure 7.3, where vertex A_0 and vertex H_3 have been joined. The new order of vertex F_1 is one (pivoting from A_0) as this is lower than its original order of two (pivoting from D_1 and then B_0 in turn). The order of vertex D_1 remains constant, as a potential new order arising from a pivot at F_1, would increase its freedom rather than decrease it.

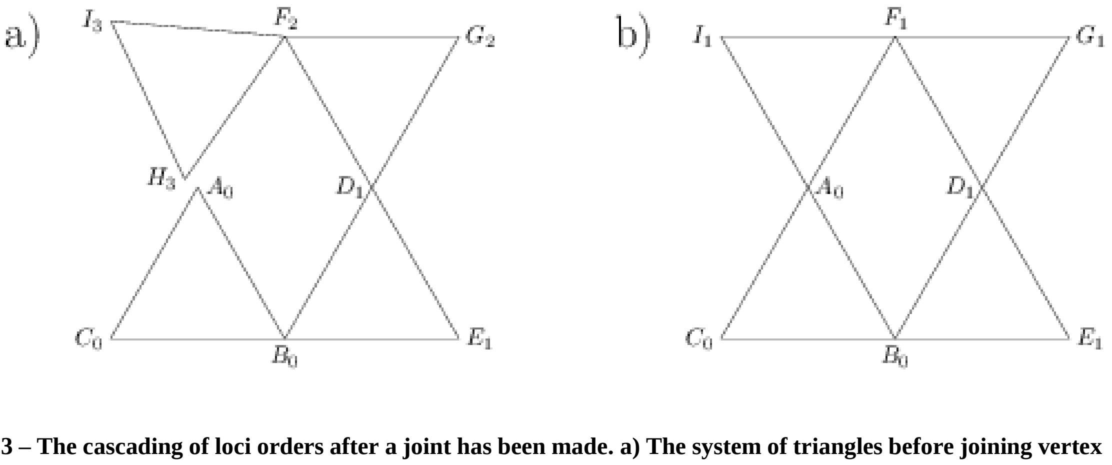

Figure 7.3 – The cascading of loci orders after a joint has been made. a) The system of triangles before joining vertex A_0 to vertex H_3, where the subscripts given are the order of the loci (i.e. A_0 and B_0 are fixed and D_1, F_2, and H_3 are first, second, an and third order respectively). b) The system of triangles after the joint has been made, where vertex H_3 has been removed and replaced with vertex A_0 in the now *FAI* triangle, and vertices F_1, G_1, and I_1 have a new order of one.

Furthermore, if the order of both the existing and new loci are equal to 1, this too becomes a fixed point in space, found by calculating the intersection of the two loci describing it. This cascading is a recursive process which propagates down each chain until the entire structure has been examined, and no further reduction in the degrees of freedom can be made.

Under certain conditions it is possible to create fixed rigid units within a structure of triangles which can behave as a single part of the framework. Figure 7.4 shows an example of an arrangement where, if A_0, B_0, and C_0 are fixed, although none of the vertices (D_1 to H_1) are yet fixed in space, they all depend on the position of the others within the unit. In this case, each locus can be represented as first order, with at a specified distance from the pivot vertex A_0.

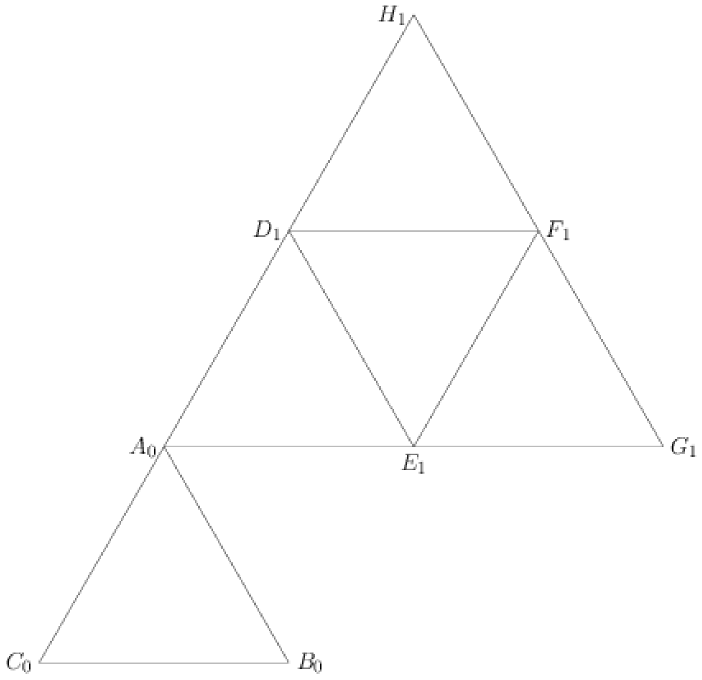

Figure 7.4 – An example of a rigid unit within a triangular structure. The larger triangle (*AHG*) is made up of the smaller triangles (*ADE*), (*EFG*), and (*DHF*). The specific arrangement allows no freedom between each of the smaller triangles and so the entire unit behaves as a single entity. If any vertex is changed, the entire unit is affected.

If a single vertex within a unit changes order, the entire unit will also change. In this case, if vertex G_1 was joined to a fixed part of the structure, vertices D_1, E_1, F_1, and H_1 would also become fixed.

7.3.4 Joining triangles to form a framework: Periodicity considerations

Within a crystalline material some bonds will be formed between atoms which are part of different unit cells. This is analogous to two vertices within a single unit cell forming a joint, but not having the same position. Instead, they remain a constant distance from each other, equal to the value of one of the lattice parameters (vectors representing the size of the unit cell). This simulates each vertex being connected to the image of the other which can be found in an adjacent periodic cell, but is not directly modelled within the structure. For the software to continue adding or joining triangles, both the periodically jointed vertices are designated as no longer free, and will take no further part in the alterations of the structure. If these are the only vertices which have been joined across this particular periodic boundary then the lattice parameter remains free to change, and is simply calculated by measuring the vector between the two. However, if a periodic joint for the direction in which the vertices are being connected already exists, the range of possible values for the lattice vector is calculated to identify if both joints can be satisfied by the same vector. Once the structure has been produced and the degrees of freedom reduced enough for the Poisson's ratio to be calculated, it is these lattice vectors, defined by the distance between periodically jointed vertices, which are used to determine the size and shape of the unit cell. Figure 7.5 part a) shows and example of periodic joints between atoms in the unit cell. The vector between vertex A and vertex C can be used to find one lattice vector, whilst vertices B and D can be used to find the other. Figure 7.5 part b) shows how these periodic vertices fit together to form a larger crystal structure.

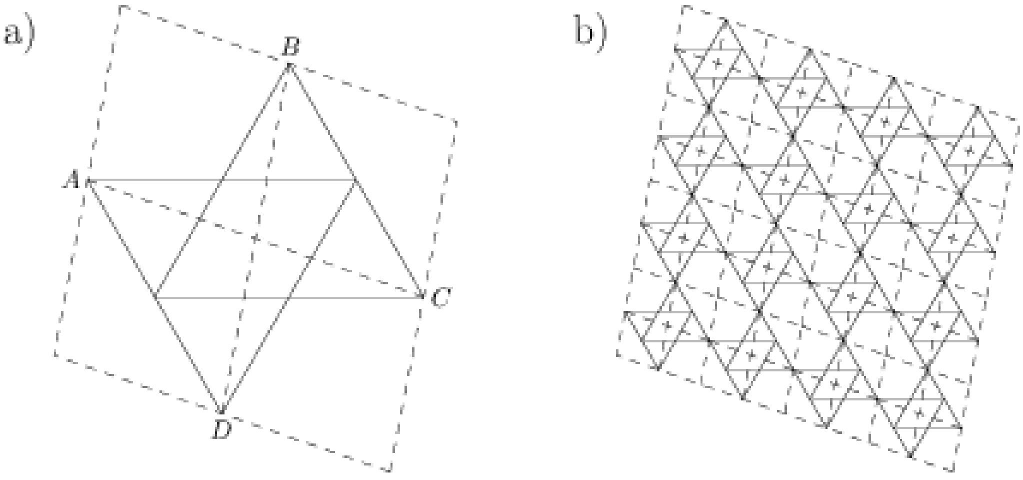

Figure 7.5 – The periodic joints between vertices. a) the lattice vectors defined by the vectors between vertex A and vertex C, and between vertex B and vertex D. b) the same structure repeated periodically, with the periodic vertices connected to the their corresponding jointed vertex in a neighbouring cell.

7.3.5 Creating structures manually, randomly, or systematically

Using the adding and joining algorithms it is possible to create two dimensional networks of connected triangles in a variety of ways. These methods are implemented within the structure creation software and allow a user to create a desired structure, or structure set, with relative ease. The three methods of creation are described as follows:

- **Manually:** A user selects a vertex (or pair of vertices) by index and chooses to join or add to the structure. This is useful if the desired structure is known and the user wishes to analyse the Poisson's ratio data, or simply view the framework orientation.

- **Randomly:** By selecting a target number of triangles to be found within the structure, the software is able to create a random arrangement which matches this. The process involves randomly adding a triangles to one of the free vertices available (until the correct number of triangles are present), then joining two random vertices which are able to form a valid link to reduce the degrees of freedom within the structure. This technique can be used to create complex arrangements of triangles which form valid structures, at a relatively low computational expense.
- **Systematically:** If every possible structure with a specified number of triangles is required then a systematic method of creating frameworks is required. This is done with a recursive algorithm which performs one choice of a list of possible actions and then continues to create the structure, only returning to a new choice once all possibilities have been exhausted further down the line. If the current structure passed to the algorithm does not yet have the required number of triangles a new one will be added. If it does then joints will be made until the degrees of freedom have been reduced sufficiently. Valid structures are compared topologically with those already created. If a new structure is found to be topologically similar to one found previously in the search (this can arise when the structure is identical but the triangles are found in a different order) the arrangement is rejected. This comparison works with exact copies of existing structures (cis), or with copies of flipped versions of existing structures (trans). The systematic algorithm quickly becomes computationally expensive with an increased number of triangles in the desired systems. To reduce some of the expense, steps are made to reduce the occurrences of topologically similar structures being

created. For example, the choice of vertex to join the second triangle to is irrelevant as all three vertices are identical. Similarly adding or joining to vertices which have a lower index than the one previously used is forbidden, as any structure created from this will have already been found.

7.3.6 Poisson's ratio calculations

For structures with only one degree of freedom the Poisson's ratio can be calculated by considering the periodic joints of the structure. By choosing a flexible bond angle (θ), and examining it over the extent of its range, the lattice vectors a and b can be found. Figure 7.6 demonstrates how the magnitudes of the lattice vectors can change dramatically with alterations of θ. Where a_1, b_1, a_2, and b_2 are the lattice vectors a and b, when θ is equal to 20° (θ_1) and 95° (θ_2) respectively.

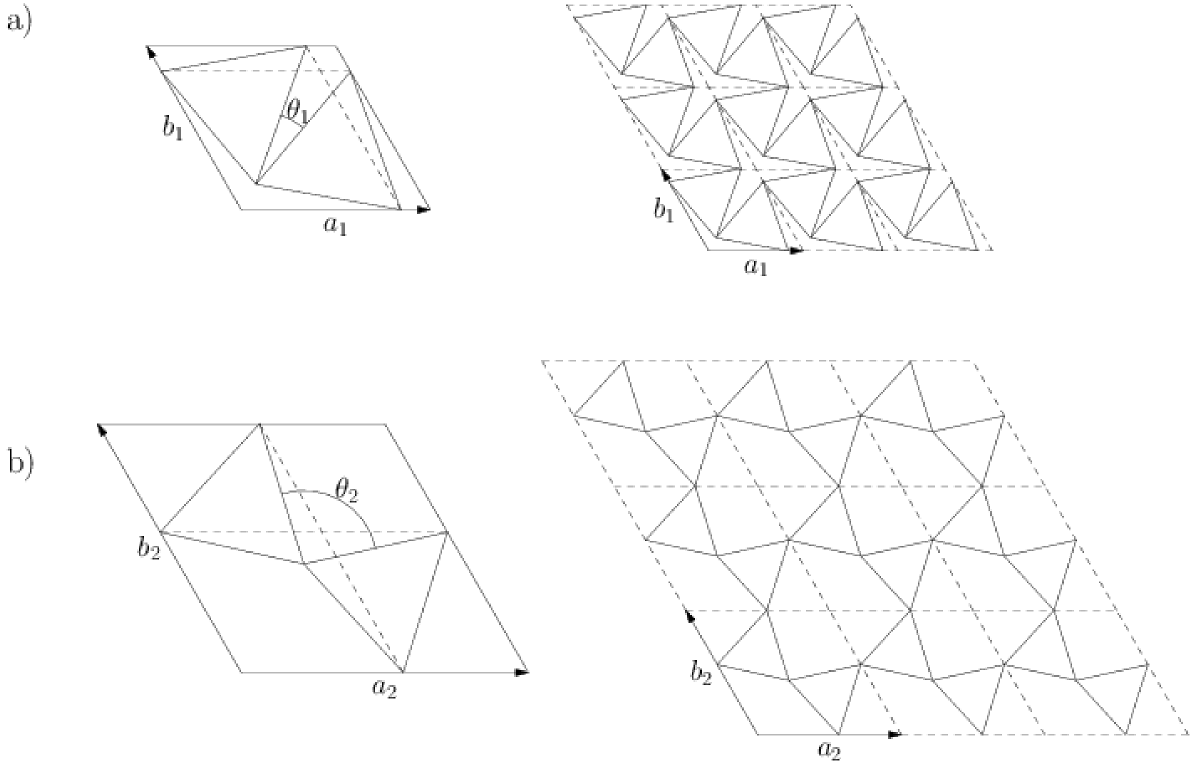

Figure 7.6 - The change in latice vectors as a result of a change in internal angle between the jointed triangles. a) The positions of the triangles, lattice vectors, and arrangment of the larger periodic structure when $\theta = 20°$. a) The positions of the triangles, lattice vectors, and arrangement of the larger periodic structure when $\theta = 95°$.

For this particular arrangement of triangles, examined in detail by Grima and Evans,[30] the Poisson's ratio can be found to be −1. This can be proved algebraically or by examining the geometry of the system. The algebraic proof first establishes a coordinate system where the x-axis is aligned with the lattice vector a, and the y-axis is perpendicular to this. The infinitesimal strains $d\varepsilon_x$ and $d\varepsilon_y$, are functions of the single variable θ and are identical, thus resulting in a Poisson's ratio of −1. The geometric proof arises from the aspect ratio of the unit cell remaining the same despite the magnitude of the vectors changing. When a system becomes uniformly larger or smaller the Poisson's ratio must be equal to −1.

With more complicated structures, this analysis becomes less trivial. Whilst it is still possible to obtain the Poisson's ratio from examining the geometric constrains alone, a more practical method is to directly use the structure creating software. By calculating the distance between periodically jointed vertices, and then deforming the structure with incremental alterations of θ, an approximation for the strains can be calculated at each point, and used to obtain the Poisson's ratio.

7.3.7 Limits on number of periodic joints

To calculate the Poisson's ratio for a structure using the above method, at least four periodic vertices are necessary (two for each unit cell vector). If there are any fewer periodic joints then the unit cell will have an undefined size and would not be able to form a periodic structure. It is possible to create structures with more than four periodically jointed vertices, provided they occur in pairs and do not conflict with other pairs which define the same cell vector. When creating a two dimensional unit cell, only two vectors are needed to fully define the unit cell. If a new periodic joint is created, the vector between the two jointed vertices must be equal to either of the existing cell vectors. For simplicity only structures with exactly four periodically jointed vertices will be considered in this work. This is sufficient for a proof of concept, as additional periodic joints can be examined in future iterations of the software.

The number of periodic vertices depends entirely on the number of triangles added to the system and the number of joints between triangles. Every joint removes two vertices from the list of those which are available to become periodic, whilst every additional triangle added to a structure adds one extra free vertex. An added triangle can be imagined as a completely detached triangle being entered into the system (an extra three vertices) which is then immediately joined with another (a reduction of two vertices), resulting in a net gain of one free vertex. Equation 3) outlines this relationship, where *f*, *n*, and *j* are the number of free vertices, triangles, and joints in the system respectively

$$f = 3n - 2j\,. \tag{7.3}$$

When *f* is equal to four $j = 1.5n - 2$, and (as both *j* and *n* must be integers) *n* must always be even.

7.4 Examples of 2D networks

7.4.1 Structures with two triangles

The simplest flexible structure which can be constructed from connected triangles has two triangles in the unit cell. This structure is the only possible arrangement (when limiting the number of triangles to two) and can be seen in Figure 7.6. As is discussed in Section 7.3.6, the Poisson's ratio for this structure is isotropic and equal to −1. For such a simple case, with an isotropic deformation, it is not necessary to use the created software for either the structure generation or the calculation of Poisson's ratio.

7.4.2 Structures with four triangles

As explained in Section 7.3.7, due to imposed constraints on the periodic joints, the number of triangles in a valid structure must be even. Systems of four triangles are realistically simple enough to analyse manually. However, they provide a useful validation of the structure generating software, which uses the same algorithms to find structures, and the Poisson's ratio of these structures, for more complex systems. Figure 7.7 and Figure 7.8 show the only two unique structures (named 4a and 4b respectively) which can be constructed with an arrangement of four connected triangles.

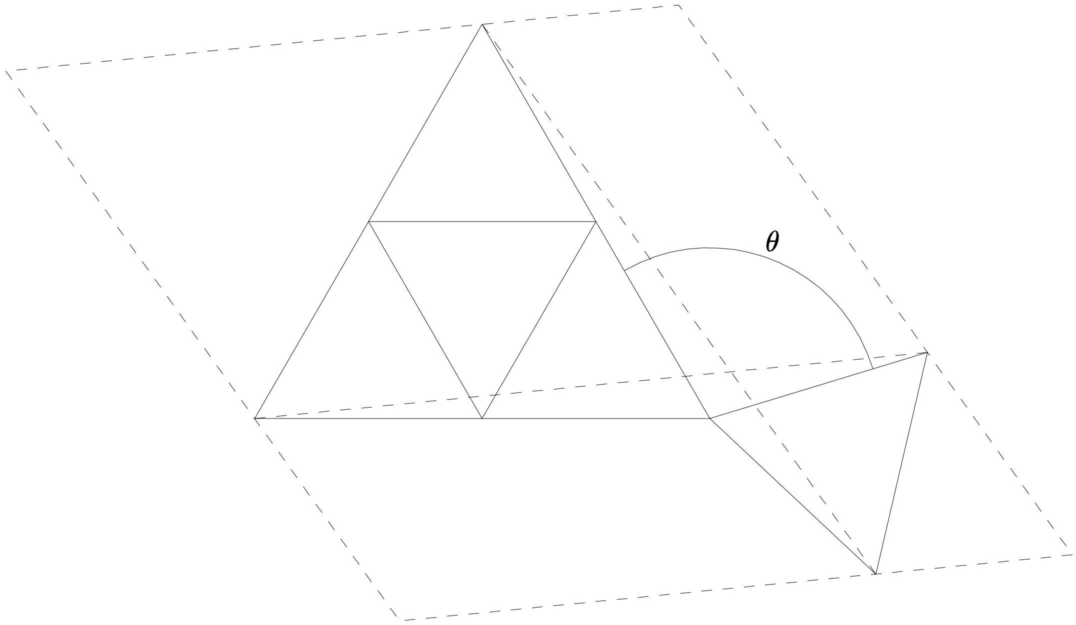

Figure 7.7 – The first of two possible structures of four connected triangles, with four periodic joints. This arrangement is designated as 4a.

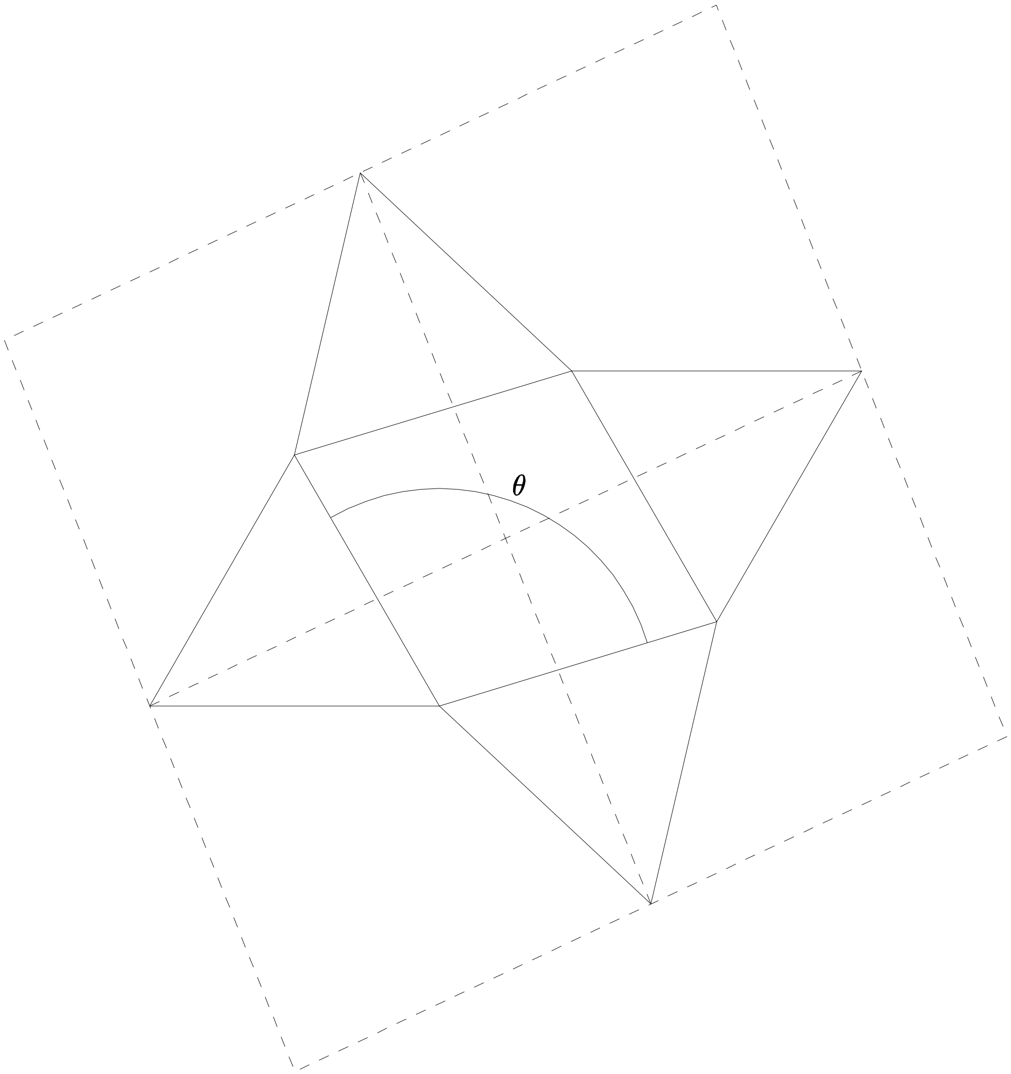

Figure 7.8 – The Second of two possible structures of four connected triangles, with four periodic joints. This arrangement is designated as 4b.

The Poisson's ratio of these two dimensional structures is directionally dependant on the axes chosen for the longitudinal and transverse strains. From the cell vectors, the length of any axis can be calculated by summing the contribution of both *a* and *b* in this direction, and hence the axis strain can be found when θ is incremented. For initial analysis of the Poisson's ratio, the longitudinal axis (x) and transverse axis (y), are chosen to be parallel and perpendicular to the *a* vector respectively.

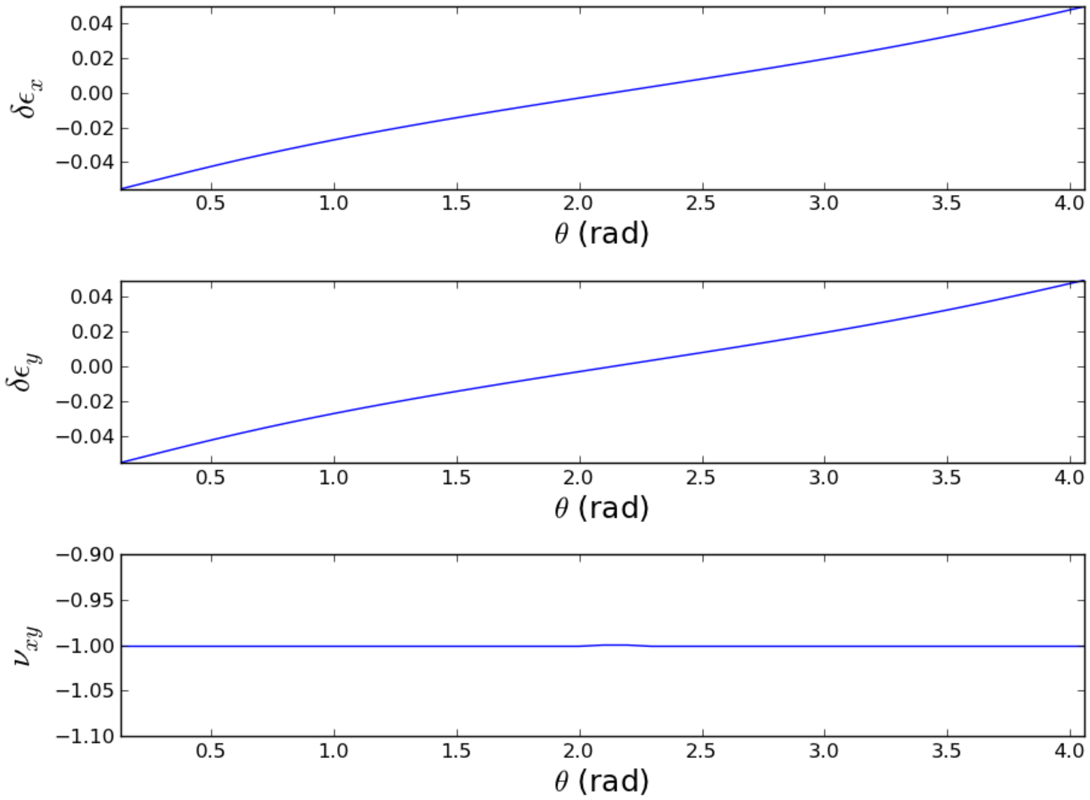

Figure 7.9 – The longitudinal strain $\delta\varepsilon_x$ (top), the transverse strain $\delta\varepsilon_y$ (middle), and Poisson's ratio ν_{xy} (bottom) of the four triangle structure 4a. With incrementally changing values of θ, the free angle within the structure.

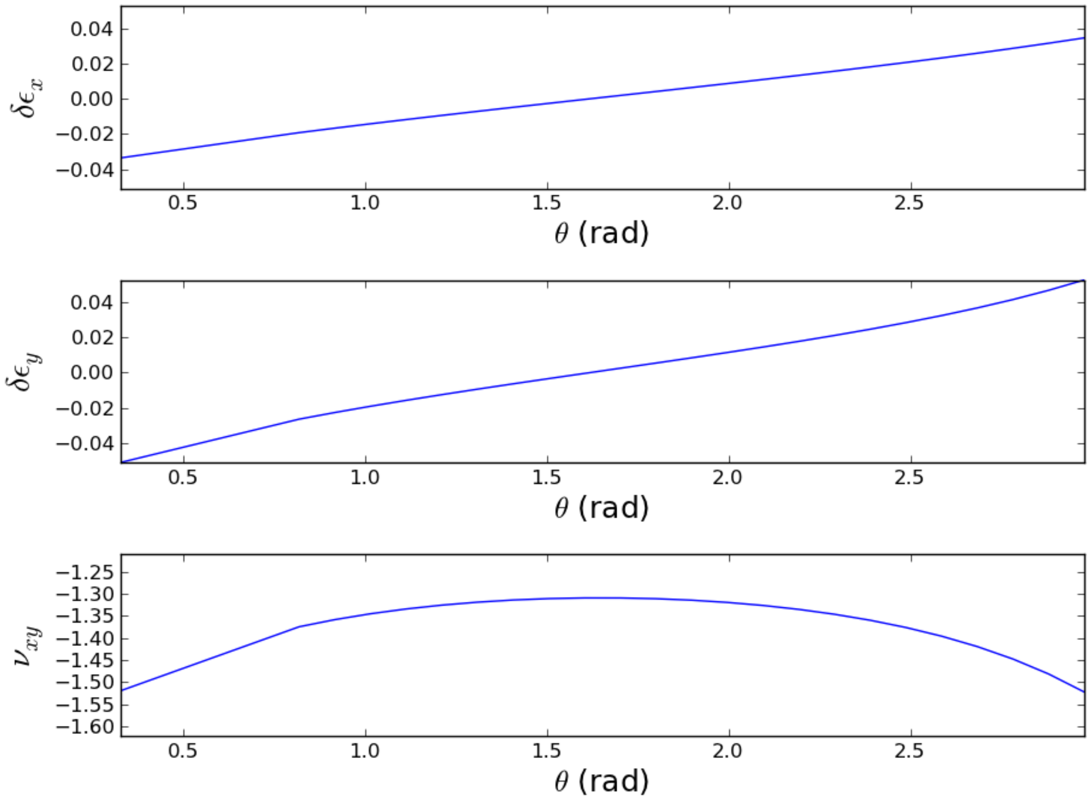

Figure 7.10 – The longitudinal strain $\delta\varepsilon_x$ (top), the transverse strain $\delta\varepsilon_y$ (middle), and Poisson's ratio v_{xy} (bottom) of the four triangle structure 4b. With incrementally changing values of θ, the free angle within the structure.

Figure 7.9 and Figure 7.10 show the strain and Poisson's ratio information for 4a and 4b structures respectively, with the lower section of each figure showing v_{xy}. The Poisson's ratio for both structures is entirely negative in the axes examined. Structure 4a is isotropically auxetic with a value of −1 throughout the range of θ used, as has been previously proved mathematically. Structure 4b however is anisotropic, with a maximum Poisson's ratio less than −1.3 when a periodic joint is chosen as the deformation axis x. For some values of θ the Poisson's ratios is as low as −1.5. These two formations of triangles suggest highly auxetic structures can be produced from simple triangular networks.

7.4.3 Structures with six triangles

By increasing the number of triangles included in the network to six, many more varied and complex structures can be produced. The vast majority of these are excluded as having either too many degrees of freedom, for the Poisson's ratio to be calculated from the structure alone, or too many periodic vertices. Given the constraints outlined in Section 7.3.7, there are only three unique structures of six triangles. These are shown in Figure 7.11, Figure 7.12, and Figure 7.13.

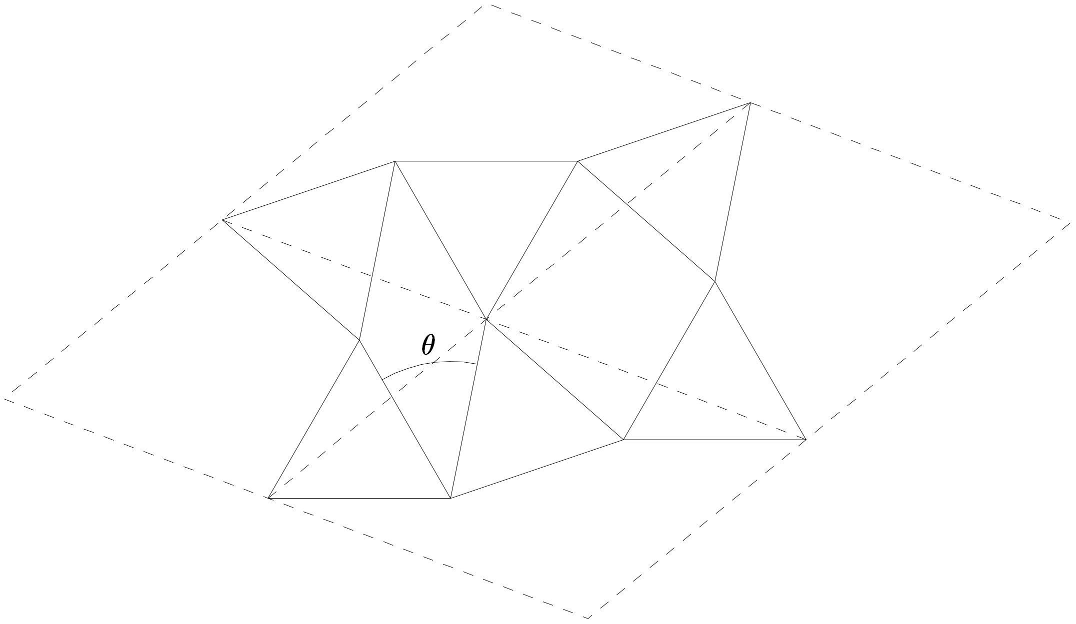

Figure 7.11 – The first of the three possible structures of six connected triangles, with four periodic joints. This arrangement is designated as 6a.

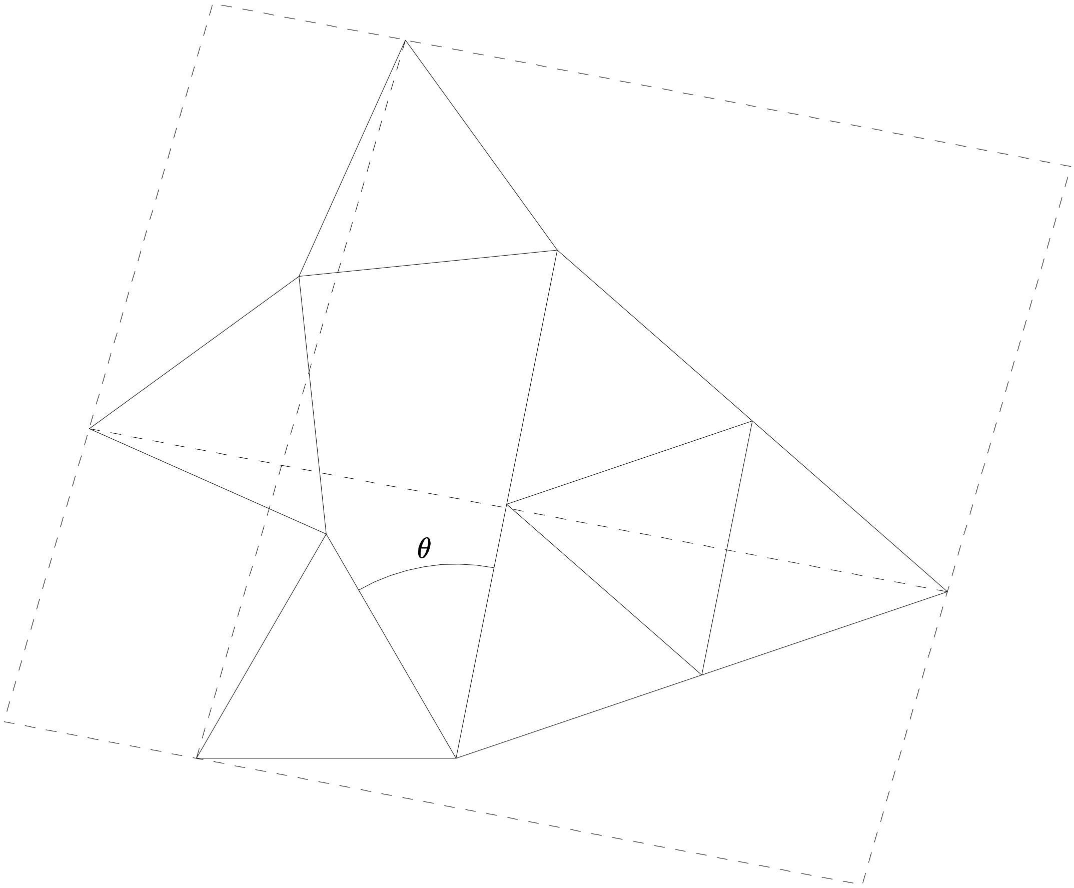

Figure 7.12 – The second of the three possible structures of six connected triangles, with four periodic joints. This arrangement is designated as 6b.

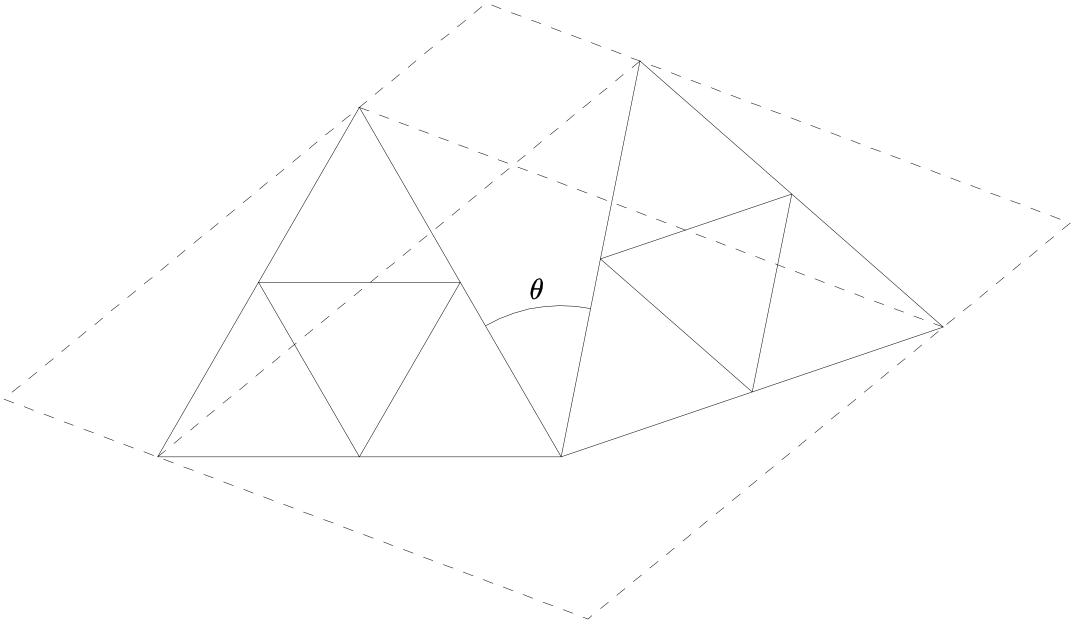

Figure 7.13 – The third of the three possible structures of six connected triangles, with four periodic joints. This arrangement is designated as 6c.

Similarities can be seen between the third structure (6c) and the simplest arrangement of two connected triangles. Each of the rigid units of three triangles, which have no movement within them, can be imagined as one larger triangle. By doing this the structure reduces to only two triangles, connected in the only possible arrangement. This explains the Poisson's ratio of −1, observed in the bottom graph of Figure 7.16 which, along with Figure 7.14 and Figure 7.15, describes the deformations within the six triangle structures.

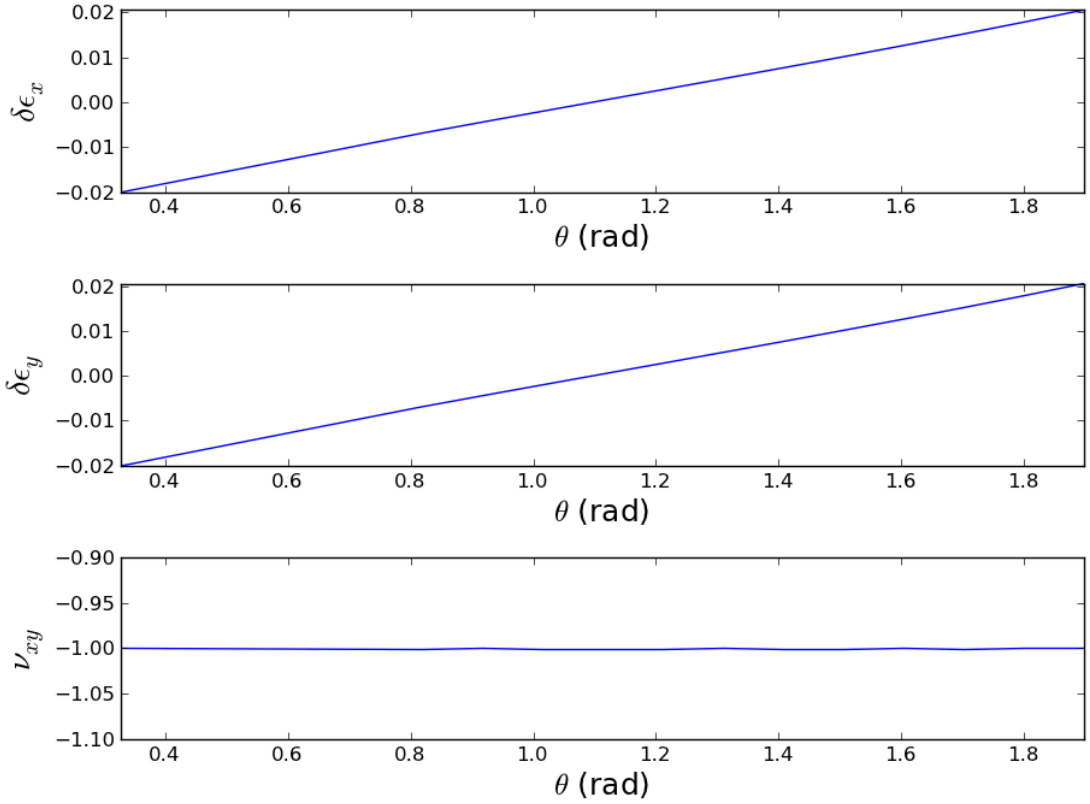

Figure 7.14 – The longitudinal strain $\delta\varepsilon_x$ (top), the transverse strain $\delta\varepsilon_y$ (middle), and Poisson's ratio v_{xy} (bottom) of the six triangle structure 6a. With incrementally changing values of θ, the free angle within the structure.

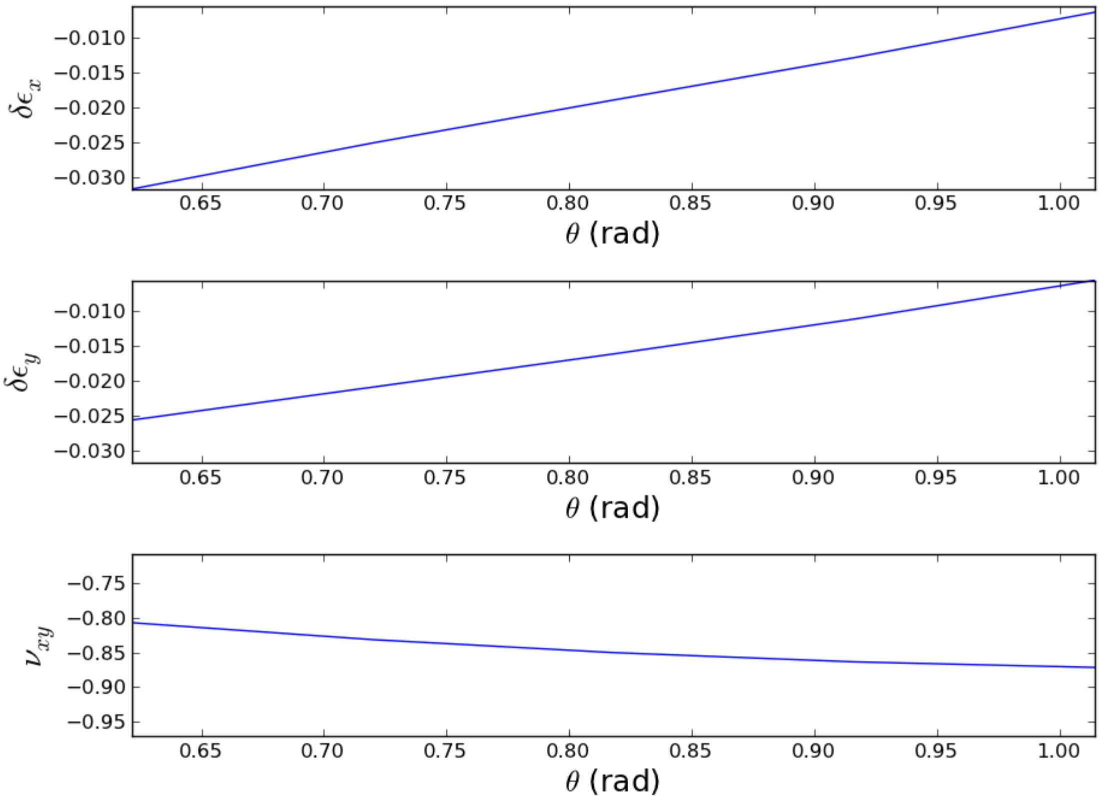

Figure 7.15 – The longitudinal strain $\delta\varepsilon_x$ (top), the transverse strain $\delta\varepsilon_y$ (middle), and Poisson's ratio ν_{xy} (bottom) of the six triangle structure 6b. With incrementally changing values of θ, the free angle within the structure.

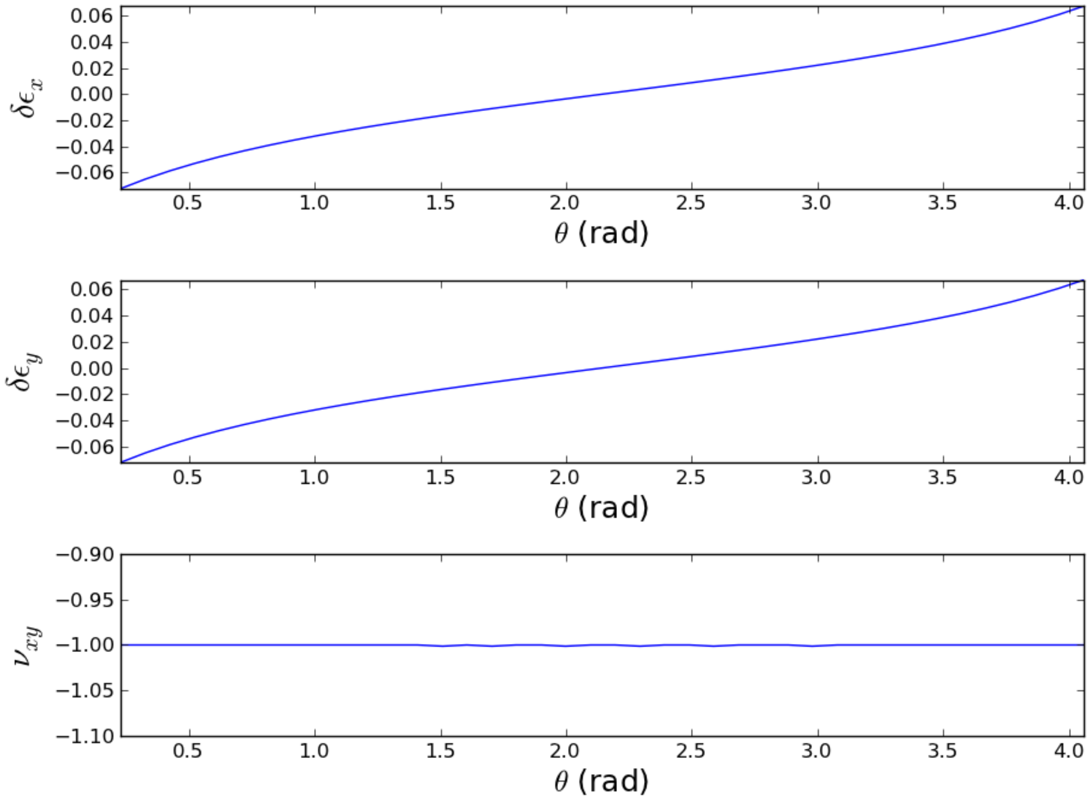

Figure 7.16 – The longitudinal strain $\delta\varepsilon_x$ (top), the transverse strain $\delta\varepsilon_y$ (middle), and Poisson's ratio ν_{xy} (bottom) of the six triangle structure 6c. With incrementally changing values of θ, the free angle within the structure.

Once more all structures are highly auxetic in the chosen directions; two of the structures are isotropically auxetic (those which are more regular), and one is anisotropic, exhibiting Poisson's ratios between −0.8 and −0.9. A hypothesis begins to emerge that all structures, composed of connected triangles with only one degree of freedom and four periodic joints, are auxetic. Whether isotropic or anisotropic, all structures so far examined have negative Poisson's ratios in the chosen axes, for all values of θ. It remains to be seen if this trend will continue to be displayed with larger and more complex structures, or with increased degrees of freedom or periodic vertices.

7.4.4 Structures with eight or more triangles

By increasing the solution set to structures with eight or more triangles, the permutations involved quickly increase the expense associated with systematic creation. Ever more of these structures are rejected on the basis of not meeting the specific requirements for degrees of freedom and periodic vertices. An example of a valid structure with eight connected triangles is given in Figure 7.17, with the associated deformation data given in Figure 7.18. This is one of only six possible unique structures with eight triangles. There are nine unique structures with ten triangles which fit the criteria for Poisson's calculation. In this work no Poisson’s ratio analysis has been attempted on the structures with 10 triangles, and no search has been performed to find the structures with 12 or more triangles.

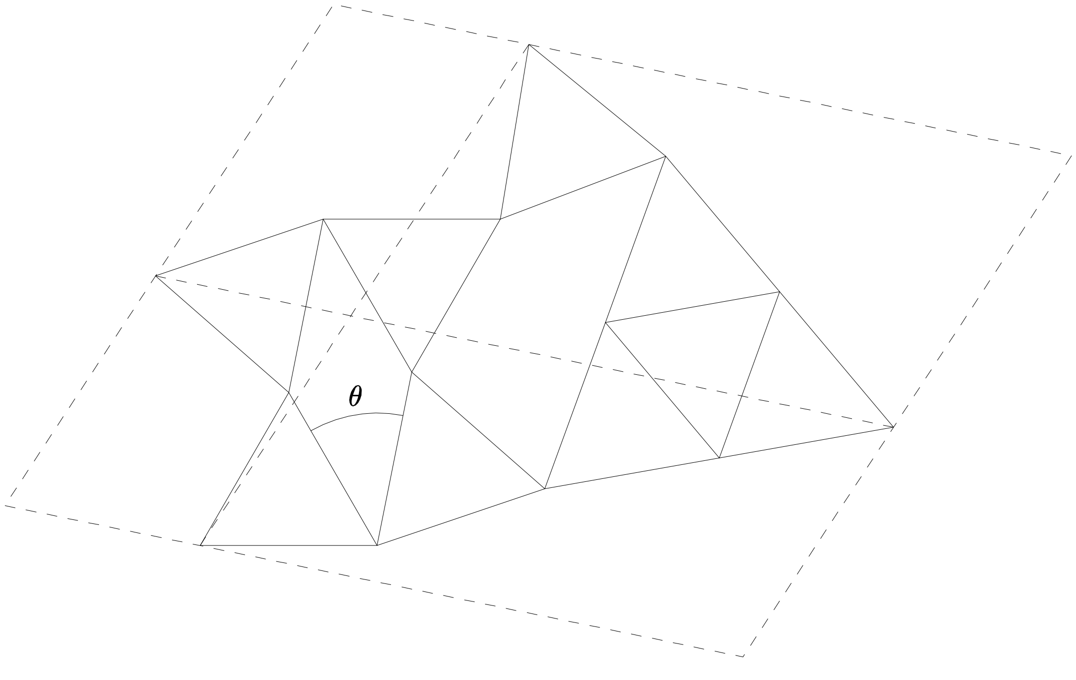

Figure 7.17 – One of six possible arrangements of triangles, when eight triangles are included in the structure.

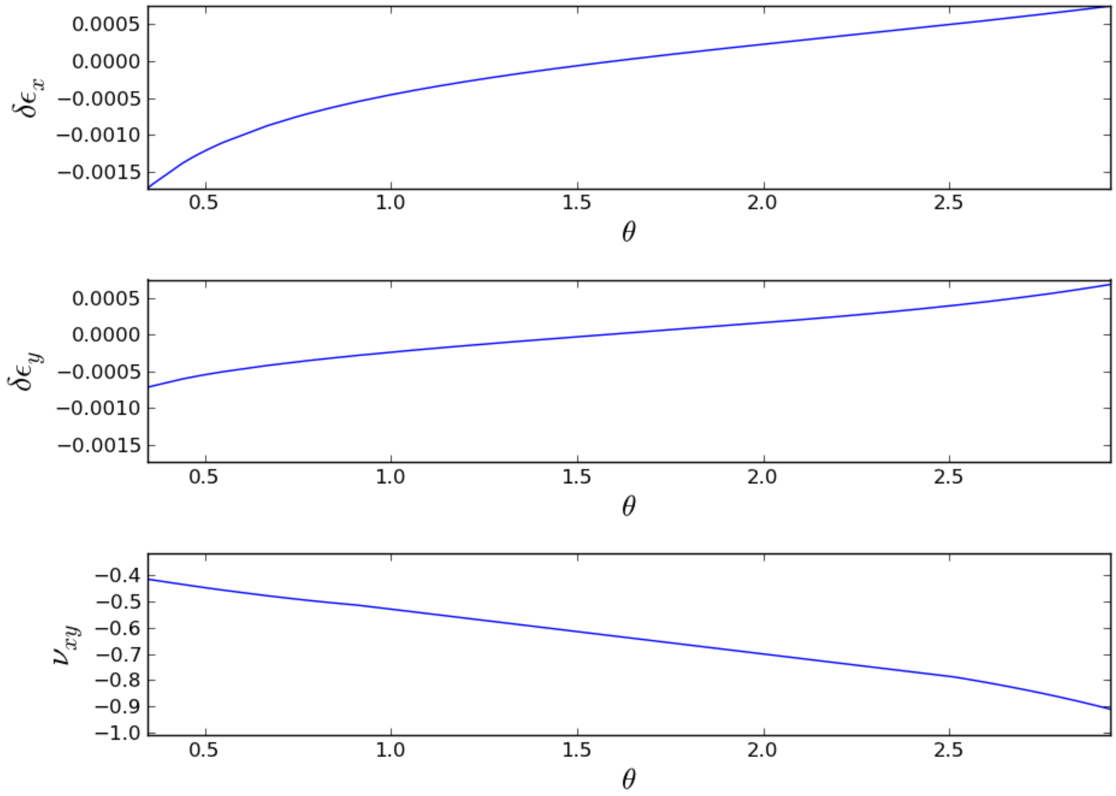

Figure 7.18 – The deformation data for the structure of eight triangles given above. As before the top, middle, and bottom graphs represent the $\delta\varepsilon_x$, $\delta\varepsilon_y$, and v_{xy} data respectively.

Following the familiar trend, this structure can be seen to display a negative Poisson's ratio. The Poisson's ratio varies from −0.4 to −0.9 for the *x* and *y* axis chosen for the calculations. So far no further structures have been used to calculate Poisson's ratio. It is thought that, as the complexity increases, the tight restrictions on degrees of freedom and periodic joints will force rigid units to be found within the valid structures, as in the example of 6c. This is supported by five of the six structures with eight triangles having at least one arrangement of three triangles connected together to form one larger similar triangle. In order to remain valid for Poisson's ratio calculations, it is expected that complex systems will have constraints which approximate them to simpler systems.

7.5 Conclusion and future development

The software for creating and examining two dimensional structures has been shown to produce meaningful results when limitations on degrees of freedom are imposed (all software created is given in the supplementary data for this work). Creation of multiple structures with a desired number of triangles is possible, enabling Poisson's ratio calculations on a wide range of triangular frameworks. The systematic production of structures, with two, four, six, and eight triangles in the unit cell, has shown a high level of auxeticity present in frameworks of this type, where rigid triangles are connected at perfectly flexible hinged joints. This supports the continued use of the software with more complex structures, to further examine their auxetic nature.

The following development suggestions could provide methods of improving the range of structures able to be examined, to allow a greater understanding of how hinged rotating units behave in a connected framework.

- **Increased number of periodic joints:** The limits imposed on number of free vertices in the final structure allow for only four periodic joints to be present. Whilst this reduces the solution set for the structures examined (thus reducing computational expense) this restriction eliminates frameworks for which the Poisson's ratio could be calculated. With four periodic joints the choices of vertices for the *a* and *b* vector are trivial, provided they alternate when traversing around the outside of the structure. However, with six or more periodic vertices (they must always exist in pairs) there become multiple options for the cell vector choices, further increasing the complexity of the problem.

- **More degrees of freedom:** There may only be one degree of freedom within the structure for the Poisson's ratio to be calculated from geometric analysis alone. To increase this freedom, more realistic models of the bonds between triangles must be included, moving away from a perfectly flexible hinged model, and towards a force field model for optimisation. The simplest method of achieving this would be to set optimum bond angles and create a series of spring forces within the structure, allowing for the Poisson's ratio to be calculated from small deformations around the lowest energy configuration. More complex approximations to atomistic bonding could be included to describe the repulsive forces between vertices; on the other hand this would reduce the value of having a simple geometric model of the structure.
- **Different geometry:** the software can be readily modified to follow the same process with units of different sizes and shapes. Non-equilateral triangles or those with a varying size could be used along with other polygons such as squares to create a structure. This diverges from the original analogy to SiO_2 frameworks but could provide value to aid understanding of flexibility in complex hybrids such as Metal-Organic-Frameworks.
- **Three dimensional structures:** The obvious progression from the two dimensional model would be to develop tetrahedral frameworks in three dimensions, exactly analogous to SiO_2 materials. This is a considerably more difficult task than creating the two dimensional software. Furthermore, with increased dimensions the freedom within the structure is also increased, with the added possibility of rotation around the joints as well as hinging. After the freedom of a three dimensional structure has been reduced as much as possible, a force field model may still be required for the Poisson's ratio to be

calculated. It is unclear at this stage whether the benefits of a purely geometrical model of SiO_2 structures could be beneficial over existing methods of elastic property calculation. However, software to systematically suggest tetrahedral networks could well provide new unexplored systems. This could work in a similar way to the two dimensional program, adding tetrahedra at available vertices (this time in three dimensions) and then joining free tetrahedra together. The additional degrees of freedom are likely to complicate the majority of the process, with valid positions of intersections, validity of loops, and periodic joins no longer trivial problems to overcome.

- **Genetic programming:** Through the use of genetic programming it will be possible to optimise a structure's Poisson's ratio, and find new frameworks which have extremely auxetic properties. The software would use genetic techniques to select and breed from a population of structures, with fitness functions designed to select structures with highly negative Poisson's ratios. Whilst the structures created with the current software are described with unique genomes, there is currently no method of mixing two structures and ensuring the properties of the parents are passed on to the child. This is a fundamental requirement of genetic techniques and without it there can be no such optimisation of properties. A possible solution lies in a hierarchical tree description of a structure rather than as a sequence of adding and joining. This description would ideally map the structure with no differences arising from a varied creation order.

Chapter 8: Conclusion

8.1 Synopsis

In this thesis, I have advanced the understanding of auxeticity: by developing a more accurate way to class materials exhibiting the property, by carrying out high-throughput atomistic simulations of frameworks materials based on the SiO_2 and GeO_2 chemistries, and by exploring mechanistic models and possible correlations with the density of plane.

8.1.1 Typology of auxeticity

My first effort has been to establish a system of typology to classify the auxeticity of materials. This system is outlined in detail in Chapter 3, where the criteria for each classification are given. The typology is applied to a large database of well-known materials which gives a demonstration of its identifying, descriptive, and comparative benefits. The extent to which α-cristobalite's elastic properties differ from the 'usual' is highlighted well. Future studies of auxetic materials will be able to make good use of the system in order to simplify comparisons and remove ambiguity in descriptions.

8.1.2 Atomistic modelling

Using a wide range of force-field potential models, the elastic properties of many zeolitic silica structures have been calculated, and are discussed in Chapter 4. These simulations confirm that there exist a relationship between the extremes of Poisson's ratio and the anisotropy of a material. On the other hand, and somewhat unexpectedly, zeolites are not found to be more auxetic than reference materials. Although the auxeticity of silica polymorphs is generally less than that of α-cristobalite, at least one structure, JST, has been suggested as being even more auxetic. It is even shown by some potential models as being isotropically auxetic, or 3C using the typology nomenclature introduced in Chapter 3.

Following the simulation of silica materials in Chapter 4, the calculated elastic properties of their germanium dioxide polymorphs are discussed in Chapter 6. With fewer potential models available and a severe lack of experimental results for comparison, the validity of these simulations is less conclusive. However, the properties predicted for the GeO_2 structures appear very similar to that of SiO_2 with the same framework. This strongly supports the need to identify chiefly “geometric” triggers for auxeticity (as opposed to “chemical”, based on the nature of the bonds).

8.1.3 Mechanistic origins of auxeticity

The relationship between the varying density of planes through a structure and the Poisson's ratios relative to these planes is explored in Chapter 5. Despite a thorough examination, for many different longitudinal and transverse directions, with both parallel and perpendicular planes, no correlation is found. The differences between the Poisson's ratios of materials with identical chemistry is shown to be unrelated to the way in which plane density varies, otherwise described as the periodicity of the crystal in a specific direction. Although the density variation cannot be used as an indicator for interesting auxetic properties, the initial hypothesis, that geometric properties (as opposed to a material's chemistry) are the primary contributors to Poisson's ratio, remains valid. Currently, explanations for the negative Poisson's ratio of some materials have been given using specific deformation mechanisms. If a systematic way to predict these mechanisms were developed, without the need for human interpretation, the search for auxetic structures could be greatly accelerated.

In an attempt to isolate the chemical and geometric contributions to Poisson's ratio, structures of corner sharing triangles (systematically and exhaustively generated) are analysed in Chapter 7. These structures represent a two-dimensional approximation to the tetrahedral frameworks of both SiO_2 and GeO_2 materials. Unit cells with increasing number of unique triangles are created and then the cell parameters under different deformations are calculated. Previous work had identified triangular structures with a negative Poisson's ratio[30] but it is now shown that for all structures studied[4] this auxeticity is present. The deformations in the structures are limited to corner rotations only with no allowed dilation of the triangles which may be the origin of the negative Poisson's ratio. I developed a software that can produce a number of different structures with 4, 6, and 8 triangles in the unit cell. However, the systematic approach employed is capable of creating much larger structures, for which there exist more unique arrangements (finding all of these comes at increased computational expense). This preliminary work only scratches the surface of the systematic production of frameworks.

8.2 Further work

Extensions of the work carried out during my PhD could follow three strands:

- Additional atomistic modelling
- Further development of the automatic generation of connected structures

---

[4] For simplicity the solution set of structures is limited to a small number (up to 8) of purely equilateral triangles and a specific number (2) of periodic joins.

- Experimental determination of elastic constants of physical models

8.2.1 Further atomistic modelling

The JST framework is very intriguing, as its properties, specifically 3C behaviour, are unique among crystals. Further examination of the JST structure would be desirable, with particular focus on the mechanistic origin of its exceptionally auxetic qualities.

The relationship between different chemistry and its effect on elastic properties could be further explored by examining a more varied range of materials, both those forming tetrahedral networks, but also those which do not. Among the former class of materials, $AlPO_4$ type frameworks would be good first candidates.

8.2.2 Development of connected structures software

For comparison with actual materials, three-dimensional structures would need to be produced; based at first around tetrahedral. Different rigid bodies, or combinations of different rigid bodies, could also be explored. Corner-sharing tetrahedra found systematically could be added to the ever expanding list of known zeolite structures and, if the right conditions are met, used to approximate elastic properties of materials where the dominant mechanisms are rotational.

One of the main attractions of the scheme I have developed is that it could be used to optimise the auxeticity of a starting structure, using methods such as Genetic Algorithms or Simulated Annealing.

8.2.3 Physical frameworks

In order to further test the competing effects of geometry vs chemistry, it would be possible to produce actual macroscopic models of the most interesting structures, chiefly α-cristobalite and JST, and to measure their Poisson's ratio directly. This would require great care. Figure 8.1 displays the early model of α-cristobalite that I intended to use as such during my PhD. Unfortunately, the data were inconclusive and with sufficiently high uncertainty as to preclude their inclusion in the final thesis. Actual physical measurement of the elasticity of such structure is undeniably difficult but certainly possible given appropriate resources. As an intermediate step, Finite Element modelling of the most promising structure would be enlightening, but it is also fraught with technical challenges.

Figure 8.1 - A macro scale model of α-cristobalite being tested under compression.

8.3 Key findings

I have designed a typology for auxetic materials, classifying materials with distinctions in the number of axes where a negative Poisson's ratio can be found, and the degree for which each axis is auxetic. The system has been demonstrated as a tool for comparing groups of materials and their auxetic properties, and the benefits of distinguishing between levels of auxeticity have also been explored, further highlighting the extraordinary properties of α-cristobalite.

The elastic properties of a large number of pure silica and pure germania zeolite frameworks have been calculated and classified with the proposed typology. After comparison of the auxetic classifications with a general database of materials, the zeolites are shown to be marginally more auxetic, but follow the same trends. I found that the JST frameworks has great potential for complete auxeticity, and have proposed an explanatory mechanism.

I have shown that there is no relation between the variation of density and the occurrence of auxeticity.

Finally, I have developed a scheme to generate periodic structures of interconnected triangles and calculate their Poisson's ratio.

Appendix A

Table A 1 – The atomic charges for silicon cores, oxygen cores, and oxygen shells used in the interatomic potential models for SiO_2.

Potential	Charges		
	Si_c(e)	O_c(e)	O_s (e)
Gale	+4.0	+0.86902	−2.86902
PMM08	+2.7226	+1.191981	−3.28111
Sastre	+4.0	+0.870733	−2.870733
SC1	+4.0	+0.86902	−2.86902
SLC	+4.0	+0.8482	−2.8482
SS96	+4.0	+1.06237	−3.06237
SS97	+4.0	+1.22858	−3.22858
AHCM	+2.4	−1.2	
BKS	+2.4	−1.2	
JA	+2.05	−1.025	
JC	+4.0	−2.0	
PMM06	+2.4	−1.2	
TTAM	+2.4	−1.2	
Vessal	+4.0	−2.0	

Table A 2 – The parameters of the two-body interactions used by the interatomic potential models for SiO_2.

Potential	Buckingham				Spring
	A(eV)	ρ(Å)	C(eV Å^6)	r_c(Å)	k(eV Å^{-2})
Gale					
Si_c-O_s	1277.514	0.32052	5.9062	12.0	
O_s-O_s	22764.000	0.14900	27.879	12.0	
O_c-O_s					79.074
PMM08					
Si_c-O_s	8166.2632	0.193884	0.0	12.0	
O_s-O_s	15039.909	0.227708	0.0	12.0	
O_c-O_s					256.71027
Sastre					
Si_c-O_s	1315.2478	0.317759	10.141118	12.0	
O_s-O_s	22764.0	0.149	10.937044	12.0	
O_c-O_s					75.96980
SC1					
Si_c-O_s	1824.2944	0.289798	0.0	10.0	
O_s-O_s	2046.0422	0.134015	14.027	12.0	
O_c-O_s					74.92
SLC					
Si_c-O_s	1283.9073	0.32052	10.6616	10.0	
O_s-O_s	22764.0	0.1490	27.8790	12.0	
O_c-O_s					74.9204
SS96					
Si_c-O_s	1550.95	0.30017	0.0	10.0	
O_c-O_s					112.7629
SS97					
Si_c-O_s	1612.45920	0.29955	0.0	10.0	
O_c-O_s					122.47853
AHCM					
Si_c-O_c	17796.1	0.2049	135.4	12.0	
O_c-O_c	1305.9	0.3594	196.1	12.0	
BKS					
Si_c-O_c	18003.7572	0.205205	133.5381	12.0	
O_c-O_c	1388.7730	0.362319	175.0	12.0	
JA					
Si_c-O_c	17796.1	0.2049	135.4	12.0	
O_c-O_c	1305.9	0.3594	196.1	12.0	
JC					
Si_c-O_c	1584.167	0.32962	52.64511	12.0	
O_c-O_c	22764.0	0.149	27.88	12.0	
TTAM					
Si_c-O_c	10721.522	0.20851	70.7345	12.0	
O_c-O_c	1756.8710	0.35132	214.7376	12.0	
Si_c-Si_c	872356662.2	0.0657	23.30007	12.0	

Vessal				
Si_c-O_c[5]	1005.1563	0.3277	25.0	7.6
O_c-O_c[6]	4978496.9	0.149	52.12	7.6
	Morse			
	De(eV)	a(Å^{-1})	r_0(Å)	r_c(Å)
PMM06				
Si_c-O_c	0.340554	2.006700	2.10	12.0
O_c-O_c	0.042395	1.379316	3.618701	12.0

Table A 3 – The parameters of the three-body interactions used by the interatomic potentials for SiO_2. All cut-off values are given in Å.

Potential	Urey-Bradley											
	K(eVÅ^{-2})	r_0(Å)	r_{12}	r_{12}	r_{12}							
Gale												
O_s-Si_c-O_s	2.30273	2.43352	2.8	2.8	2.8							
	Harmonic					Vessal						
	k(eVrad^{-2})	θ_0(deg)	r_{12}	r_{13}	r_{32}	k(eVrad^{-2})	θ_0(deg)	ρ_1	ρ_2	r_{12}	r_{13}	r_{23}
Sastre												
O_s-Si_c-O_s	1.2614	109.47	2.0	2.0	2.4							
SC1												
O_s-Si_c-O_s	2.0972	109.47	1.8	1.8	3.2							
Si_c-O_s-Si_c						729.0189	144.0	0.328	0.328	2.9	2.9	2.9
SLC												
O_s-Si_c-O_s	2.097	109.47	1.8	1.8	3.2							
SS96												
O_s-Si_c-O_s	0.18397	109.47	1.8	1.8	3.2							
SS97												
O_s-Si_c-O_s	0.144703	109.47	1.8	1.8	3.2							
AHCM												
O_c-Si_c-O_c						729.0189	109.47	0.328	0.328	2.9	2.9	2.9
JA												
O_c-Si_c-O_c						729.0189	109.47	0.328	0.328	2.9	2.9	2.9
JC												
O_c-Si_c-O_c	4.5815	109.47	1.8	1.8	3.2							
Vessal												
O_c-Si_c-O_c						729.0189	109.47	0.328	0.328	2.9	2.9	2.9

---

[5] The Vessal potential implements a four term Buckingham potential with r_1, r_2, and r_3 having values of 1.5, 2.5, and 3.5 Å respectively for Si_c-O_c bonds.

[6] The r_1, r_2, and r_3 values for O_c-O_c bonds in the Vessal potential are 2.9, 3.6, and 4.2 Å respectively.

Appendix B

Table B 1 – Potential parameters for the two-body and three-body interactions of the GeO_2 potential models

Potential	Charge	Buckingham				Spring
	Q (e)	A (eV)	ρ (Å)	C (eVÅ^6)	r_c (Å)	k (eVÅ^{-2})
Woodley						
Ge	+4.0					
O_c	−2.0					
Ge-O_c		3703.725	0.2610	0.0	10.0	
O_c-O_c		25.410	0.6937	32.32	12.0	
Oeffner						
Ge	+0.94174					
O_c	−0.47087					
Ge-O_c		81989.6607	0.16315	93.2784227	12.0	
O_c-O_c		3032.4815	0.304404	51.665882	12.0	
Sastre						
Ge	+4.0					
O_c	+1.733957					
O_s	−3.733957					
Ge-O_s		1497.3996	0.325646	16.808599	12.0	
O_s-O_s		22764.0	0.149	10.937044	12.0	
O_c-O_s						180.31577

Bibliography

1. Evans, K.E. and A. Alderson, *Auxetic materials: functional materials and structures from lateral thinking!* Advanced Materials, 2000: p. 617-628.
2. Mcclintock, F.A. and A.S. Argon, *Mechanical Behaviour of Materials*1966.
3. Love, A.E.H., *A Treatise on the Mathematical Theory of Elasticity*1944: Dover.
4. Evans, K.E., et al., *Molecular network design.* Nature, 1991. **353**(6340): p. 124-124.
5. Howell, B., P. Prendergast, and L. Hansen, *Examination of acoustic behavior of negative poisson's ratio materials.* Applied Acoustics, 1994. **43**(2): p. 141-148.
6. Alderson, K.L., et al., *Auxetic polyethylene: The effect of a negative poisson's ratio on hardness.* Acta Metallurgica et Materialia, 1994. **42**(7): p. 2261-2266.
7. Scarpa, F., L. Ciffo, and J. Yates, *Dynamic properties of high structural integrity auxetic open cell foam.* Smart Materials and Structures, 2004. **13**(1): p. 49.
8. Alderson, A., et al., *An Auxetic Filter: A Tuneable Filter Displaying Enhanced Size Selectivity or Defouling Properties.* Industrial & Engineering Chemistry Research, 2000. **39**(3): p. 654-665.
9. Rasburn, J., et al., *Auxetic structures for variable permeability systems.* AIChE Journal, 2001. **47**(11): p. 2623-2626.
10. Evans, K.E., *The design of doubly curved sandwich panels with honeycomb cores.* Composite Structures, 1991. **17**(2): p. 95-111.
11. Nye, J.F., *Physical Properties of Cristals: Their Representation by Tensors and Matrices*1985: Oxford University Press.
12. Voigt, W., *Lehrbuch der Kristallphysik.* Leipzig Teubner, 1928: p. 962.
13. Reuss, A., *Berechnung der Fließgrenze von Mischkristallen auf Grund der Plastizitätsbedingung für Einkristalle.* ZAMM - Journal of Applied Mathematics and Mechanics / Zeitschrift für Angewandte Mathematik und Mechanik, 1929. **9**(1): p. 49-58.
14. Hill, R., *The elastic behaviour of a crystalline aggregate.* Proceedings of the Physical Society. Section A, 1952. **65**(5): p. 349.
15. Williams, J. and J. Lewis, *Properties and an anisotropic model of cancellous bone from the proximal tibial epiphysis.* Journal of Biomechanical Engineering, 1982. **104**(1): p. 50-56.
16. Veronda, D. and R. Westmann, *Mechanical characterization of skin—finite deformations.* Journal of biomechanics, 1970. **3**(1): p. 111-124.
17. Lakes, R., *Foam structures with a negative Poisson's ratio.* Science, 1987: p. 235.
18. Baughman, R., et al., *Negative Poisson's ratios as a common feature of cubic metals.* Nature, 1998: p. 362-365.
19. Rovati, M., *Directions of auxeticity for monoclinic crystals.* Scripta materialia, 2004. **51**(11): p. 1087-1091.
20. Yeganeh-Haeri, A., D. Weidner, and J. Parise, *Elasticity of a-Cristobalite : A Silicon Dioxide with a Negative Poisson ' s Ratio.* Science, 1992. **257**(5070): p. 650-652.
21. Alderson, A., et al., *Modelling of the mechanical and mass transport properties of auxetic molecular sieves: an idealised inorganic (zeolitic) host–guest system.* Molecular Simulation, 2005: p. 889-896.
22. Alderson, K., et al., *Auxetic warp knit textile structures.* physica status solidi (b), 2012. **249**(7): p. 1322-1329.
23. Miller, W., et al., *The manufacture and characterisation of a novel, low modulus, negative Poisson's ratio composite.* Composites Science and Technology, 2009. **69**(5): p. 651-655.
24. Smith, W. *Optimizing electromechanical coupling in piezocomposites using polymers with negative Poisson's ratio*. in *Ultrasonics Symposium, 1991. Proceedings., IEEE 1991*. 1991. IEEE.
25. Alderson, A., et al., *Modelling of the mechanical and mass transport properties of auxetic molecular sieves: an idealised organic (polymeric honeycomb) host-guest system.* Molecular Simulation, 2005: p. 897-905.
26. Davis, M.E. and R.F. Lobo, *Zeolite and molecular sieve synthesis.* Chemistry of Materials, 1992. **4**(4): p. 756-768.
27. J., G.L., et al., *The mechanics of two-dimensional cellular materials.* Proceedings of the royal society of London. series a, mathematical and physical sciences (1934-1990), 1982: p. 382.
28. Grima, J.N., R. Gatt, and P.S. Farrugia, *On the properties of auxetic meta-tetrachiral structures.* physica status solidi (b), 2008. **245**(3): p. 511-520.

29. Grima, J.N. and K.E. Evans, *Auxetic behavior from rotating squares.* Journal of Materials Science Letters, 2000. **19**(17): p. 1563-1565.
30. Grima, J.N. and K.E. Evans, *Auxetic behavior from rotating triangles.* Journal of materials science, 2006. **41**(10): p. 3193-3196.
31. Alderson, A. and K. Evans, *Rotation and dilation deformation mechanisms for auxetic behaviour in the alpha-cristobalite tetrahedral framework structure.* Physics and Chemistry of Minerals, 2001: p. 711-718.
32. Grima, J.N., A. Alderson, and K.E. Evans, *Auxetic behaviour from rotation rigid units.* physica satus solidi (b), 2005: p. 561-575.
33. Grima, J.N., et al., *Auxetic behaviour from rotation semi-rigid units.* physica status solidi (b), 2007: p. 866-882.
34. Milton, G.W., *Composite materials with Poisson's ratios close to—1.* Journal of the Mechanics and Physics of Solids, 1992. **40**(5): p. 1105-1137.
35. Wojciechowski, K., *Two-dimensional isotropic system with a negative Poisson ratio.* Physics Letters A, 1989. **137**(1): p. 60-64.
36. Alderson, A. and K. Evans, *Modelling concurrent deformation mechanisms in auxetic microporous polymers.* Journal of materials science, 1997: p. 2797-2809.
37. He, C., P. Liu, and A.C. Griffin, *Toward negative Poisson ratio polymers through molecular design.* Macromolecules, 1998. **31**(9): p. 3145-3147.
38. Ogi, H., M. Fukunga, and M. Hirao, *Elastic constants, internal friction, and piezoelectric coefficient of alpha-*TeO_2*.* Physical Review B, 2004: p. 024104.
39. Lakes, R., *Advances in negative Poisson's ratio materials.* Advanced Materials, 1993. **5**(4): p. 293-296.
40. Ju, J. and J.D. Summers, *Compliant hexagonal periodic lattice structures having both high shear strength and high shear strain.* Materials & Design, 2011. **32**(2): p. 512-524.
41. Lethbridge, Z.A.D., et al., *Elastic anisotropy and extreme Poisson's ratios in single crystals.* Acta Materialia, 2010. **58**(19).
42. Zener, C., *Contributions to the theory of beta-phase alloys.* Physical Review, 1947. **71**(12): p. 846.
43. Ledbetter, H. and A. Migliori, *A general elastic-anisotropy measure.* Journal of Applied Physics, 2006. **100**(6): p. 063516.
44. Makishima, A. and J.D. Mackenzie, *Calculation of bulk modulus, shear modulus and Poisson's ratio of glass.* Journal of non-crystalline solids, 1975. **17**(2): p. 147-157.
45. Yang, W., et al., *Review on auxetic materials.* Journal of materials science, 2004. **39**(10): p. 3269-3279.
46. Brańka, A., D. Heyes, and K. Wojciechowski, *Auxeticity of cubic materials.* physica status solidi (b), 2009. **246**(9): p. 2063-2071.
47. Sanchez-Valle, C., S. Sinogeikin, and Z.A.D. Lethbridge, *Brillouin scattering study on the single-crystal elastic properties of natrolite and analcime zeolites.* Journal of Applied Physics, 2005: p. 053508.
48. Taylor, S., *Abundance of chemical elements in the continental crust: a new table.* Geochimica et Cosmochimica Acta, 1964. **28**(8): p. 1273-1285.
49. Revesz, A.G., *The defect structure of vitreous* SiO_2 *films on silicon. I. Structure of vitreous* SiO_2 *and the nature of the Si-O bond.* physica status solidi (a), 1980. **57**(1): p. 235-243.
50. Wei, P.-H., *The Structure of [alpha]-Quartz*, 1935, University of Chicago, Department of Physics.
51. Bragg, W. and R. Gibbs, *The Structure of α and β Quartz.* Proceedings of the Royal Society of London. Series A, 1925. **109**(751): p. 405-427.
52. Damjanovic, D., *Ferroelectric, dielectric and piezoelectric properties of ferroelectric thin films and ceramics.* Reports on Progress in Physics, 1998. **61**(9): p. 1267.
53. Walker, A. and E. Buehler, *Growing large quartz crystals.* Industrial & Engineering Chemistry, 1950. **42**(7): p. 1369-1375.
54. Bechmann, R., *Elastic and piezoelectric constants of alpha-quartz.* Physical Review, 1958. **110**(5): p. 1060.
55. Guo, C. and L. Wheeler, *Extreme Poisson's ratios and related elastic crystal properties.* Journal of the Mechanics and Physics of Solids, 2006: p. 690-707.
56. Kimizuka, H., H. Kaburaki, and Y. Kogure, *Mechanism for Negative Poisson Ratios over the alpha-beta Transition of Cristobalite,* SiO_2*: A Molecular-Dynamics Study.* Physical Review Letters, 2000: p. 5548-5551.
57. Grima, J.N., et al., *Do Zeolites Have Negative Poisson's Ratios?* Advanced Materials, 2000: p. 1912-1918.
58. Grima, J.N., R. Gatt, and V. Zammit, *Natrolite: A zeolite with negative Poisson's ratios.* Journal of Applied Physics, 2007: p. 086102.

59. Williams, J.J., et al., *An analytical model for producing negative Poisson ' s ratios and its application in explaining off-axis elastic properties of the NAT-type zeolites.* Acta Materialia, 2007: p. 56975707.
60. Kimizuka, H., S. Ogata, and Y. Shibutani, *Atomistic characterization of structural and elastic properties of auxetic crystalline SiO_2.* physica status solidi (b), 2007. **244**(3): p. 900-909.
61. Beest, B., G. Kramer, and R. Santen, *Force fields for silicas and aluminophosphates based on ab initio calculations.* Physical Review Letters, 1990. **64**(16).
62. Huang, L. and J. Kieffer, *Molecular dynamics study of cristobalite silica using a charge transfer three-body potential: Phase transformation and structural disorder.* The Journal of Chemical Physics, 2003. **118**(3): p. 1487-1498.
63. Van Duin, A.C., et al., *ReaxFFSiO reactive force field for silicon and silicon oxide systems.* The Journal of Physical Chemistry A, 2003. **107**(19): p. 3803-3811.
64. Sierka, M. and J. Sauer, *Structure and reactivity of silica and zeolite catalysts by a combined quantum mechanics [ndash] shell-model potential approach based on DFT.* Faraday Discussions, 1997. **106**: p. 41-62.
65. Coudert, F.-X., *Systematic investigation of the mechanical properties of pure silica zeolites: stiffness, anisotropy, and negative linear compressibility.* Physical Chemistry Chemical Physics, 2013. **15**(38): p. 16012-16018.
66. Frenkel, D. and B. Smit, *Understanding molecular simulation: from algorithms to applications*2001: Access Online via Elsevier.
67. Parr, R.G. and W. Yang, *Density-functional theory of atoms and molecules*. Vol. 16. 1989: Oxford university press.
68. Gale, J. *gulp3.1_manual*. http://projects.ivec.org/gulp, 2007.
69. Finnis, M., *Interatomic forces in condensed matter*2003: Oxford University Press.
70. Burchart, E., et al., *A consistent molecular mechanics force field for all-silica zeolites.* Zeolites, 1992. **12**(2).
71. Mott, N. and M. Littleton, *Conduction in polar crystals. I. Electrolytic conduction in solid salts.* Transactions of the Faraday Society, 1938. **34**: p. 485-499.
72. Ewald, P.P., *Ewald summation.* Ann. Physik, 1921. **64**: p. 253-371.
73. Catlow, C., et al., *Molecular dynamics studies of hydrocarbon diffusion in zeolites.* Journal of the Chemical Society, Faraday Transactions, 1991. **87**(13): p. 1947-1950.
74. Dick Jr, B. and A. Overhauser, *Theory of the dielectric constants of alkali halide crystals.* Physical Review, 1958. **112**(1): p. 90.
75. Pan, X.-W., et al., *Nuclear shell-model calculations with fundamental nucleon-nucleon interactions.* Physics reports, 1996. **264**(1): p. 311-323.
76. Sanders, M., M. Leslie, and C. Catlow, *Interatomic potentials for SiO_2.* Journal of the Chemical Society, Chemical Communications, 1984(19): p. 1271-1273.
77. Schröder, K.-P. and J. Sauer, *Potential Functions for Silica and Zeolite Catalysts Based on ab Initio Calculations. 3. A Shell Model Ion Pair Potential for Silica and Aluminosilicates†.* The Journal of Physical Chemistry, 1996. **100**(26): p. 11043-11049.
78. Gale, J.D., *Analytical free energy minimization of silica polymorphs.* The Journal of Physical Chemistry B, 1998. **102**(28): p. 5423-5431.
79. Sastre, G. and A. Corma, *Rings and strain in pure silica zeolites.* The Journal of Physical Chemistry B, 2006. **110**(36): p. 17949-17959.
80. Pedone, A., et al., *FFSiOH: a New Force Field for Silica Polymorphs and Their Hydroxylated Surfaces Based on Periodic B3LYP Calculations.* Chemistry of Materials, 2008. **20**(7): p. 2522-2531.
81. Pedone, A., et al., *A New Self-Consistent Empirical Interatomic Potential Model for Oxides, Silicates, and Silica-Based Glasses.* The Journal of Physical Chemistry B, 2006. **110**(24): p. 11780-11795.
82. Sastre, G. and J.D. Gale, *Derivation of an interatomic potential for germanium-and silicon-containing zeolites and its application to the study of the structures of octadecasil, ASU-7, and ASU-9 Materials.* Chemistry of Materials, 2003. **15**(9): p. 1788-1796.
83. Jackson, R. and C. Catlow, *Computer simulation studies of zeolite structure.* Molecular Simulation, 1988. **1**(4): p. 207-224.
84. Jaramillo, E. and S.M. Auerbach, *New force field for Na cations in faujasite-type zeolites.* The Journal of Physical Chemistry B, 1999. **103**(44): p. 9589-9594.
85. Auerbach, S.M., et al., *Transport theory for cationic zeolites: Diffusion of benzene in Na-Y.* The Journal of Physical Chemistry, 1995. **99**(26): p. 10600-10608.
86. Vessal, B., *Simulation studies of silicates and phosphates.* Journal of non-crystalline solids, 1994. **177**: p. 103-124.

87. Tsuneyuki, S., et al., *First-Principles Interatomic Potential of Silica Applied to Molecular Dynamics.* Physical Review Letters, 1988. **61**(7): p. 869-872.
88. Woodley, S., et al., *The prediction of inorganic crystal structures using a genetic algorithm and energy minimisation.* Physical Chemistry Chemical Physics, 1999. **1**(10): p. 2535-2542.
89. Oeffner, R.D. and S.R. Elliott, *Interatomic potential for germanium dioxide empirically fitted to an ab initio energy surface.* Physical Review B, 1998. **58**(22): p. 14791.
90. Marmier, A., et al., *ElAM: A computer program for the analysis and representation of anisotropic.* Computer Physics Communications, 2010. **181**.
91. Catlow, C. and G. Price, *Computer modelling of solid-state inorganic materials.* Nature, 1990. **347**(6290).
92. Combariza, A.F., D.A. Gomez, and G. Sastre, *Simulating the properties of small pore silica zeolites using interatomic potentials.* Chemical Society Reviews, 2013. **42**(1): p. 114-127.
93. Baerlocher, C. and L.B. McCusker. *Database of zeolite structures*. 1996 10/05/2012; Available from: http://iza-structure.org/databases/.
94. Head, J.D. and M.C. Zerner, *A Broyden—Fletcher—Goldfarb—Shanno optimization procedure for molecular geometries.* Chemical physics letters, 1985. **122**(3): p. 264-270.
95. Stelzer, J., et al., *Hydrophobic properties of all-silica zeolite beta.* Microporous and mesoporous materials, 1998. **22**(1-3).
96. Sanchez-Valle, C., et al., *Negative Poisson's ratios in siliceous zeolite MFI-silicalite.* Journal of Chemical Physics, 2008. **128**(18): p. 184503-184503.
97. Han, Y., et al., *A Gallogermanate Zeolite Constructed Exclusively by Three-Ring Building Units.* Angewandte Chemie International Edition, 2011. **50**(13): p. 3003-3005.
98. Hughes, J., *Why functional programming matters.* The computer journal, 1989. **32**(2): p. 98-107.
99. Søndergaard, H. and P. Sestoft, *Referential transparency, definiteness and unfoldability.* Acta Informatica, 1990. **27**(6): p. 505-517.
100. Haskell.org. *The Haskell Programming Language*. 2013 [cited 2013 15/11/2013]; Available from: http://www.haskell.org/haskellwiki/Haskell.
101. Huggins, M.L., *The crystal structure of quartz.* Physical Review, 1922. **19**(4): p. 363.
102. *Introduction*, in *Haskellwiki*2012, Haskell.org.
103. Smith, G.S. and P.B. Isaacs, *The crystal structure of quartz-like GeO2.* Acta Crystallographica, 1964. **17**(7): p. 842-846.
104. Bennett, J.M., et al., *Crystal structure of* $AlPO_4$*-21, a framework aluminophosphate containing tetrahedral phosphorus and both tetrahedral and trigonal-bipyramidal aluminum in 3-, 4-, 5-, and 8-rings.* Inorganic Chemistry, 1985. **24**(2): p. 188-193.
105. Sowa, H., *The crystal structure of* $GaPO_4$ *at high pressure.* Zeitschrift für Kristallographie, 1994. **209**(12): p. 954-960.
106. Ghobadi, E. and J. Capobianco, *Crystal properties of α-quartz type* GeO_2. Physical Chemistry Chemical Physics, 2000. **2**(24): p. 5761-5763.
107. Balitsky, D., et al. *Growth of germanium dioxide single crystals with α-quartz structure and investigation of their crystal structure, optical, elastic, piezoelectric, dielectric and mechanical properties*. in *Annales de Chimie Science des Materiaux*. 2001. Elsevier.
108. Grant, F.A., *Properties of rutile (titanium dioxide).* Rev. Mod. Phys., 1959. **31**(646): p. 242.
109. Philippot, E., et al., *A general survey of quartz and quartz-like materials: packing distortions, temperature, and pressure effects.* Journal of Solid State Chemistry, 1996. **123**(1): p. 1-13.
110. Baerlocher, C., L.B. McCusker, and D.H. Olson, *Atlas of zeolite framework types*2007: Elsevier.
111. Dawson, C.J., et al., *Ab Initio Calculations of the Energy Dependence of Si–O–Si Angles in Silica and Ge–O–Ge Angles in Germania Crystalline Systems.* Chemistry of Materials, 2014. **26**(4): p. 1523-1527.
112. Sastre, G. and A. Corma, *Predicting Structural Feasibility of Silica and Germania Zeolites.* The Journal of Physical Chemistry C, 2010. **114**(3): p. 1667-1673.
113. Wang, Y., J. Song, and H. Gies, *The substitution of germanium for silicon in AST-type zeolite.* Solid State Sciences, 2003. **5**(11): p. 1421-1433.
114. Blasco, T., et al., *Preferential location of Ge in the double four-membered ring units of ITQ-7 zeolite.* The Journal of Physical Chemistry B, 2002. **106**(10): p. 2634-2642.
115. Kamakoti, P. and T.A. Barckholtz, *Role of Germanium in the Formation of Double Four Rings in Zeolites.* The Journal of Physical Chemistry C, 2007. **111**(9): p. 3575-3583.
116. Grimsditch, M., et al., *Elastic constants of α-*GeO_2. Journal of Applied Physics, 1998. **83**(6): p. 3018-3020.
117. Jorgensen, J., *Compression mechanisms in α-quartz structures—SiO2 and* GeO_2. Journal of Applied Physics, 2008. **49**(11): p. 5473-5478.

118. Böhm, H., *The cristobalite modification of GeO_2.* Naturwissenschaften, 1968. **55**(12): p. 648-649.
119. Kapko, V., et al., *Flexibility of ideal zeolite frameworks.* Physical Chemistry Chemical Physics, 2010. **12**(30): p. 8531-8541.
120. Masters, I. and K. Evans, *Models for the elastic deformation of honeycombs.* Composite Structures, 1996. **35**(4): p. 403-422.
121. Dove, M.T., V. Heine, and K.D. Hammonds, *Rigid unit modes in framework silicates.* Mineralogical Magazine, 1995. **59**(397): p. 629-640.
122. Lira, C., P. Innocenti, and F. Scarpa, *Transverse elastic shear of auxetic multi re-entrant honeycombs.* Composite Structures, 2009. **90**(3): p. 314-322.
123. Goodwin, A.L., *Rigid unit modes and intrinsic flexibility in linearly bridged framework structures.* Physical Review B, 2006. **74**(13): p. 134302.